# Fundamental and Applied Investigations in Solid-State Polymer Mechanochemistry

Michael B. Larsen

A dissertation

submitted in partial fulfillment of the

requirements for the degree of

Doctor of Philosophy

University of Washington

2015

Reading Committee:

Prof. Andrew J. Boydston, Chair

Prof. Christine K. Luscombe

Prof. Forrest Michael

Program Authorized to Offer Degree:

Department of Chemistry

University of Washington

## Abstract

Fundamental and Applied Investigations in Solid-State Polymer Mechanochemistry

Michael B. Larsen

Chair of the Supervisory Committee:
Professor Andrew J. Boydston
Department of Chemistry

The translation of mechanical force to specific chemical reactivity within polymeric materials is known as polymer mechanochemistry. While this phenomenon has long been observed in homopolymers, it has recently attracted much interest as researchers have developed systems capable of site-specific activation and defined outputs in response to mechanical inputs. This thesis aims to contribute to the study of polymer mechanochemistry by describing our fundamental and applied investigations in the field, with a particular emphasis on activation in the solid state. Chapter 1 is an introduction to polymer mechanochemistry, beginning with the characteristics and behavior of polymers under applied load, tracing the historical origins and recent developments in the field, and describing the methods with which systems capable of mechanochemical activation are studied. Chapter 2 discusses our work developing a new mode of mechanochemical activation, which we term “flex activation”, in which bond bending motions are the primary geometric deformation responsible for activation. It describes both initial proof-

of-concept studies of oxanorbornadiene mechanophores and the extension of this system to robust scaffolds capable of multiple mechanochemical activation cycles. Chapter 3 describes our ongoing efforts in the extension of the flex activation concept to a new mechanophore capable of releasing N-heterocyclic carbenes upon activation. Finally, Chapter 4 introduces the use of 3D printing to fabricate functional materials containing a mechanochemically-active polymer, along with demonstrating the advantages of this method in making prototype force sensors that would be difficult, if not impossible, to fabricate otherwise.

# TABLE OF CONTENTS

# LIST OF FIGURES

# LIST OF SCHEMES

# LIST OF TABLES

# ACKNOWLEDGEMENTS

The past five years have not been easy – nor should they have been, as it is supposed to be difficult to earn a PhD – and there are many people to whom I need to express sincere gratitude for helping me along the way. First and foremost, my advisor, Prof. AJ Boydston, has been an incredible source of inspiration for me. Joining the lab as the first student (well, co-first student – Greg was there with me) was daunting, but it has been everything I could have asked for in a grad school experience. AJ was a great advisor – I always knew I had his support and he has been instrumental in everything I have done. He pushed me harder than I have ever been pushed before, and none of the publications, conference presentations, patents, or experiences I have had in the past five years would be possible without him. I also need to thank other members of the Boydston lab, in particular Greg Peterson, Derek Church, and Kelli Ogawa. We were the original four students that made up the lab in that first year, and they served as great support for me throughout the process. Whether griping together about TAing, going out for drinks after finishing work on Fridays, or playing Cards Against Humanity in the conference room, they made the whole crazy and overwhelming experience of grad school better and more bearable.

Outside the Boydston lab, I would like to thank my committee members, Profs. Forrest Michael, Christine Luscombe, and Julie Kovacs. Their advice and insight during my exams and other presentations were a source of great help to me. Joseph May and his advisor, Prof. Xiaosong Li, taught me the basics of using Gaussian and I owe them any comprehension of computational chemistry I may have. My understanding of organic chemistry – and the world of academic chemistry as a whole – would not be where it is without Prof. Gojko Lalic. His class,

although a rude awakening to grad school, was instrumental in my development as a scientist, as were his efforts during our problem set meetings. Profs. Mark Ganter and Duane Storti from the Department of Mechanical Engineering at UW were instrumental in our various 3D printing projects, and without their guidance and expertise in the subject I very highly doubt Chapter 4 would exist. Profs. Jeremiah Johnson at MIT and Steve Craig at Duke (and their groups) were also great collaborators, and their willingness to share unpublished results and discuss projects – in particular NHC-CDI flex activation – was extremely gracious, not to mention scientifically invaluable.

Aside from professors, I need to thank the people that really make the department here at UW run. Paul Miller trained me on the NMR and made the whole NMR facility run amazingly smoothly. Martin Sadilek was always very nice and helpful in the mass spec facility, and I could always count on not just an answer from him but also genuine interest in my research. I taught a lot of organic lab courses during my time here, and Leesa Kurtz was great at making the whole process of teaching that many undergrads somehow run easily and was always helpful when I needed it, especially when I first started teaching.

I also need to thank everybody in the Department of Chemistry at my undergrad alma mater, Colorado College. They contacted me during my fourth year and asked if I would like to teach my own class on the block plan, which was an incredible experience for me and is probably going to affect my career choices down the line. By putting that amount of faith in me (which I hope was not ill-placed!) they were a great source of inspiration to really work hard and take pride in my teaching. As weird as it was to be at the front of a classroom in which I used to learn organic chemistry, I really did enjoy it and I am immensely grateful for the opportunity.

Outside the world of chemistry, I need to thank my friends and family for keeping me sane and always providing a shoulder to lean on. Even though they were in different cities, my friends from undergrad have been as great as they ever were, hosting me for visits, distracting me from work with fantasy football, and sending me random texts or emails. Of my friends here in Seattle, Tom Porter deserves a special mention for providing an escape from lab and a couch to crash on when those escapes went on a little too late. Kim Hartstein has been an amazing source of love and support, and I am grateful every day for having her in my life. I could write pages about how great she has been to me, but she would probably get embarrassed and ask me to take them out.

Finally, I absolutely could not have gotten through this without my parents and brother. Knowing that you have always supported me in whatever I do and that I can always call when I need someone to talk to has had an immeasurable impact in my life, and I have an endless amount of love and gratitude for all of you.

# DEDICATION

To my parents, without whom none of this would be possible
(in both the literal and figurative sense)

# Chapter 1. Introduction to Polymer Mechanochemistry

## Section 1: Mechanical Behavior of Polymers

### *1.1.a Polymer Viscoelasticity*

In order to understand and rationally design methods by which polymeric materials translate macroscopic mechanical deformation to specific chemical reactivity, it is necessary to possess a basic understanding of the behavior of polymers under applied loads. A defining characteristic of these systems is the time-dependence of their response to stress or strain, a phenomenon known as viscoelasticity.[1] Empirically, this results in the ability of polymers to exhibit differing mechanical characteristics depending on the temperature and time scale of measurement; for example, a given polymer may behave as a rigid, glassy solid at low temperatures and high strain rates and as a soft, elastic rubber at higher temperatures and lower strain rates.[2] An important parameter for characterizing viscoelastic behavior is the glass transition temperature ($T_g$), the temperature at which the bulk solid transitions from a hard, relatively brittle state to a softer, more elastic one. Experimentally, this is observed as a marked decrease in the elastic modulus of the material with increased temperature.[3]

At the molecular level, $T_g$ represents the onset of localized segmental motion of individual polymer chains. Below this transition, there is not enough kinetic energy for this type of mobility, and the relatively poor ability of polymer chains to dissipate mechanical input leads to more brittle behavior in the bulk solid. As is the case with many properties of polymeric materials, $T_g$ is largely determined by chemical composition, degree of polymerization, and the amount of entanglement and crosslinking.[2]

In a sense, the explanation of $T_g$ at the molecular level is a first step toward understanding the phenomenon of polymer mechanochemistry, as it relates molecular chemical

properties to the mechanical behavior of the bulk solid as a whole. The viscoelasticity of polymeric materials manifests in their response to mechanical deformation, both at the macroscopic and molecular levels. In the context of polymer mechanochemistry, it is important to consider the effects at each length scale, as the effectiveness of the transduction of mechanical energy to chemical energy between the two is of paramount importance.[4,5]

*1.1.b Macroscopic Responses to Mechanical Force*

When classified according to their rheological properties, polymers generally fall into three groups: thermoplastics, elastomers, and thermosets.[1] The defining characteristic of thermoplastics is their ability to be molded when heated due to the reduction in viscosity above the $T_g$ and, if semi-crystalline, the melting temperature ($T_m$). A typical stress-strain curve for thermoplastics above the $T_g$ is shown in Figure 1.1 (blue). Initially, the material experiences elastic deformation, in which the slope of the response between stress and strain is the Young's modulus. In this region, removal of applied force results in full recovery of the original shape.

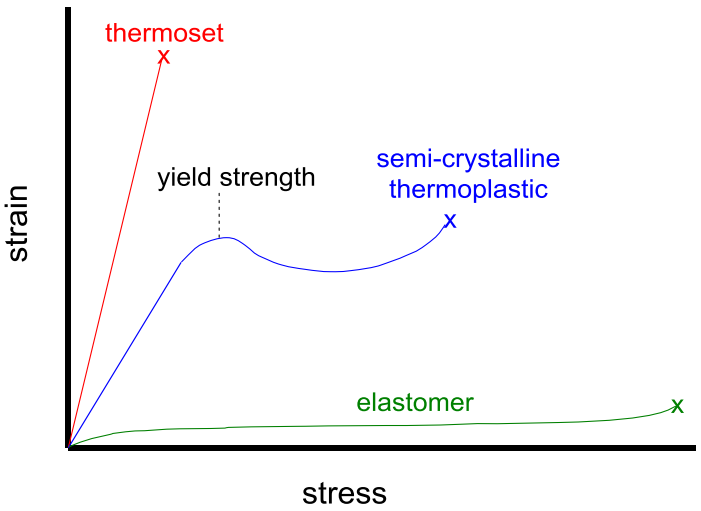


**Figure 1.1**. Representative stress-strain curves of different types of polymeric materials.

As more force is applied, relatively large amounts of stress localize in small regions of the material, and plastic deformation will begin to occur. The onset of this deformation is known as the yield strength, and the change in shape is permanent. Further application of force results in increasing amounts of plastic deformation, until the ultimate strength is reached and fracture occurs.

In contrast to the complexity of the stress-strain curves of thermoplastics, both elastomers and thermosets often display relatively simple macroscopic behavior in response to deformation (Figure 1.1, green and red, respectively). The crosslinking present in both types of polymer results in networks that are unable to undergo high degrees of large-scale chain mobility (see Section 1.1.c), resulting in little or no plastic deformation prior to bulk fracture. The primary difference between the two is the degree of crosslinking and the rigidity of the chains between crosslinks, which is reflected in their moduli and strain to fracture. Thermosets consist of relatively rigid monomers that are permanently covalently crosslinked to a high degree, providing little opportunity to compensate for any applied force via chain deformation or movement. As a result, they are relatively brittle and require a low amount of strain to fracture. In contrast, the chain segments of elastomers are highly flexible. They are able to compensate for an applied stress via chain extension, resulting in relatively large strain to fracture. Additionally, elastomers tend to possess a relatively low degree of crosslinking, which further decreases the modulus and allows for increased chain mobility.

### *1.1.c Microscopic and Molecular Responses to Mechanical Force*

The behavior of individual polymer chains in response to applied force differs based on whether the bulk polymer is amorphous or semi-crystalline. The characteristics of amorphous

polymers under reversible deformation are well-understood, and can primarily be rationalized via the kinetic theory of rubber elasticity.[6] This theory considers elasticity to originate from the reduction of entropy associated with main-chain conformational changes, the result of which is to elongate the polymer chain in the direction of the applied force. Anchor points, whether chemical crosslinks or physical chain entanglements, restrict the large-scale translational motion of individual chains. At low strains, thermodynamic equilibrium can be re-established once the applied force is released, with concomitant macroscopic recovery of the original shape (Figure 1.2).

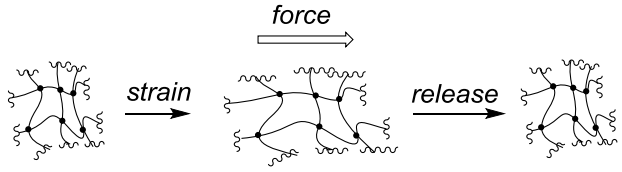


**Figure 1.2**. Chain elongation under applied force and elastic recovery in crosslinked networks. • = anchor point.

Experimentally, these molecular-level deformations can be observed and quantified via differential infrared (IR) spectroscopy of stressed and unstressed polymer samples.[7] In a seminal study,[7c] Wool and Boyd combined theoretical treatment and experimental shifts in IR frequencies to determine the relative contributions of different types of molecular perturbations to the elastic deformation of polypropylene (Figure 1.3). Importantly in the context of polymer mechanochemistry, they determined that although dihedral angles were most affected by the application of force, both bond angle bending and internuclear stretching were observed to a significant degree. The precise relative contribution of each type of deformation was found to be 1 : 2.4 : 9 for stretching, valence bending, and dihedral changes, respectively. Thus, the elastic response of individual chains can be envisioned as an uncoiling process, wherein the three main modes of molecular deformation all play an important role. In semi-crystalline polymers, the

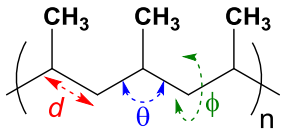


**Figure 1.3**. Molecular deformations in polypropylene, consisting of stretching of internuclear axes *d*, bending of bond angles θ, and changes in dihedral angles ϕ.

elastic response is dominated by the amorphous regions, which act similarly to those found in bulk amorphous materials.

In contrast to the Hookean behavior displayed in the elastic regime, plastic deformation is explained as the force-induced flow of a viscous liquid, a characteristic property of viscoelastic materials.[3,8] It is driven by shearing stresses, and thus is the result of large-scale translational motion of individual chains past each other. In amorphous, non-crosslinked polymers, this is activated by the disruption of noncovalent inter- and intramolecular interactions.[9] In effect, the application of stress reduces the thermal activation barrier to the onset of liquid-like flow. This can be modeled in an Eyring-type rate equation that describes the effect of force on lowering the activation energy of a chemical process (Equation 1):

$$k = k_0 exp[F\Delta x/k_B T] \quad (1)$$

In the case of an applied external force $F$ that acts along the reaction coordinate $x$ through a finite distance $\Delta x$ from the reactant to the transition state, the force-free rate constant $k_0$ is lowered to the new rate constant $k$ ($k_B$ and $T$ are Boltzmann's constant and temperature, respectively).[10] In considering the onset of plastic deformation, Equation 1 relates to the disruption of noncovalent interactions which hold the chains in place.[2] Thus, once enough force is applied such that the activation barrier for disrupting these interactions can be accessed under the thermal conditions of the system, translational chain motion will occur with bulk plastic deformation as the macroscopic result.

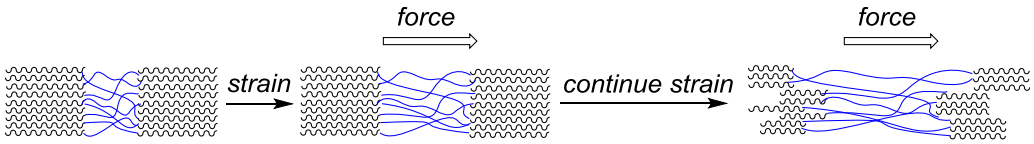


**Figure 1.4**. The effect of increasing force on semi-crystalline polymers. At low strains, elastic deformation of amorphous regions (blue) dominates. At higher strains, breakup of crystalline phases (black) leads to plastic deformation.

In semi-crystalline polymers, the precise mechanism of plastic deformation is still the subject of debate.[11,12] However, it is generally agreed upon that it involves shear-induced rearrangements of crystalline regions from folded, closely-packed lamellar phases to unfolded, more amorphous microstructures (Figure 1.4).[8,13] It is a similar process as that described above, in which applied stress results in the ability of the system to overcome the activation barrier for disruption of crystalline phases; in other words, the noncovalent inter- and intramolecular forces driving crystallization are overcome through the application of mechanical stress. Given this understanding of plasticity in polymeric materials, it is not surprising that the concept of force-enabled transformations would eventually be extended to the targeted scission of specific molecular structures within the polymer chain.

## Section 2: Historical Perspective

### *1.2.a Early Observations in Homopolymers*

The development of covalent polymer mechanochemistry – that is, the direct scission of covalent bonds in response to applied force – can be traced to the early investigations of polymer chemistry itself. In a series of publications in the 1930s, Staudinger reported the reduction of the molecular weight of natural rubber upon grinding in the solid state.[14] Given that the mechanical properties of polymers are correlated with molecular weight, grinding represents a facile method for obtaining the desired mechanical characteristics to suit a particular application, and remains the primary means of treatment for natural rubber to reach desired rheological properties.[5,15] The theoretical basis of polymer mechanochemistry was first explored by Kauzmann and Eyring, who suggested that modification of the Morse potential of stressed bonds led to homolytic scission in mechanically perturbed macromolecules (Figure 1.5).[16] Bell further elaborated this theory to state that, in systems in which the mechanical potential energy decreases as the chemical potential energy increases toward the transition state, the activation energy of the

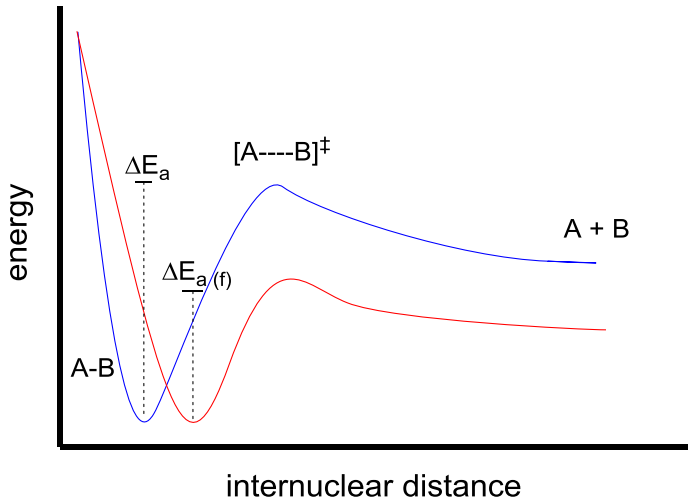


**Figure 1.5**. Morse potentials of a homolytic dissociation reaction between A and B in the absence (blue) and presence (red) of applied force. The coupled force leads to a reduction in the activation energy of $\Delta(\Delta E_a) = \Delta E_a - \Delta E_{a\,(f)}$. Adapted from ref. 23f.

reaction is lowered by the application of force.[17] That is, if mechanical energy can be productively coupled to geometric transformations that bring the molecule closer to the transition state for a particular reaction, that reaction will be accelerated through mechanical input (see Equation 1).

Support for this theory came in the form of electron paramagnetic resonance (EPR) spectroscopy of all manner of stressed polymeric materials, both in the solid state and in solution.[18] The detection of carbon-centered radicals, consistent with structures indicative of scission in the polymer main chain and supported by decreases in molecular weight, firmly established the susceptibility of homopolymers to mechanochemical homolytic chain scission. Both nuclear magnetic resonance (NMR)[19] and IR[20] spectroscopies have been utilized to determine the fate of mechanogenerated radicals; in the absence of radical trapping agents, both olefinic products typical of radical disproportionation and aerobic oxidation products are readily observed. The potential for productive chemical pathways of these mechanogenerated radicals was realized relatively early by Sohma.[21] By subjecting solid samples of poly(tetrafluoroethylene) to ball milling in the presence of methyl methacrylate or vinyl acetate, block copolymers were obtained via initiation of the second monomer by the chain end radical (Figure 1.6). Thus, by the early 1970s, both theoretical and experimental treatments had firmly established the propensity of macromolecules to undergo covalent bond scission in response to applied mechanical force, and this phenomenon had been utilized for productive transformations.

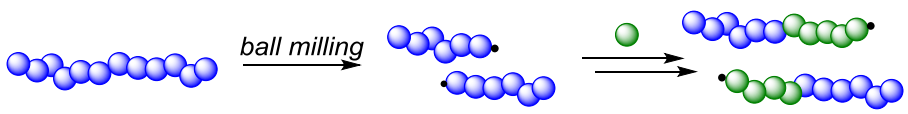


**Figure 1.6.** Application of force via ball milling results in homolytic chain scission and subsequent initiation of radical polymerization, producing diblock copolymers. Blue = poly(tetrafluoroethylene); green = poly(methyl methacrylate) or poly(vinyl acetate); • = chain-end radical.

*1.2.b Development of Targeted Bond Scission*[1]

With the concept of mechanochemical chain scission firmly established, a natural next route of inquiry concerned the factors controlling the efficiency of mechanochemical transduction at the molecular level. A key early effort in this area was described by Encina and coworkers in 1980, who compared the mechanochemical degradation rates of poly(vinyl pyrrolidone) with and without random peroxide linkages in the backbone.[22] By incorporating these weak links (O–O bond dissociation energy = 35 kcal/mol, versus C–C bond dissociation energy = 83 kcal/mol), the macromolecular degradation rate when exposed to ultrasound was estimated to be enhanced tenfold as measured by intrinsic viscosity; however, the authors noted that difficulties in characterizing the exact number of peroxide linkages per backbone precluded more quantitative conclusions. Perhaps due to these analytical difficulties, the investigation of selective mechanochemical bond scission in polymeric materials went relatively dormant after this study. Together with more effective analytical techniques, the ability of modern polymer chemists to manipulate the molecular structure of macromolecules to a high degree of precision has led to a resurgence in the field of covalent polymer mechanochemistry.[4,5,23]

Precise control over the distribution of forces at the molecular level can be achieved through the development of polymeric materials capable of channeling elongational forces to mechanophores – functional groups that are designed to undergo selective bond scission in response to external force. In the past decade, investigations of the effects of mechanical stress upon polymeric materials have provided macromolecules capable of undergoing well-defined chemical changes in response to the application of mechanical force (Figure 1.7). By introducing

[1] Reproduced with permission from Larsen, M. B.; Boydston, A. J. "Flex-Activated Mechanophores: Using Polymer Mechanochemistry to Direct Bond Bending Activation" *J. Am. Chem. Soc.* **2013**, *135*, 8189. Copyright 2013 American Chemical Society.

a mechanophore at a specific point along the polymer chain, the application of stress to the polymer as a whole can be coupled to reactivity at a single site. Early efforts in mechanochemical control and design demonstrated selective homolytic scission of weak bonds and site-specificity.[24] Dative metal-ligand bonds have also been shown to be mechanochemically sensitive, giving rise to force-activated catalysts.[25] Additionally, ring opening and cycloreversion reactions have provided exciting breakthroughs in force-guided reactivity, mechanochromics, and potential self-healing or reinforcing materials. Key examples include ring opening of strained three- and four-membered rings,[26–29] formal retro-cycloaddition,[30–32] and electrocyclic ring opening of spiropyran chromophores.[33] In addition to these experimental studies, a robust theoretical framework for understanding covalent polymer mechanochemistry has also been developed, which has enabled a better understanding of the factors that affect the efficiency of chemomechanical coupling and provided design rules for new mechanophores.[10,34] Collectively,

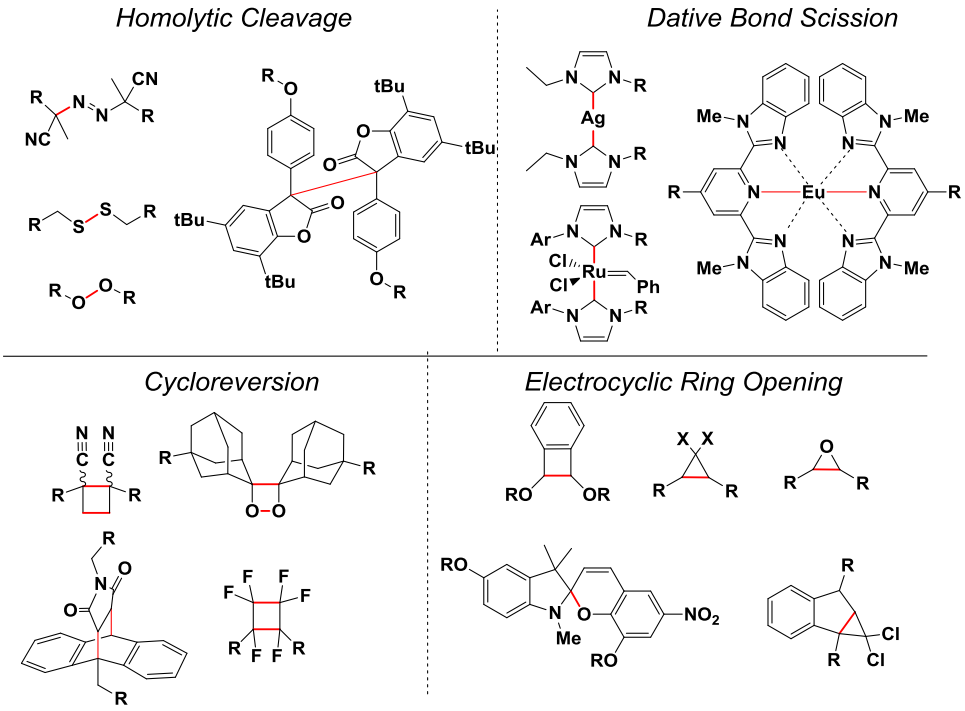


**Figure 1.7**. Generalized examples of moieties capable of mechanochemical activation, with the scissile bond(s) highlighted in red. R = site of polymer attachment; X = F, Cl, Br.

the assortment of demonstrated mechanochemical reactions accessible via polymer elongation spans a range of organic, organometallic, and inorganic transformations.

## Section 3: Methods to Achieve Mechanochemical Transduction

### *1.3.a Solution-Based Methods*

The fundamental molecular deformation that gives rise to the scission of covalent bonds in polymeric materials is an elongation of the polymer chain. Thus, any method in which such an elongation is achieved can conceivably be adapted to induce a mechanochemical reaction, given appropriate experimental conditions can be identified. To date, the techniques utilized to activate mechanochemical events in polymers can be broadly categorized as occurring in dilute solution, in the bulk solid, or on individual chains via single molecule force spectroscopy (SMFS). They differ widely in their achievable regimes of stress and strain rates (Figure 1.8). This section will provide a brief overview of the effective methods for mechanochemical transduction in

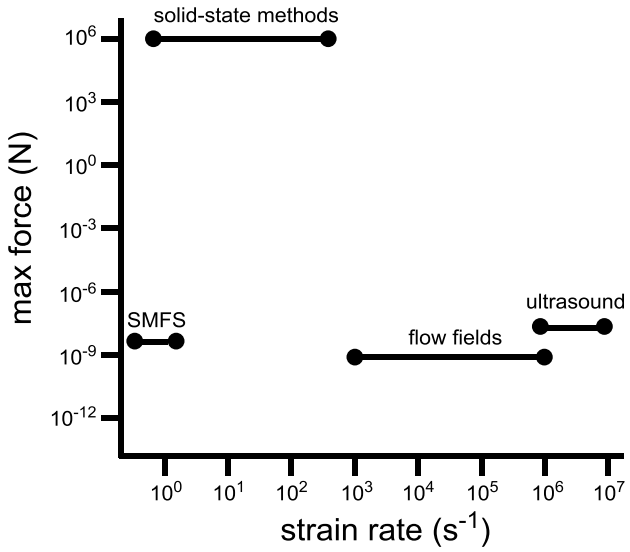


**Figure 1.8**. Relative stress and strain rates of different methods used to apply force to polymers. Adapted from refs. 4 and 22c.

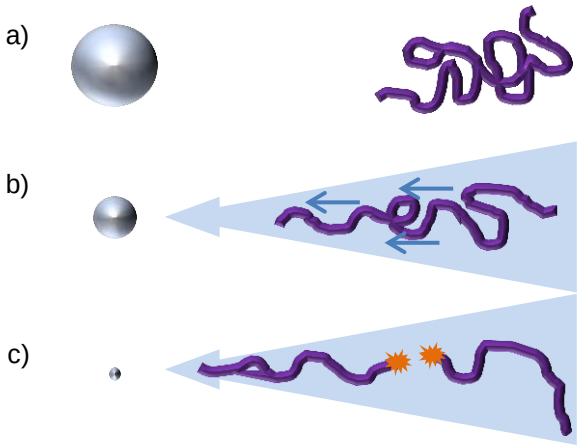


**Figure 1.9**. (a) Ultrasonication causes cavitation bubbles to grow in solution. (b) Collapse of bubbles results in solvodynamic shear forces acting on polymer chain (purple). (c) Weak point of polymer breaks in response to buildup of stress in backbone.

polymers, with special emphasis placed upon those utilized most commonly in the activation of mechanophores.

The various methods by which force is applied to polymers in dilute solution all rely on the action of flow fields to extend the polymer.[23a,b] Elongational flow in particular exerts strong hydrodynamic shear forces on polymer chains. In response to these forces, the chain stretches, re-orients, and extends in the direction of flow, a phenomenon known as the coil-stretch transition. If the rate of chain stretching (i.e. strain rate) far exceeds the rate of chain relaxation, covalent bonds can be severed.[35] A variety of approaches to generate elongational flow in the context of mechanochemical activation have been investigated, including turbulent flow fields,[36] opposed jets,[37] and contraction flows.[38] However, ultrasonication of dilute polymer solutions has proven to be especially fruitful in studying polymer mechanochemistry.

The mechanism for converting ultrasound to elongational flow occurs via a process known as cavitation (Figure 1.9).[39,40] As an ultrasonic wave moves through a liquid medium, it produces pressure oscillations throughout the solution according to the phase of the wave – that is, during the compression cycle pressure is increased, and during rarefaction it is decreased. If

the wave is of sufficient frequency and intensity, the decrease in pressure during rarefaction can be significant enough to create voids and cavities within the liquid, forming cavitation bubbles. These bubbles rapidly collapse during the succeeding compression cycle, and in doing so create solvodynamic shear forces in any nearby dissolved polymer as the proximal chain end is pulled toward the collapsing bubble. The relatively large size of the polymer chain results in an anisotropic distribution of these forces along the chain, resulting in a buildup of stress and eventual chain scission. Experimentally, it has been demonstrated that chain scission in homopolymers occurs in the middle 15% of the chain, where the forces are greatest.[41] Thus, by deliberate placement of a mechanophore in the middle of a polymer chain (as opposed to a chain end), the influence of mechanical force versus thermal or pressure-induced effects can be easily probed.

The relatively high strain rates achieved during ultrasonication, as opposed to other solution-based techniques (ca. $10^6$ – $10^7$ $s^{-1}$ versus $10^3$ – $10^6$ $s^{-1}$ for other elongational flow techniques)[23b] permit the use of lower molecular weight polymers to study chemomechanical coupling. Polymers on the order of 30 – 100 kDa successfully undergo mechanochemical activation in ultrasonication studies, and this range is easily achieved using modern controlled polymerization techniques. In addition, polymer chemists are able to precisely control the location and amount of mechanophore in each polymer chain. In combination with the ease of experimental setup, the ability to use familiar solution-based characterization techniques, and the well-known effects of a variety of factors upon the efficiency of cavitation,[4,39] the relatively low molecular weight requirements for ultrasonication studies make it an attractive option for probing mechanochemical activation.

*1.3.b Solid-state Methods*

In general, solid-state methods of mechanochemical activation are capable of achieving higher maximum forces than solution-phase techniques, albeit at lower strain rates (see Figure 1.8). While chain elongation must still occur faster than relaxation, this latter transition is much slower in solid polymers, and thus mechanochemical activation can still occur even though the strain rate is much lower.[23c] Due to the simple fact that the majority of applications of polymeric materials are found in the solid state, the behavior of mechanochemically-active bulk polymers under familiar mechanical testing conditions is of paramount importance in eventually moving these platforms beyond the laboratory. To date, most studies of the activation of mechanophores have applied force to polymers in the solid-state via either elongation or compression.

Simple manual elongation of solid polymer samples, while it cannot provide precise measurements of applied stress or strain, nevertheless may provide rapid preliminary assessment of the mechanochemical activity of a polymeric material, particularly in cases in which the result of activation is a marked color change or other easily detected spectroscopic signal.[42] Much more common is the use of either rheometers or tensile testing load frames to apply elongational force, as they are able to quantify the applied stress and control strain rates. The resultant stress-strain curves, and the properties derived from them, are important in identifying potential applications. Moreover, in cases in which activation of the mechanophore produces a spectroscopic signal or shift, optical spectroscopic measurements can be collected simultaneously to provide information pertaining to the onset of mechanochemical activation during the stressing of the bulk material.[30b,33,43] A prime example of these advantages is the work of Braun, Sottos, White, and Moore, who have added to the understanding of how time,[43e] chain mobility and alignment,[43c,f,h] and microenvironment[43d] affect the activation of spiropyran mechanophores in tensile testing

specimens. However, these studies require relatively large amounts of material that are processed into well-defined shapes, which can make studying crosslinked polymers or those with limited solubility challenging.

An alternative to tensile elongation methods is the use of compressive forces, which generally do not require samples of well-defined shape, making it an attractive option for polymers that are more difficult to process. For quantification, the applied force can be simply calculated from the pressure on the sample and the cross-sectional area of the compression chamber. As the compression is not isotropic, it still acts to elongate individual polymer chains as the sample deforms outward from the axis of compression, thus giving rise to mechanophore activation. While piston cells,[44] diamond anvil cells,[45] and custom setups[33b] have all been utilized for compressive studies, the simplest method is compression in a hydraulic benchtop press. In these experiments, compression chambers similar to those used for making KBr pellets for IR spectroscopy are used to hold the polymer sample, and pressure is applied with a simple hydraulic press. When force is applied to the die, the uniaxial compression of polymer samples causes deformation until the sample fills the cross-sectional area of the compression chamber. This deformation causes elongational stress on individual polymer chains, and compression on a different axis has been shown to increase mechanophore conversion.[27c,46] A main drawback of compressive testing is the difficulty of coupling the apparatus to *in situ* spectroscopic monitoring techniques, particularly when using relatively simple hydraulic presses.

### *1.3.c Single Molecule Force Spectroscopy*

The measurements and results obtained using the activation methods described above are all ensemble averages, in which it is impossible to determine the forces and dynamics acting

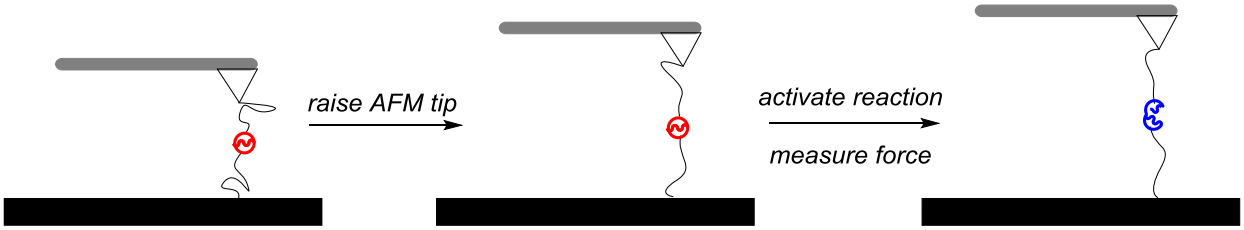


**Figure 1.10**. Use of SMFS to study activation of mechanophores in individual polymers. As the AFM tip is raised, accumulated stress in the main chain leads to mechanochemical activation, and the force is recorded and quantified. Red = mechanophore before activation; blue = reacted mechanophore.

upon a single polymer chain. In contrast, SMFS provides precise quantification of the forces required to activate a mechanochemical event.[47] Briefly, a polymer containing a putative mechanophore is either covalently attached or adsorbed onto an atomic force microscopy (AFM) stage (Figure 1.10). Subsequent contact, polymer adhesion, and withdrawl of the AFM cantilever stretches an individual polymer chain, and bond scission can be observed via plateaus or drops in the force-displacement curve.

Studying the interactions and unfolding of biopolymers is the most widespread use of SMFS,[48] but pioneering work by Craig and coworkers has firmly demonstrated the value of this method in exploring synthetic polymer mechanochemistry.[27a,49] In addition to direct quantification of the forces required to activate mechanophores – typically on the order of 1 – 2 nanonewtons – the effects of both local stereochemistry[49c] and the polymer backbone[27a] on mechanochemical activation have yielded important design parameters for increasing the efficiency of chemomechanical coupling. However, the highly specialized nature of the measurement, synthetic modifications required for good adhesion to the AFM tip, and inability to spectroscopically characterize the polymer after mechanochemical activation may limit the scope of this method. In addition, only non-scissile mechanophores – i.e. those whose activation does not result in total chain scission – are suitable for study using this method.

**Section 4: Summary**

The study of the effects of force on polymeric materials encompasses a broad range of disciplines, from engineering and materials science to polymer chemistry. The viscoelastic behavior of polymers is perhaps the defining characteristic of their behavior in the solid state, and the experimental and theoretical understanding of both elastic and plastic deformation laid the foundations for explorations of the mechanochemical scission of bonds in polymeric materials. Beginning with the study of the decrease in molecular weight in homopolymers subject to milling and grinding, the field of polymer mechanochemistry has matured to the point of targeted scission of specific sites within polymeric architectures. The extension of theoretical concepts of polymer viscoelasticity and force-modified potential energy surfaces has enabled a thorough understanding of the various factors affecting the efficiency of mechanochemical transduction. In conjunction with modern analytical techniques and controlled polymerization methods, researchers have developed a full suite of methods – i.e. solution phase, solid state, and single molecule – for studying the activation of mechanophores.

**Notes and References for Chapter 1**

[1]Young, R. J. and Lovell, P. A. *Introduction to Polymers*, 3rd ed.; CRC Press: Boca Raton, FL, 2011.
[2] Ward, I. M. and Sweeney, J. *Mechanical Properties of Solid Polymers*, 3rd ed.; John Wiley & Sons: Sussex, UK, 2013.
[3] Menard, K. P. *Dynamic Mechanical Analysis: A Practical Introduction*, 1st ed.; CRC Press: Boca Raton, FL, 1999.
[4] Caruso, M. M.; Davis, D. A.; Shen, Q.; Odom, S. A.; Sottos, N. R.; White, S. R.; Moore, J. S. *Chem. Rev.* **2009**, *109*, 5755.
[5] Beyer, M. K.; Clausen-Schaumann, H. *Chem. Rev.* **2005**, *105*, 2921.
[6] Treloar, L. R. G. *Physics of Rubber Elasticity*, 3rd ed.; Oxford University Press: Oxford, UK, 2009.
[7] (a) Wool, R. P. *J. Polym. Sci., Polym. Phys. Ed.* **1975**, *13*, 1795. (b) Wool, R. P. *Polym. Eng. Sci.* **1980**, *20*, 805. (c) Wool, R. P.; Boyd, R. H. *J. Appl. Phys.* **1980**, *51*, 5116. (d) Wool, R. P.; Statton, W. O. *J. Polym. Sci., Polym. Phys. Ed.* **1974**, *12*, 1575.
[8] Argon, A. S. *The Physics of Deformation and Fracture in Polymers*, 1st ed.; Cambridge University Press: Cambridge, UK, 2013.
[9] Launey, M. E.; Ritchie, R. O. *Adv. Mater.* **2009**, *21*, 2103.
[10] Ribas-Arino, J.; Marx, D. *Chem. Rev.* **2012**, *112*, 5412.
[11] Bartczak, Z.; Galeski, A. *Macromol. Symp*. **2010**, *294-1*, 67.
[12] Oleinik, E. F.; Rudnev, S. N.; Salamatina, O. B. *Polym. Sci. A* **2007**, *49*, 1302.
[13] Jabbari-Farouji, S.; Rottler, J.; Lame, O.; Makke, A.; Perez, M.; Barrat, J.-L. *ACS Macro Lett.* **2015**, *4*, 147.
[14] (a) Staudinger, H.; Bondy, H. F. *Ber. Dtsch. Chem. Ges.* **1930**, *63*, 734. (b) Staudinger, H.; Heuer, W. *Ber. Dtsch. Chem. Ges.* **1934**, *67*, 1159. (c) Staudinger, H.; Leupold, E. O. *Ber. Dtsch. Chem. Ges.* **1930**, *63*, 730.
[15] Casale, A.; Porter, R. S.; Johnson, J. F. *Rubber Chem. Technol.* **1971**, *44*, 534.
[16] Kauzmann, W.; Eyring, H. *J. Am. Chem. Soc.* **1940**, *62*, 3113.
[17] Bell, G. I. *Science* **1978**, *200*, 618.
[18] Sohma, J. *Prog. Polym. Sci.* **1989**, *14*, 451.
[19] Kolbert, A. C.; Didier, J. G.; Xu, L. *Macromolecules* **1996**, *29*, 8591.
[20] Zhurkov, S. N.; Korsukov, V. E. *J. Polym. Sci. Polym. Phys. Ed.* **1974**, *12*, 385.
[21] Sakaguchi, M.; Sohma, J. *J. Appl. Polym. Sci.* **1978**, *22*, 2915.
[22] Encina, M. V.; Lissi, E.; Sarasua, M.; Gargallo, L.; Radic, D. *J. Polym. Sci.* **1980**, *18*, 757.
[23] For additional recent reviews, see: (a) Brantley, J. N.; Bailey, C. B.; Wiggins, K. M.; Ketinge-Clay, A. T.; Bielawski, C. W. *Polym Chem.* **2013**, *4*, 3916. (b) May, P. A.; Moore, J. S. *Chem. Soc. Rev.* **2013**, *42*, 7497. (c) Wiggins, K. M.; Brantley, J. N.; Bielawski, C. W. *Chem. Soc. Rev.* **2013**, *42*, 7130. (d) Brantley, J. N.; Wiggins, K. M.; Bielawski, C. W. *Polym. Int.* **2012**, *62*, 2. (e) Ariga, K.; Mori, T.; Hill, J. P. *Adv. Mater.* **2012**, *24*, 158. (f) Black, A. L.; Lenhardt, J. M.; Craig, S. L. *J. Mater. Chem.* **2011**, *21*, 1655.
[24] (a) Imato, K.; Irie, A.; Kosuge, T.; Ohishi, T.; Nishihara, M.; Takahara, A.; Otsuka, H. *Angew. Chem. Int. Ed.* **2015**, *127*, 6266. (b) Fitch, K. R.; Goodwin, A. P. *Chem. Mater.* **2014**, *26*, 6771. (c) Park, I.; Sheiko, S. S.; Nese, A.; Matyjaszewski, K. *Macromolecules* **2009**, *42*, 1805 (d)

Berkowski, K. L; Potisek, S. L.; Hickenboth, C. R.; Moore, J. S. *Macromolecules* **2005**, *38*, 8975.
[25] (a) Paulusse, J. M.; Sijbesma, R. P. *Chem. Commun.* **2008**, 4416. (b) Piermattei, A.; Karthikeyan, S.; Sijbesma, R. P. *Nat. Chem.* **2009**, *1*, 133. (c) Jakobs, R. T. M.; Ma, S.; Sijbesma, R. P. *ACS Macro Lett.* **2013**, *2*, 613. (d) Balkenende, D. W. R.; Coulibaly, S.; Balog, S.; Simon, Y. C.; Fiore, G. L.; Weder, C. *J. Am. Chem. Soc.* **2014**, *136*, 10493.
[26] For an example of epoxide ring opening, see: Klukovich, H. M.; Kean, Z. S.; Ramirez, A. L. B.; Lenhardt, J. M.; Lin, J.; Hu, X.; Craig, S. L. *J. Am. Chem. Soc.* **2012**, *134*, 9577.
[27] For examples of cyclopropane ring opening, see: (a) Klukovich, H. M.; Kouznetsova, T. B.; Kean, Z. S.; Lenhardt, J. M.; Craig, S. L. *Nat. Chem.* **2013**, *5*, 110. (b) Kean, Z. S.; Craig, S. L. *Polymer* **2012**, *53*, 1035. (c) Lenhardt, J. M.; Black, A. L.; Beiermann, B. A.; Steinberg, B. D.; Rahman, F.; Samborski, T.; Elsakr, J.; Moore, J. S.; Sottos, N. R.; Craig, S. L. *J. Mater. Chem.* **2011**, *21*, 8454. (d) Lenhardt, J. M.; Black, A. L.; Craig, S. L. *J. Am. Chem. Soc.* **2009**, *131*, 10818.
[28] For an example of tandem ring opening/dehydrohalogenation, see: Diesendruck, C. E.; Steinberg, B. D.; Sugai, S. N.; Silberstein, M. N.; Sottos, N. R.; White, S. R.; Braun, P. V.; Moore, J. S. *J. Am. Chem. Soc.* **2012**, *134*, 12446.
[29] For examples of electrocyclic ring opening of benzocyclobutene, see: (a) Hickenboth, C. R.; Moore, J. S.; White, S. R.; Sottos, N. R.; Baudry, J.; Wilson, S. R. *Nature* **2007**, *446*, 423. (b) Potisek, S. L.; Davis, D. A.; Sottos, N. R.; White, S. R.; Moore, J. S. *J. Am. Chem. Soc.* **2007**, *129*, 13808.
[30] For examples of retro [2+2] cycloaddition, see: (a) Kean, Z. S.; Gossweiler, G. R.; Kouznetsova, T. B.; Hewage, G. B.; Craig, S. L. *Chem. Commun.* **2015**, *51*, 9157. (b) Chen, Y.; Spiering, A. J. H.; Karthikeyan, S.; Peters, G. W. M.; Meijer, E. W.; Sijbesma, R. P. *Nat. Chem.* **2012**, *4*, 559. (c) Klukovich, H. M.; Kean, Z. S.; Iacono, S. T.; Craig, S. L. *J. Am. Chem. Soc.* **2011**, *133*, 17882. (d) Kryger, M. J.; Munaretto, A. M.; Moore, J. S. *J. Am. Chem. Soc.* **2011**, *133*, 18992. (e) Kryger, M. J.; Ong, M. T.; Odom, S. A.; Sottos, N. R.; White, S. R.; Martínez, T. J.; Moore, J. S. *J. Am. Chem. Soc.* **2010**, *132*, 4558.
[31] For an example of retro [3+2] cycloaddition, see: Brantley, J. N.; Konda, S. S. M.; Makarov, D. E.; Bielawski, C. W. *J. Am. Chem. Soc.* **2012**, *134*, 9882.
[32] For examples of retro [4+2] cycloaddition, see: (a) Church, D. C.; Peterson, G. I.; Boydston, A. J. *ACS Macro Lett.* **2014**, *3*, 648. (b) Li, J.; Shiraki, T.; Hu, B.; Wright, R. A. E.; Zhao, B.; Moore, J. S. *J. Am. Chem. Soc.* **2014**, *45*, 15925. (c) Larsen, M. B.; Boydston, A. J. *J. Am. Chem. Soc.* **2013**, *135*, 8189.
[33] For representative examples, see: (a) Gossweiler, G. R.; Hewage, G. B.; Soriano, G.; Wang, Q.; Welshofer, G. W.; Zhao, X.; Craig, S. L. *ACS Macro Lett.* **2014**, *3*, 216. (b) Lee, C. K.; Davis, D. A.; White, S. R.; Moore, J. S.; Sottos, N. R.; Braun, P. V. *J. Am. Chem. Soc.* **2010**, *132*, 16107. (c) Davis, D. A.; Hamilton, A.; Yang, J.; Cremar, L. D.; Van Gough, D.; Potisek, S. L.; Ong, M. T.; Braun, P. V.; Martínez, T. J.; White, S. R.; Moore, J. S.; Sottos, N. R. *Nature* **2009**, *459*, 68.
[34] (a) Avdoshenko, S. M.; Makarov, D. E. *J. Chem. Phys.* **2015**, *142*, 174106. (b) Konda, S. S. M.; Avdoshenko, S. M.; Makarov, D. E. *J. Chem. Phys.* **2014**, *140*, 104114. (c) Konda, S. S. M.; Brantley, J. N.; Varghese, B. T.; Bielawski, C. W.; Makarov, D. E. *J. Am. Chem. Soc.* **2013**, *135*, 12722. (d) Tian, Y.; Boulatov, R. *Chem. Commun.* **2013**, *49*, 4187. (e) Huang, Z.; Boulatov, R. *Chem. Soc. Rev.* **2011**, *40*, 2359. (f) Boulatov, R. *Pure Appl. Chem.* **2011**, *83*, 25. (g) Ribas-

Arino, J.; Shiga, M.; Marx, D. *J. Am. Chem. Soc.* **2010**, *132*, 10609. (h) Ribas-Arino, J.; Shiga, M.; Marx, D. *Angew. Chem. Int. Ed.* **2009**, *48*, 4190. (i) Beyer, M. K. *J. Chem. Phys.* **2000**, *112*, 7307.

[35] Buchholz, B. A.; Zahn, J. M.; Kenward, M.; Slater, G. W.; Barron, A. E. *Polymer* **2004**, *45*, 1223.

[36] (a) Culter, J.; Zakin, J. L.; Patterson, G. K. *J. Appl. Polym. Sci.* **1975**, *19*, 3235. (b) Moussa, T.; Tiu, C. *Chem. Eng. Sci.* **1994**, *29*, 1681. (c) Horn, A. F.; Merrill, E. W. *Nature*, **1984**, *312*, 140. (d) Vanapalli, S. A.; Ceccio, S. L.; Solomon, M. J. *Proc Natl. Acad. Sci. USA*, **2006**, *103*, 16660.

[37] (a) Keller, A.; Odell, J. A. *Colloid Polym. Sci.* **1985**, *263*, 181. (b) Odell, J. A.; Miles, M. J. *Polymer*, **1985**, *26*, 1219. (c) Odell, J. A.; Keller, A. *J. Polym. Sci. Part B: Polym. Phys.* **1986**, *24*, 1889. (d) Odell, J. A.; Muller, A. J.; Narh, K. A.; Keller, A. *Macromolecules* **1990**, *23*, 3092.

[38] (a) Yu, G.; Nguyen, T. Q.; Kausch, H. H. *J. Polym. Sci. Part B: Polym. Phys*. **1998**, *36*, 1483. (b) Nguyen, T. Q.; Kausch, H. H. *Adv. Polym. Sci.* **1992**, *100*, 74. (c) Nguyen, T. Q.; Kausch, H. H. *J. Non-Newtonian Fluid Mech.* **1988**, *30*, 125.

[39] Mason, T. J. and Lorimer, J. P. *Applied Sonochemistry: The Uses of Power Ultrasound in Chemistry and Processing* 1st ed.; Wiley-VCH Verlag GmbH: Weinheim, Germany 2002.

[40] Suslick, K. S. *Science* **1990**, *247*, 1439.

[41] Suslick, K. S.; Price, G. J. *Annu. Rev. Mater. Sci.* **1999**, *29*, 295.

[42] For an example in which manual elongation was the only method utilized, see: Cho, S.-Y.; Kim, J.-G.; Chung, C.-M. *Sens. Actuators B*, **2008**, *134*, 822.

[43] (a) Kim, J. W.; Jung, Y.; Coates, G. W.; Silberstein, M. N. *Macromolecules* **2015**, *48*, 1335. (b) Ducrot, E.; Chen, Y.; Bulters, M. J. H.; Sijbesma, R. P.; Creton, C. *Science* **2014**, *344*, 186. (c) Beiermann, B. A.; Kramer, S. L. B.; May, P. A.; Moore, J. S.; White, S. R.; Sottos, N. R. *Adv. Funct. Mater.* **2014**, *24*, 1529. (d) Lee, C. K.; Beiermann, B. A.; Silberstein, M. N.; Wang, J.; Moore, J. S.; Sottos, N. R.; Braun, P. V. *Macromolecules* **2013**, *46*, 3746. (e) Degen, C. M.; May, P. A.; Moore, J. S.; White, S. R.; Sottos, N. R. *Macromolecules* **2013**, *46*, 8917. (f) Beiermann, B. A.; Kramer, S. L. B.; Moore, J. S.; White, S. R.; Sottos, N. R. *ACS Macro Lett.* **2012**, *1*, 163. (g) Kingsbury, C. M.; May, P. A.; Davis, D. A.; White, S. R.; Moore, J. S.; Sottos, N. R. *J. Mater. Chem.* **2011**, *21*, 8381. (h) Beiermann, B. A.; Davis, D. A.; Kramer, S. L. B.; Moore, J. S.; Sottos, N. R.; White, S. R. *J. Mater. Chem.* **2011**, *21*, 8443.

[44] Moses, D.; Feldblum, A.; Ehrenfreund, E.; Heeger, A. J.; Chung, T.-C.; MacDiarmid, A. G. *Phys. Rev. B.: Condens. Matter Mater. Phys.* **1982**, *26*, 3361.

[45] Muramatsu, Y.; Yamamoto, T.; Hasegawa, M.; Yagi, T.; Koinuma, H. *Polymer*, **2001**, *42*, 6673.

[46] Larsen, M. B.; Boydston, A. J. *J. Am. Chem. Soc.* **2014**, *136*, 1276.

[47] For recent reviews, see: (a) Claridge, S. A.; Schwartz, J. J.; Weiss, P. S. *ACS Nano* **2011**, *5*, 693. (b) Liang, J.; Fernández, J. M. *ACS Nano* **2009**, *3*, 1628.

[48] For representative examples, see: (a) Bull, M. S.; Sullan, R. M. A.; Li, H.; Perkins, T. T. *ACS Nano* **2014**, *8*, 4984. (b) Kim, B.-H.; Palermo, N. Y.; Lovas, S.; Zaikova, T.; Keana, J. F. W.; Lyubchenko, Y. L. *Biochemistry*, **2011**, *50*, 5154. (c) Dougan, L.; Ainavarapu, S. R. K.; Genchev, G.; Lu, H.; Fernández, J. M. A. *ChemPhysChem* **2008**, *9*, 2836. (d) Wittia, A. P.; Ainavarapu, S. R. K.; Huang, H. H.; Fernández, J. M. *Proc. Natl. Acad. Sci. USA* **2006**, *103*, 7222.

[49] (a) Brown, C. L.; Craig, S. L. *Chem. Sci.* **2015**, *6*, 2158. (b) Gossweiler, G. R.; Kouznetsova, T. B.; Craig, S. L. *J. Am. Chem. Soc.* **2015**, *137*, 6148. (c) Wang, J.; Kouznetsova, T. B.; Kean,

Z. S.; Fan, L.; Mar, B. D.; Martínez, T. J.; Craig, S. L. *J. Am. Chem. Soc.* **2014**, *136*, 15162. (d) Wu, D.; Lenhardt, J. M.; Black, A. L.; Akhremitchev, B. B.; Craig, S. L. *J. Am. Chem. Soc.* **2010**, *132*, 15936.

# Chapter 2. Flex Activation of Oxanorbornadiene Mechanophores[1,2]

## Section 1: Introduction

### *2.1.a "Flex" versus "Stretch" Activation*

A unifying theme in mechanophore designs aimed at bond scission remains an intuitive approach in which the bonds to be broken are integral components of the polymer main chains, and elongated in accordance with the general force vectors being applied to the flanking polymer segments. An exciting possibility would be the use of polymer scaffolds to effect mechanochemical activation of bonds that were neither components of the main chain nor directly elongated by the tensile force within the polymer backbone.[1] This mode of reactivity could enable release of small molecules from side chains while preserving overall macromolecular structure, and provide new fundamental knowledge on how mechanical force can be coupled with chemical potential.

To investigate, we considered the effects of bond angle distortions for in modulating chemical reactivity. Geometric distortions can greatly influence reactivity and ground state hybridization, as observed in contemporary approaches toward Cu-free azide-alkyne cycloaddition and more traditional variations in, for example, carbonyl stretching frequencies in cyclic ketones of varying ring size.[2] Mechanical activation of isolated small organic and inorganic molecules, metals and metalloids, and molecular dopants within polymer matrices has been intensely studied. In many instances, activation by shearing can occur via bond bending motions that augment ground state geometries and lower HOMO-LUMO energy gaps.[3–5]

[1] Reproduced with permission from Larsen, M. B.; Boydston, A. J. "Flex-Activated Mechanophores: Using Polymer Mechanochemistry to Direct Bond Bending Activation" *J. Am. Chem. Soc.* **2013**, *135*, 8189. Copyright 2013 American Chemical Society.

[2] Reproduced with permission from Larsen, M. B.; Boydston, A. J. "Successive Mechanochemical Activation and Small Molecule Release in an Elastomeric Material" *J. Am. Chem. Soc.* **2014**, *136*, 1276. Copyright 2014 American Chemical Society.

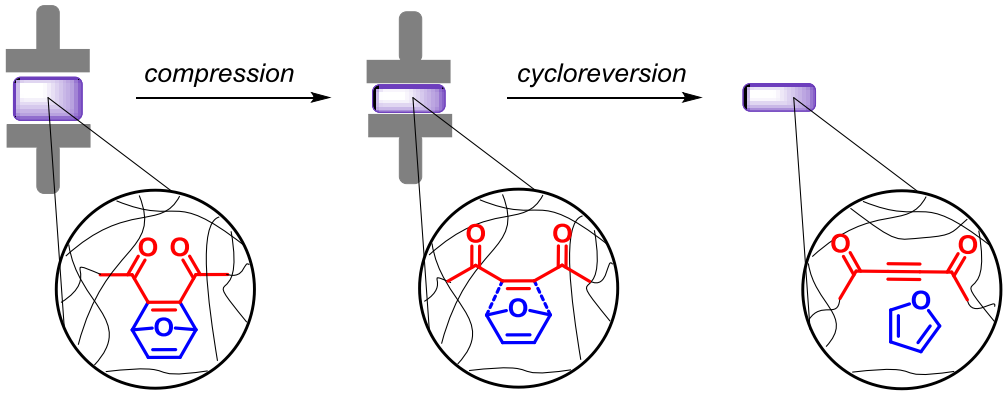


**Figure 2.1**. Generalized depiction of mechanophore activation via bond "flexing" motions induced by application of force.

Recently, application of pressure to a polymer matrix doped with small molecule mechanophores was found to catalyze mechanochemical isomerization. In this system, as opposed to ground state destabilization, a negative activation volume for the reaction lead to an overall lowering of the activation energy with increasing pressure.[6] In contrast, polymer mechanochemistry utilizes the macromolecular scaffold to precisely direct force vectors to a covalently attached mechanophore. Using this approach to accomplish activation primarily through transient bond angle distortions, however, has not been fully investigated.

Application of stress causes a combination of conformational changes as a polymer chain is elongated, including both bond stretching and bending. In most cases, changes in bond angles require less energy than bond stretching, and thus utilizing bending motions that occur during application of stress to a polymer may provide an overall more efficient means of energy transduction. We envisioned "flex-activation" could occur in reactions in which structural changes were consistent with linearization that occurs during polymer elongation. An example of such reactivity would be cycloreversion reactions that convert main chain alkene moieties into alkyne groups (Figure 2.1). Notably, although the internuclear distance of the vinylic atoms

would be lengthened in the overall transformation, the covalent bonds in the mechanophore that are located along the polymer main chain actually become shorter and stronger.

*2.1.b Multiple Activation Cycles in Polymer Mechanochemistry*

One limitation of most mechanoresponsive materials that have been demonstrated is that a single application of stress sufficient for mechanochemical activation results in macroscopic failure or permanent plastic deformation, thus irreversibly altering the material or precluding additional cycles of mechanochemical transduction. One exception, recently reported by Craig and coworkers,[7] involved mechanochemical activation of gem-dihalocyclopropanes embedded within poly(butadiene).[8] Compression of the material up to twelve times resulted in a linear increase in the % activation of mechanophores, ultimately reaching 2.8%. Additional studies to correlate the load history and extent of mechanochemical activation, combined with a mechanophore able to release small molecules could enable advancements in drug delivery, catalysis, sensory materials, and self-healing systems. Challenges to developing such materials include the need to balance the force required to activate the mechanophore with that which results in macroscopic failure, and the incorporation of a mechanophore that can release the desired small molecules. Thus, we consider the primary design components of a mechano-responsive release platform to be a) minimal change in the mechanical and material properties of the bulk matrix upon application of sufficient force; and b) release of the desired species in a manner that does not inherently degrade the macromolecular architecture.

Our initial studies of the flex-activated oxanorbornadiene centered on examination of the mechanochemical activity of the system within crosslinked poly(methyl acrylate) (PMA) networks (See Section 2.2a). Unfortunately, the compressive force necessary for

mechanochemical transduction led to macroscopic failure of the sample. As a result, the amount of activated mechanophore was limited to that achieved in a single compression, and the relative inability of the polymer matrix to withstand mechanochemically-relevant pressures limits its use in practical applications. Adaptation of this system to an elastomeric scaffold able to recover its initial shape after experiencing forces necessary for activation would enable multiple compression-activation cycles, thereby increasing the conversion of mechanophores in a dose-responsive fashion.

## Section 2: Results and Discussion

### *2.2.a Activation in Crosslinked Poly(methyl acrylate)*

To model the effect of force upon the oxonorbornadiene architecture, we conducted a modified version of the CoGEF (Constrained Geometries Simulate External Force) method developed by Beyer and recently demonstrated to be in good agreement with empirical reactivity of mechanophores.[9–11] Briefly, this method entails incremental distortions of the molecule along

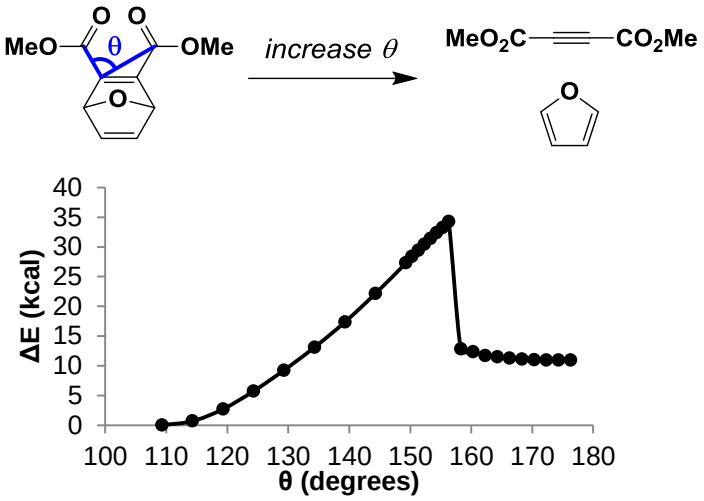


**Figure 2.2**. Calculated potential energies (kcal/mol) resulting from incremental increase in the angle θ. Density functional theory (DFT) calculations were performed at the B3LYP 6-31G* (d) level of theory using the Gaussian program package.

a specified coordinate, which upon relaxation of the rest of the molecule models the effects of mechanical force. As a simplified version of our experimental mechanophore, we applied this method to the oxanorbornadiene Diels-Alder adduct of furan and dimethylacetylene dicarboxylate (DMAD). To mimic linearization of the ene diester moiety, the angle (θ) indicated in Figure 2.2 was incrementally increased relative to the ground state geometry.[12,13] As can be seen in Figure 2.2, an expected increase in the calculated potential energy of the mechanophore was observed until a point at which cycloreversion occurred spontaneously. The ΔE just prior to cycloreversion corresponds to an estimated activation energy ($E_a$) of 35 kcal/mol for the mechanochemical reaction. Importantly, this $E_a$ value is well within the established range of mechanochemically-accessible pathways.

Encouraged by the computational results, we prepared two types of crosslinked networks each comprising oxanorbornadiene mechanophores (Scheme 2.1): one in which the mechanophore was used as a crosslinking unit that would experience extensional force upon application of stress, and another in which the mechanophore was adsorbed into a crosslinked material. Diol **1** was prepared from acetylene dicarboxylic acid and 1,6-hexanediol via Fischer esterification. Benzyl furfuryl ether (**2**) was chosen as the diene in place of furan to avoid issues of volatility with the latter. Diol **1** and furan **2** reacted smoothly via [4+2] cycloaddition to provide the corresponding oxanorbornadiene (not shown) in moderate yield. Subsequent reaction with methacryloyl anhydride furnished difunctionalized crosslinker mechanophore **3**. Formation of crosslinked network **4-CL**, in which the mechanophore serves as the crosslinking unit, was prepared according to a procedure previously reported by Moore and coworkers.[14] For comparison, we also prepared a mechanophore (**5**) incapable of functioning as a crosslinking unit during acrylate polymerization. For this control system, 1,6-hexanediol dimethacrylate (**6**) was

**Scheme 2.1**. Synthesis of network with mechanophore crosslinking units (**4-CL**), and control network with adsorbed mechanophore units (**4-ads**).

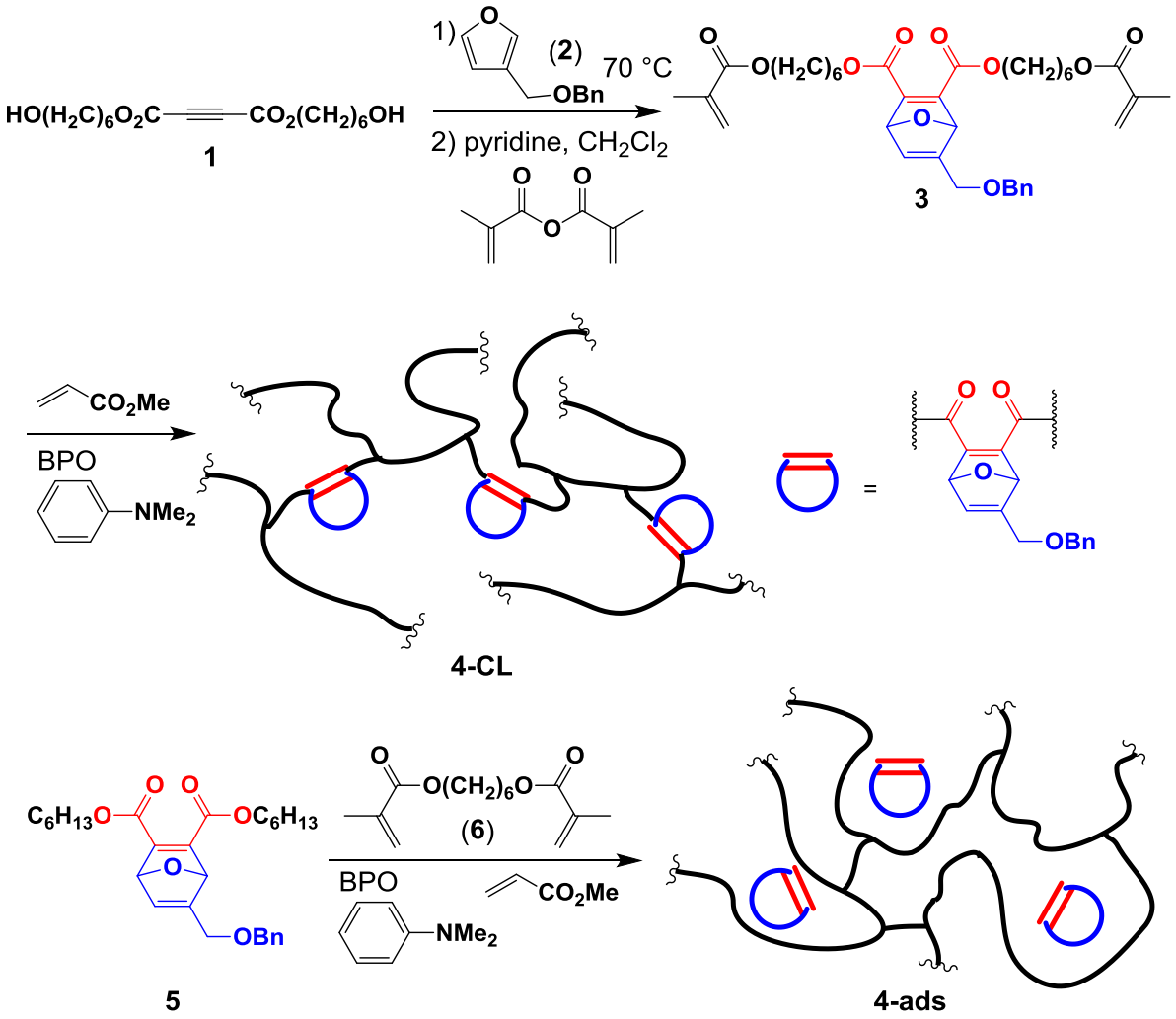


used as a crosslinker to ultimately provide a material in which the oxanorbornadiene mechanophore was adsorbed into the matrix, but not covalently attached (**4-ads**). Copolymerization of a monoacrylate variant of **3** and methyl acrylate in the presence of benzoyl peroxide (BPO) and N,N-dimethylaniline confirmed the stability of the mechanophore under the polymerization conditions (see Experimental).

After polymerization and crosslinking had ensued, each network was soaked in $CH_2Cl_2$ or MeOH for 2-hour cycles to remove unincorporated small molecules. Multiple soak cycles

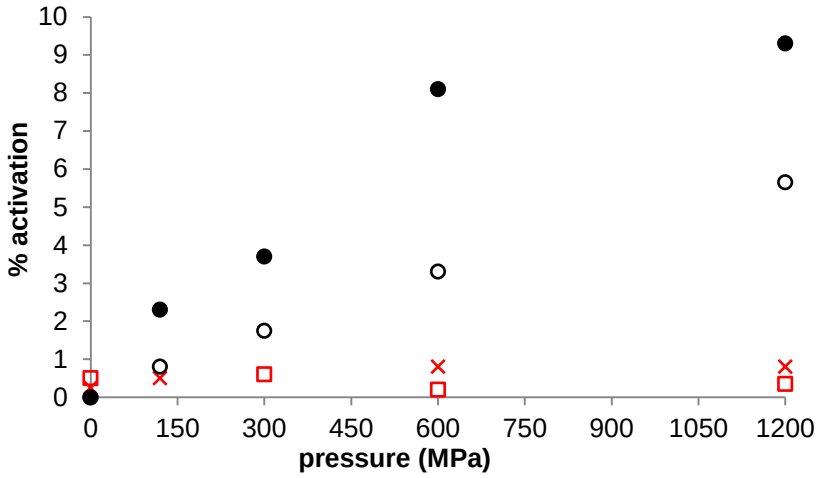


**Figure 2.3.** Plot of applied pressure versus activation of mechanophore, as judged by GC/MS analysis of soak solutions after compression of 4-CL with 14 mol% 3 (●), 4-CL with 5 mol% 3 (○), 4-ads with 17 mol% 5 and 19 mol% 6 (×), and 4-ads with 7 mol% 5 and 11 mol% 6 (□). Each data point is an average of two independent compression experiments.

were conducted until no additional small molecules were detected in the solution, as judged by GC-MS. The amount of **3**, **5**, and **6** in the combined soak solutions were each quantified and used to infer the amount of each species that was incorporated into the crosslinked networks. By adjusting the feed ratios of the reactants, we prepared samples of **4-CL** with estimated mechanophore/crosslinker (**3**) compositions of ca. 5 and 14 mol%. Similarly, samples of 4-ads were prepared and determined to contain 17 mol% mechanophore (**5**) and 19 mol% crosslinker (**6**); a **4-ads** network of lower mechanophore and crosslinker composition was also prepared, containing 7 and 11 mol% of each component, respectively.

To evaluate the mechanochemical reactivity of each network, we conducted compression experiments of each sample at different pressures. Samples were loaded into a Carver press and subjected to a sustained pressure as indicated in Figure 2.3. After 30 min of sustained stress, the sample was placed in $CH_2Cl_2$ to facilitate diffusion of released small molecules. The $CH_2Cl_2$ solutions were then analyzed by GC-MS, and NMR spectroscopy. The GC-MS method was optimized such that analysis of solutions containing **3** and **5** would not result in false positive

detection of **2**. Without applied stress, no furan was observed in the soak solution, indicating to us that no background amount of furan was released due to, for example, mechanochemical activation upon swelling or inadvertent physical adsorption during synthesis. Over the range of 0 to 1200 MPa of applied pressure, we observed a monotonic increase in the % activation of the crosslinked mechanophore for both samples of **4-CL**. While the same trend was observed for **4-CL** containing 5 and 14 mol% of mechanophore **3**, greater activation was observed from the network having a greater density of **3**. These results support a non-thermal activation mechanism, since thermal effects would be expected to influence reactivity to the same extent in the two different variants of **4-CL**. Additionally, compression of **4-CL** for 1 min at 600 MPa gave essentially the same % activation (3.0%) as a 30-min compression (3.3%), consistent with mechanical activation mechanisms.[7] Importantly, compression and analysis of each **4-ads** sample resulted in little or no activation at each pressure, further supporting the mechanochemical origins of the cycloreversion reaction. These results suggested to us that released amounts of **2** detected in compression experiments could not be attributed to thermal or pressure-induced activation.

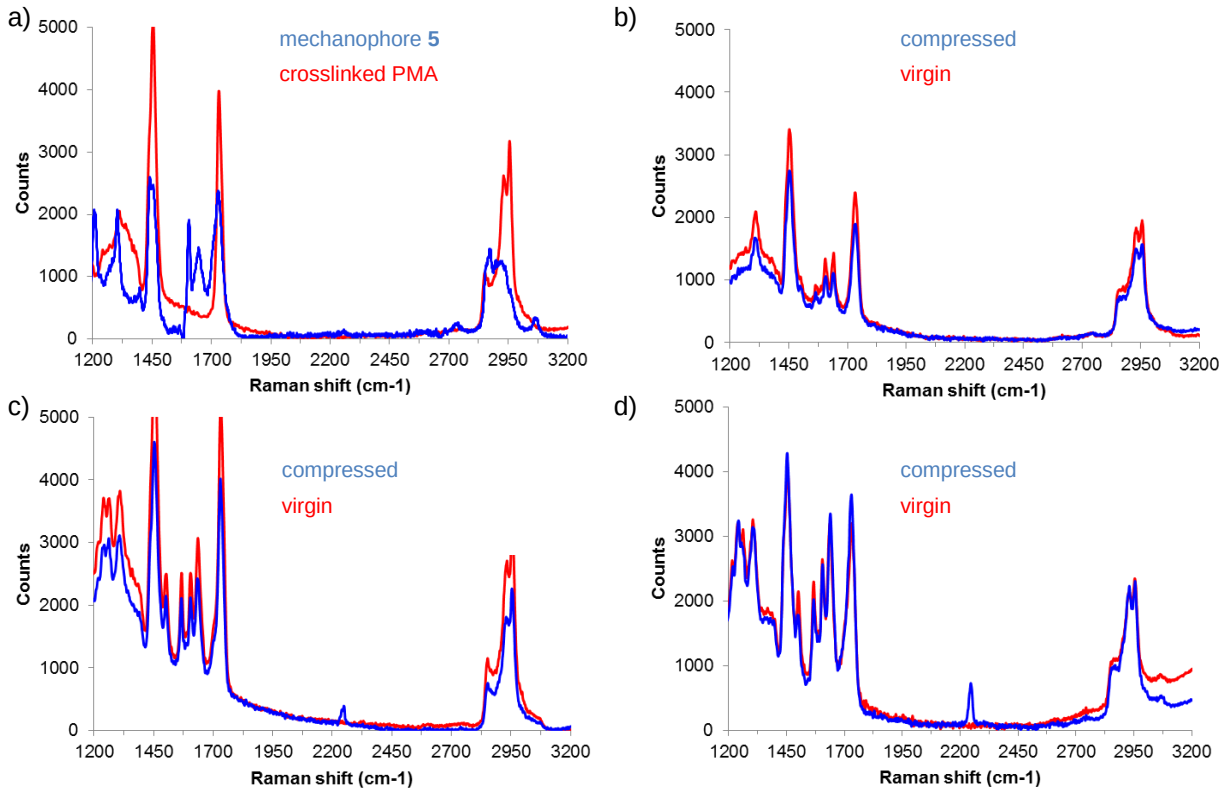


**Figure 2.4**. Raman spectra on HOPG of (a) control mechanophore **5** and crosslinked PMA absent any mechanophore; (b) network **4-ads** (17 mol% **5**) before and after compression at 1200 MPa for 30 min; (c) **4-CL** (5 mol% **3**) before and after compression at 1200 MPa for 30 min; and (d) **4-CL** (14 mol% **3**) before and after compression at 1200 MPa for 30 min. $\lambda_{ex}$ = 785 nm.

Additional support for the proposed origin of **2** was obtained via confocal Raman spectroscopy (Figure 2.4). Control mechanophore **5** and PMA crosslinked via incorporation of **6**, but without any mechanophore, are shown in the top spectrum for reference. Prior to compression, the Raman spectrum of each **4-CL** sample shows only signals consistent with the mechanophore and polymer network. After compression at 1200 MPa, each sample of **4-CL** displayed a new band at ca. 2250 $cm^{-1}$, consistent with known stretching frequencies of acetylene dicarboxylates. This indicated to us that cycloreversion with concomitant alkyne formation as the likely origin of **2**, consistent with computational predictions and envisioned flex-activation.

Raman spectra of **4-ads** before and after compression at 1200 MPa were essentially indistinguishable from one another, and no alkyne formation was apparent.

*2.2.b Multiple Activation Cycles in Elastomeric Polyurethane*

To obtain a material with a lower elastic modulus than the crosslinked PMA networks previously employed, we incorporated the flex activated mechanophore into an elastomeric segmented polyurethane network. These networks comprise flexible polyether segments joined by short, hard diisocyanates and diol chain extenders, resulting in the phase separation between hard and soft segments responsible for their superior strength and elasticity.[15] Toward this end, diol **7** was first reacted with an excess of methylene diphenyldiisocyanate (MDI) to form a diisocyanate-capped mechanophore (Scheme 2.2). Polymerization and crosslinking was effected via addition of dihydroxy-terminated poly(ethylene glycol) and triol **8** to the reaction mixture, resulting in full gelation of the network within 48 h. After curing at 30 °C, solid materials were obtained with a mechanophore concentration of 6.7 wt% (0.13 mmol of mechanophore **7** per gram of material), based upon the feed ratios. Comparison of analogous non-crosslinked (i.e.,

**Scheme 2.2**. Synthesis of polyurethane networks.

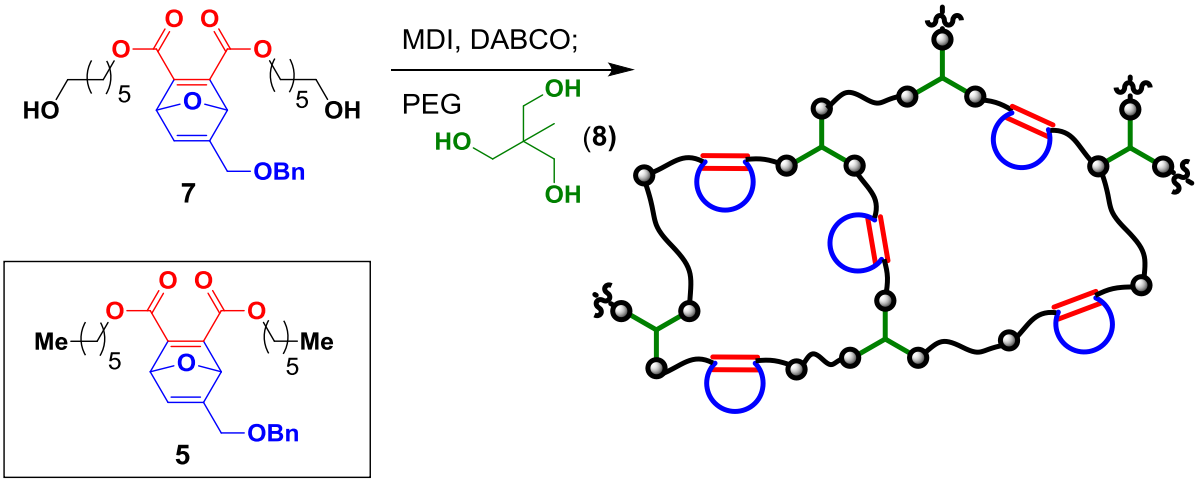

linear polymers) systems revealed excellent mechanophore stability during polymerization and curing (see Experimental). A control system was also prepared, in which mechanophore chain extender **7** was replaced by inert 1,6-hexanediol and mechanophore **5** was physically adsorbed into the material, thus enabling determination of the mechanical (as opposed to thermal or pressure-induced) activation.

The mechanochemical reactivity of each network cured at 30 °C was evaluated by subjecting each to compression in a hydraulic press at sustained pressures as indicated in Figure 2.5. After 1 min of sustained stress, the sample was placed in $CH_2Cl_2$ to facilitate diffusion of released small molecules. The $CH_2Cl_2$ solutions were then analyzed by GC-MS in the presence of an internal standard. Without applied stress, only a small amount of benzyl furfuryl ether was observed in the soak solution, corresponding to activation of roughly 1% of the incorporated mechanophores. As the pressure was increased in each subsequent experiment using fresh samples of the polyurethane material, we observed a monotonic increase in the % activation of

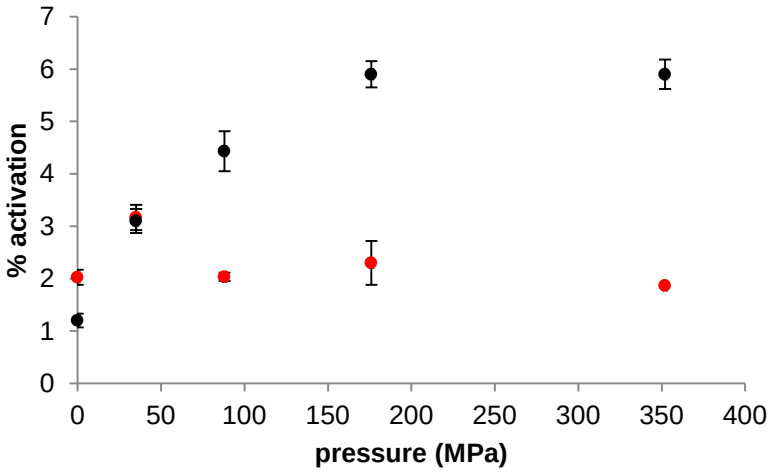


**Figure 2.5**. Plot of applied pressure versus activation of crosslinking (●) and control (●) mechanophore, as judged by GC-MS analysis of soak solutions after compression. Error bars represent standard deviations.

the crosslinked mechanophore up 176 MPa of applied pressure. At higher pressures, we saw consistent % activation but no additional increase. Importantly, the control network only gave ca. 2% activation, and we observed no increase in the % activation with increasing pressure. Collectively, these results confirmed the mechanical origins of the cycloreversion reaction.

We next explored the feasibility of using multiple compressions to achieve iterative increases in the % mechanophore activation from the same sample of material. Samples were compressed at 35 or 88 MPa for 1 min, and pressure was then released and the sample was folded before subjecting to another 1-min compression. The process was repeated for each fresh sample until the target number of compressions was reached, at which point the sample was soaked in $CH_2Cl_2$ and the soak solution analyzed by GC-MS. As shown in Figure 2.6, we observed a discernible positive correlation between the number of compressions and the % activation. The amount gained with each compression began to diminish, which we speculate is likely due to a strain softening effect (see below). When compressed at either 35 or 88 MPa,

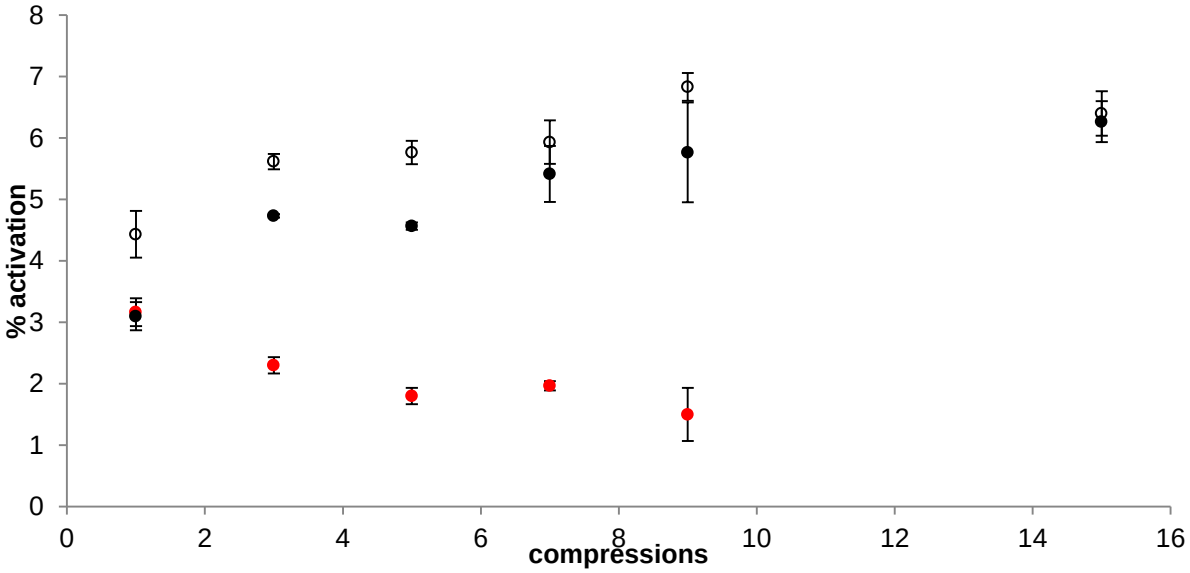


**Figure 2.6**. Plot of % activation of mechanophores versus number of successive compressions (1 min each) at 35 (●) and 88 MPa (○). Control network (●) was compressed at 35 MPa. Error bars represent standard deviations.

increases in activation were apparent up to 9 compression-activation cycles, reaching a maximum of 6 – 7% activation. This suggested to us that once a sufficient load history was imposed to cause this maximum % activation, the material had softened to the extent that additional mechanophore activation could not be achieved. In comparison, however, no increase in % activation was observed for > 1 compression when using the previously reported PMA networks, nor the polyurethane control networks containing **5**.

To investigate the effects of load history on the physical properties of the material, we measured the flexural modulus after increasing numbers of compressions on the same sample.[16] Shown in Figure 2.7 are representative examples of the % of initial flexural modulus versus number of compressions at 35 and 88 MPa. As expected, the material softened more quickly under higher load (88 MPa), reducing to 68% of initial after just one compression. For comparison, at 35 MPa the material retained 68% of its initial flexural modulus for up to nine compressions. In segmented polyurethanes, strain softening is generally attributed to the breakup of hard domains in response to applied force.[17,18] A possible explanation for the observed upper

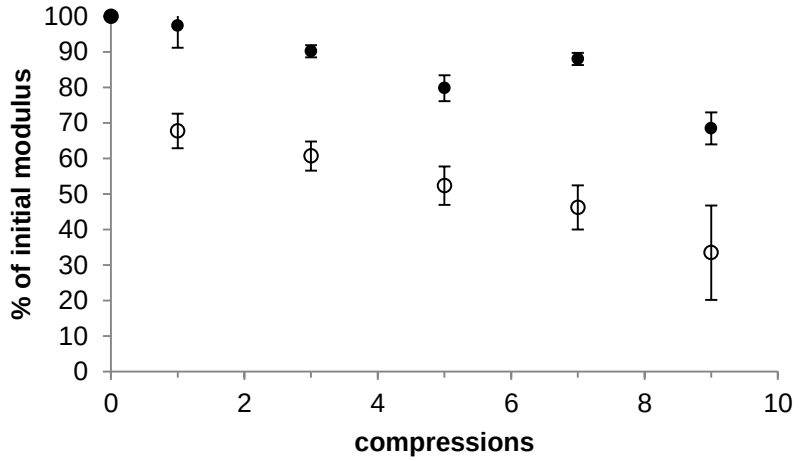


**Figure 2.7**. Changes in measured flexural modulus after compressions at 35 (●) and 88 MPa (○), plotted as percent of modulus of initial, uncompressed material. Error bars represent standard deviations.

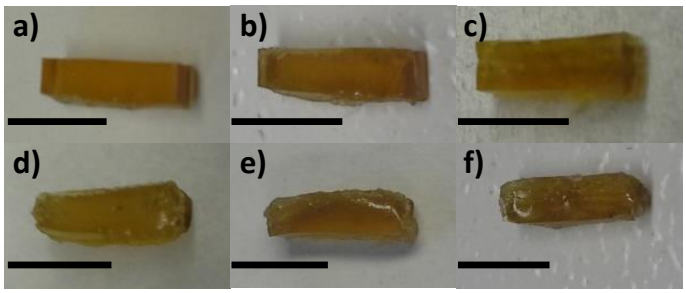


**Figure 2.8.** Polyurethane material after compressions at 35 MPa. Images a) through f) were taken after 0, 1, 3, 5, 7, and 9 compressions, respectively, of the same sample piece. Scale bars = 5 cm.

limit of mechanophore reactivity lies in both random scission of chemical crosslinks and destruction of the physical crosslinks provided by hard domains. As described in Section 2.2.a, the mechanochemical reactivity of the oxanorbornadiene is directly related to crosslink density, and it is possible that the lower limit of crosslink density sufficient for mechanochemical activation has been reached after strain-induced softening by ca. 30%. Despite softening, the material clearly resisted permanent physical deformation, as shown in Figure 2.8. Notably, it has been demonstrated that more efficient mechanochemical activation is associated with plastic deformation of the bulk material,[19,20] a limit not reached under our experimental conditions as judged by the nearly identical physical measurements of samples when subjected to repeated compressions (see Experimental). Thus, the conditions experienced by the mechanophores may not be optimal for reaching high levels of activation, yet sequential increase in small molecule release was still achievable.

*2.2.c Effects of Oxanorbornadiene Substitution on Mechanochemical Transduction*

A convenient feature of the oxanorbornadiene mechanophore is the facile means of quantifying % activation. Particularly in the case of scissile mechanophores, the % activation can be difficult to accurately determine; typically, rates of polymer chain scission are calculated and

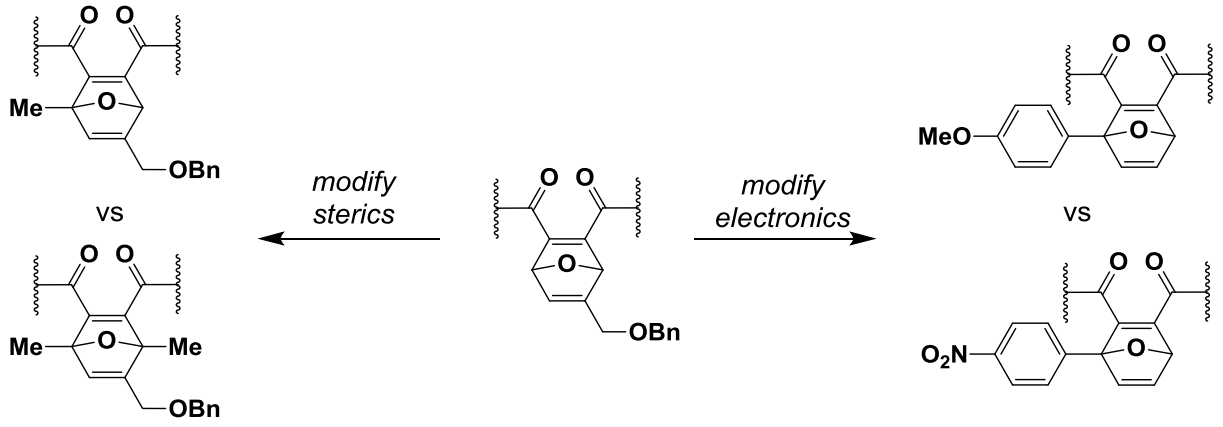


**Figure 2.9**. Potential studies of structure-activity relationships in the mechanochemical activation of oxanorbornadienes.

compared to infer mechanophore reactivity in the place of calculation of precise % activation.[10,21] In contrast, the release of a small molecule enables the rapid, facile detection and quantification of mechanochemical activity. This could enable detailed investigation of the factors affecting the efficiency of mechanochemical transduction in the oxanorbornadiene, and combined with the wide range of substitution patterns available for furans we sought to obtain a set of structure-activity relationships for this mechanophore (Figure 2.9). By comparing the % activation of a series of oxanorbornadienes to, for example, the thermal retrocyclization of the same series, the relationship between the ground state and the force-modified potential energy surface can be better elucidated. While many regio- and stereochemical structure-activity relationships of mechanophores are known,[9,22,23] the discrete modification of a single mechanophore to study both steric and electronic effects is much more rare.[10]

As a starting point, we probed the effect of sterics on the efficiency of mechanochemical transduction in the oxanorbornadiene by introducing a methyl group at the bridgehead. Detailed studies of the structural effects controlling the rate of retro-Diels Alder reactions are sparse; however, studies of anthracene cycloadducts suggest that sterics of the diene play a role in determining the activation barrier of the thermal retrocyclization reaction, albeit a smaller one

than electronics.[24] To investigate, we synthesized the 5-methylated congener of the original benzyl furfuryl ether (see Experimental). We then incorporated the methylated oxanorbornadiene **9** in an elastomeric polyurethane and assessed the mechanochemical reactivity of the network (Scheme 2.3a), using the procedure described in Section 2.2.b. However, none of the desired methylated benzyl furfuryl ether was detected after compression at any pressure tested, up to 352 MPa. A mixed network was also prepared, which contained equimolar amounts of parent diol **7** and **9** (Scheme 2.3b). Upon compression, activation of the parent oxanorbornadiene **7** was observed, along with the expected monotopic increase in % activation with pressure (Figure 2.10). However, again no activation of **9** was detected. Thus, we concluded that bridgehead methylation inactivated the mechanochemical response of the oxanorbornadiene.

**Scheme 2.3**. (a) Synthesis of polyurethane network containing bridgehead-alkylated congener **9**. (b) Synthesis of mixed network containing **7** and **9**.

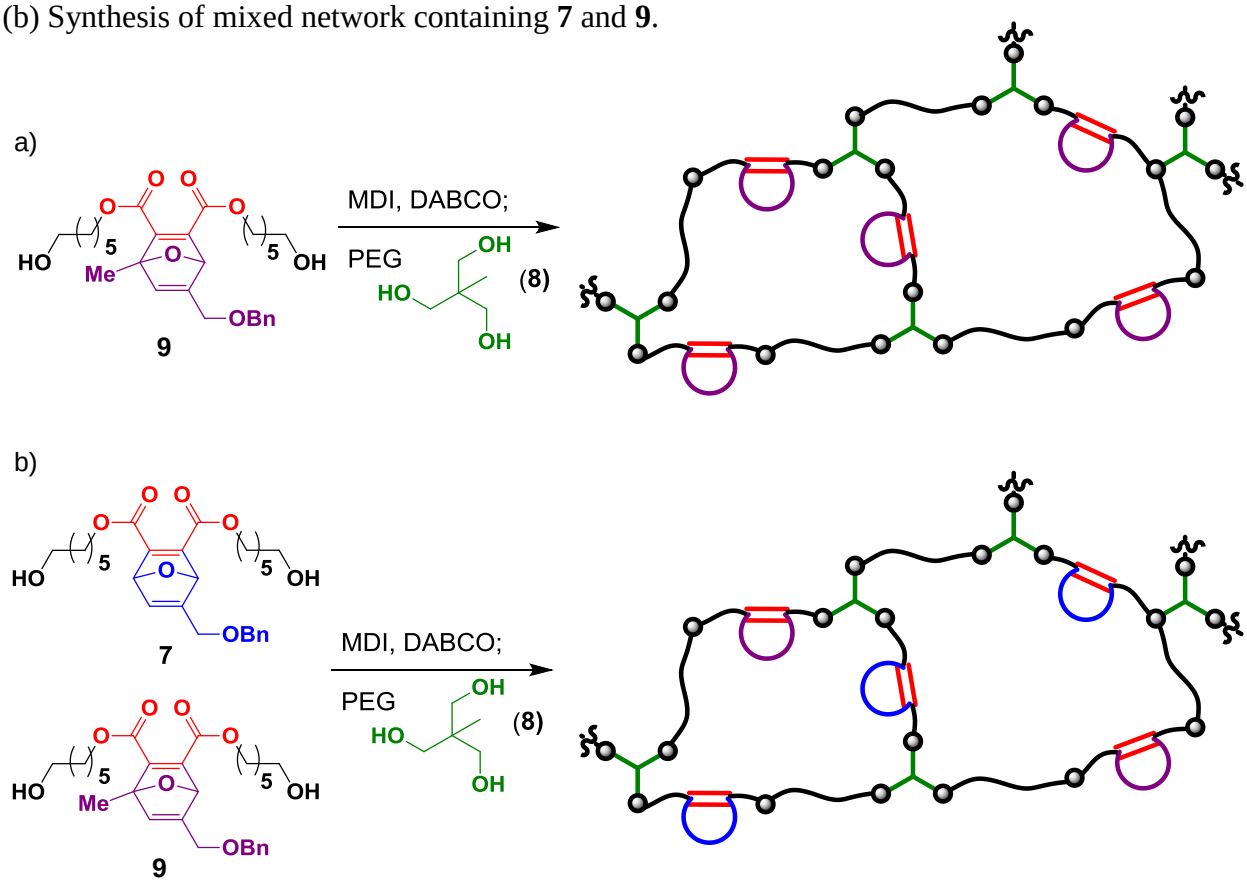

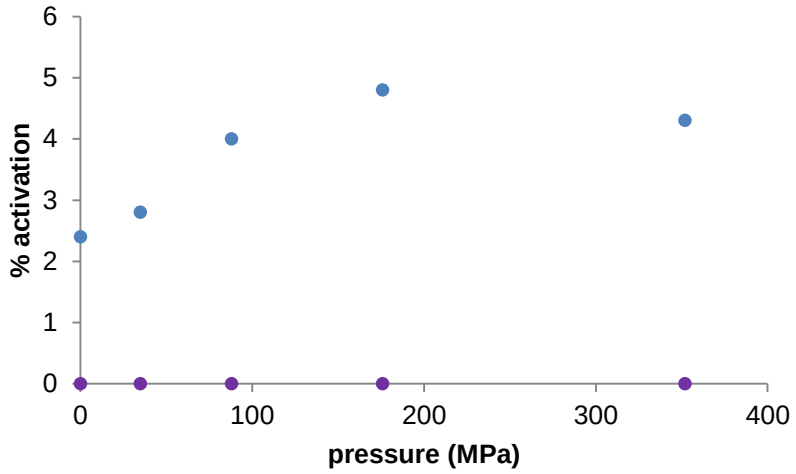


**Figure 2.10**. Plot of applied pressure versus activation of oxanorbornadiene **7** (●) and **9** (●), as judged by GC-MS analysis of soak solutions after compression.

The cause does not appear to be a higher intrinsic activation barrier to the retrocyclization reaction. Thermolysis of small molecule adducts of the parent and methylated oxanorbornadienes showed similar rates of thermal decomposition ($1.96 \times 10^{-5}$ $s^{-1}$ and $4.03 \times 10^{-5}$ $s^{-1}$ for the parent and methylated congeners, respectively). As the ground state potential energy surface (PES) does not appear to be intrinsically biased against retrocyclization, the answer must lie in a perturbation particular to the force-modified PES. A potential explanation may be a rotation out of conjugation of the ester group proximal to the bridgehead methyl of the oxanorbornadiene. This may then require more mechanical deformation to reach the transition state, i.e. an additional dihedral rotation. IR spectroscopy shows a slight difference in the carbonyl stretching frequencies between the parent and methylated oxanorbornadienes in the ground state (1719 $cm^{-1}$ and 1724 $cm^{-1}$, respectively). In addition, $^{13}C$ NMR of the methylated oxanorbornadiene congener shows two distinct carbonyl resonances (δ 165.0, 162.9), with one signal appearing downfield from the corresponding resonance in the parent oxanorbornadiene (δ 163.3). These observations are consistent with a decrease in conjugation in the carbonyl pi orbitals of the

methylated congener, manifested as an out-of-plane dihedral rotation. Additional computational investigations are currently underway to more completely elaborate the role of steric encumbrance in the flex activation of oxanorbornadienes.

**Section 3: Conclusions**

In summary, we have demonstrated a fundamentally unique mechanochemical transduction process in mechanophores that undergo scission along bonds that are not components of the elongated polymer main chain, resulting in a net strengthening of the bonds in the polymer backbone. A unique aspect of the design is the use of the macromolecular scaffold to direct activation by means of bond bending induced by mechanical stress on the material. This "flex activation" method has been supported through experimental and computational studies. An exciting feature of these materials is their ability to undergo mechanochemical transduction to release small molecules capable of diffusing out of the polymer matrix. We anticipate that the successful development of flex-activated mechanophores will open a new avenue for the investigation of materials that respond to physical stimulus, both from the standpoint of mechanophore design and in the incorporation of these structures in advanced functional materials.

Additionally, we have demonstrated the ability to use elastomeric polyurethane scaffolds combined with a flex-activated mechanophore to achieve force-activated release of small molecules over multiple load cycles. Mechanical analysis of the compressed material revealed the ability of the bulk polymer matrix to maintain its elasticity and shape after the application of force sufficient for mechanophore activation. This advancement is an important step toward realizing force-coupled capabilities, including reloadable sensory materials, refillable reservoirs

of therapeutics or catalysts, and composites capable of healing fractures from repeated, low-level stresses.

Preliminary investigations of structural factors affecting the mechanochemical transduction of oxanorbornadienes have revealed that subtle changes in the structure have the ability to greatly impact chemomechanical coupling. In contrast to thermal retrocyclization, the addition of a methyl substituent at the bridgehead position completely deactivates the ability of the mechanophore to undergo flex activation. While the precise origin of this effect is currently unknown, it suggests a perturbation particular to the force-modified PES, rendering flex activation inaccessible to even moderately sterically encumbered oxanorbornadienes.

**Section 4: Experimental**

*General Considerations***.** Dimethylformamide, pyridine, and tetrahydrofuran were obtained from a solvent purification system. $^{1}$H and $^{13}$C NMR spectra were recorded on Bruker AVance 300 MHz or 500 MHz spectrometers. Chemical shifts are reported in delta (δ) units, expressed in parts per million (ppm) downfield from tetramethylsilane using the residual protio-solvent as an internal standard ($CDCl_3$, $^{1}$H: 7.26 ppm and $^{13}$C: 77.0 ppm; DMSO-$d_6$, $^{1}$H: 2.49 ppm and $^{13}$C: 39.5 ppm). GC-MS analysis was performed on a HP 5971A gas chromatograph-mass spectrometer (electron impact ionization). The thermal profile was optimized so as to preclude thermal activation of residual oxanorbornadiene upon injection and/or chromatographic separation. LRMS was performed on a Bruker Esquire equipped with either an electrospray ionization (ESI) or IonSense SVP100 DART source. HRMS was performed by the Department of Chemistry Mass Spectrometry Facility at the University of Washington. Confocal Raman microscopy was performed on a Renishaw inVia Raman microscope at the Nanotech User

Facility in the Molecular Engineering and Sciences Institute at the University of Washington. Mechanical analysis was performed with a Perkin Elmer DMA 7e Dynamic Mechanical Analyzer. IR spectroscopy was performed with a Perkin Elmer Spectrum RX I FTIR spectrometer. All reagents and solvents were obtained from commercial sources and used as received unless otherwise specified.

***2.4.****a Experimental for Activation in Crosslinked Poly(methyl acrylate)*

**Scheme 2.4**. Synthesis of small molecule components.

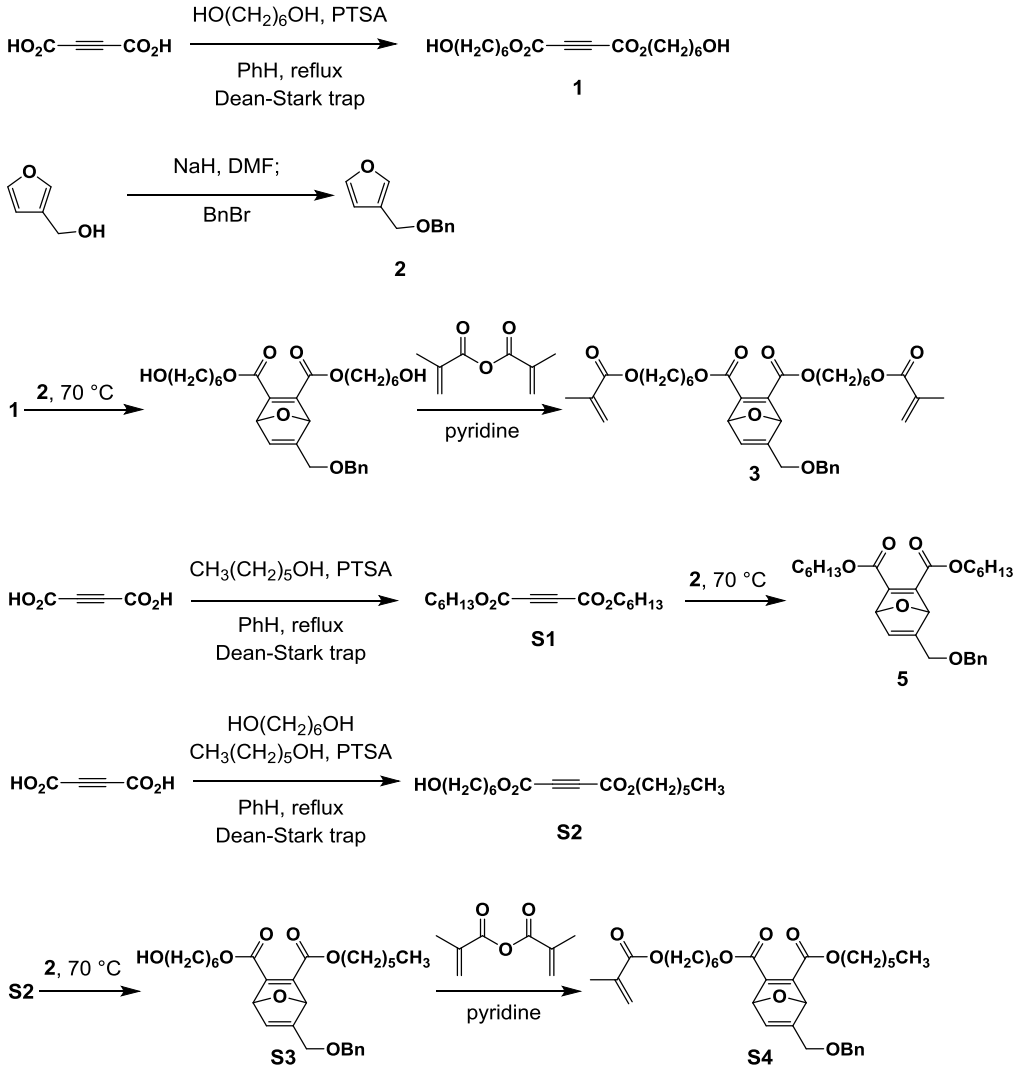

Preparation of **1**. Acetylene dicarboxylate (5.0 g, 43.8 mmol), 1,6-hexanediol (52 g, 438 mmol), and *p*-toluenesulfonic acid monohydrate (833 mg, 4.38 mmol) were dissolved in benzene (70 mL). The reaction flask was equipped with a reflux condenser fitted with a Dean-Stark trap and heated at 100 °C. After 20 h, ca. 1.5 mL of water had collected in the trap. The solution was removed from heat and once at room temperature, diluted with $Et_2O$ (50 mL), and then cooled to -10 °C for 1 h. The solution was decanted and the solids rinsed with additional portions of $Et_2O$. The combined organic layers were washed successively with saturated $NaHCO_3$ solution (2 × 50 mL), water (4 × 50 mL), and brine (1 × 50 mL). The organic layer was dried with $MgSO_4$, filtered through a thin pad of Celite, and concentrated under reduced pressure yielding **1** as a pale yellow oil (8.79 g, 64%). $^1$H NMR (300 MHz, $CDCl_3$) δ 4.17 (t, *J* = 6.6 Hz, 4H), 3.58 (t, *J* = 6.5 Hz, 4H), 1.71 – 1.57 (m, 4H), 1.52 (m, 4H), 1.41 – 1.28 (m, 8H). $^{13}$C NMR (126 MHz, $CDCl_3$) δ 152.0, 128.3, 74.7, 67.0, 32.5, 28.3, 25.6, 25.3. LRMS (DART): $[M+H]^+$ calcd for $C_{16}H_{27}O_6$, 315.18; found 314.9.

Preparation of **2**. To a solution of 3-furfuryl alcohol (4.14 g, 42.1 mmol) in dry DMF (80 mL) under $N_2$ atmosphere was added NaH (1.52 g, 63.2 mmol). After 30 min, benzyl bromide (5.51 mL, 46.4 mmol) was added and the reaction mixture was stirred at room temperature and monitored by TLC (15% EtOAc/hexanes). After 6 h, the solution was opened to air and the excess NaH was consumed via dropwise addition of water (50 mL). The solution was extracted with hexanes (4 × 30 mL) and the combined organic layers rinsed with brine (1 × 40 mL). The solution was dried with $MgSO_4$, filtered through a thin pad of Celite, and concentrated under reduced pressure. The crude product was purified by eluting through a silica gel plug (15% EtOAc/hexanes) to yield **2** as a pale yellow liquid (7.73 g, 98%). $^1$H NMR (300 MHz, $CDCl_3$) δ

7.45 – 7.26 (m, 7H), 6.45 (d, *J* = 0.8 Hz, 1H), 4.54 (s, 2H), 4.43 (s, 2H). $^{13}$C NMR (75 MHz, $CDCl_3$) δ 143.4, 140.8, 138.3, 128.5, 127.9, 127.7, 110.5, 71.9, 63.4. LRMS (EI) $[M]^+$ calcd for $C_{12}H_{12}O_2$ 188.08; found 188.1. Spectral data were consistent with previously reported values.[25]

Preparation of **3**. Compounds **1** (3.5 g, 11.1 mmol) and **2** (2.31 g, 12.2 mmol) were combined in a sealed vial and heated at 70 °C. The reaction progress was monitored via $^1$H NMR spectroscopy. After 18 h, nearly full conversion of **2** was achieved. The reaction mixture was removed from heat and triturated with hexanes (3 × 15 mL) to remove excess unreacted starting materials. Residual solvent was removed under reduced pressure to yield the intermediate diol as an orange oil (4.86 g, 87%).

To a solution of the intermediate diol (298 mg, 0.59 mmol) in dry pyridine (5 mL) under $N_2$ atmosphere was added methacrylic anhydride (660 µL, 4.4 mmol). The solution was stirred at room temperature and monitored via TLC (85% EtOAc/hexanes). After 18 h, the reaction was diluted with $Et_2O$ (10 mL) and washed successively with water (2 × 10 mL), 10 wt% $CuSO_4$ solution (3 × 10 mL), and saturated $NaHCO_3$ solution (2 × 10 mL). The organic layer was dried with $MgSO_4$, filtered, and the solvents removed under reduced pressure. The crude product was purified by column chromatography (20% EtOAc/hexanes) to yield **3** as a pale yellow oil (54 mg, 14%). $^1$H NMR (500 MHz, $CDCl_3$) δ 7.38 – 7.27 (m, 5H), 6.92 (s, 1H), 6.08 (s, 2H), 5.65 (s, 1H), 5.59 (s, 1H), 5.54 (s, 2H), 4.55 (d, *J* = 11.9 Hz, 1H), 4.46 (d, *J* = 11.9 Hz, 1H ), 4.32 (s, 2H), 4.22 – 4.08 (m, 8H), 1.93 (s, 6H), 1.76 – 1.58 (m, 8H), 1.47 – 1.30 (m, 8H). $^{13}$C NMR (126 MHz, $CDCl_3$) δ 167.5, 162.9, 156.0, 153.0, 152.7, 137.8, 137.0, 136.5, 128.4, 127.8, 127.7, 125.3, 85.9, 85.6, 72.5, 66.1, 65.4, 64.5, 28.5, 28.4, 25.7, 25.5, 18.4. LRMS (DART): $[M+NH_4]^+$

calcd for $C_{36}H_{50}NO_{10}$, 656.34; found 656.3. HRMS (ESI): $[M+H]^+$ calcd for $C_{36}H_{47}O_{10}$, 639.3169; found 639.3192.

Preparation of **4-CL**. In a screw cap vial under $N_2$ atmosphere, compound **3** (64 mg, 0.10 mmol) and recrystallized benzoyl peroxide (4.8 mg, 0.02 mmol) were dissolved in freshly distilled methyl acrylate (0.11 mL, 1.25 mmol). *N*,*N*-Dimethylaniline was added (2.5 µL, 0.02 mmol) and the vial was sealed with a Teflon-lined screw cap and immediately transferred to a freezer (-10 °C). After 40 h, the vial was opened and $CH_2Cl_2$ (5 mL) was added. After 1 h, the solution was decanted and replaced with a fresh portion of $CH_2Cl_2$, and the soaking process repeated until no reactants were observed by GC. The remaining solids were dried on a Schlenk line to yield **4-CL** as a rubbery orange solid (118 mg). The final loading of **3** within the polymer network was determined via $^1$H NMR analysis of the combined $CH_2Cl_2$ soaking solutions and determined to be 14 mol%.

An analogous procedure using **3** (64 mg, 0.10 mmol), benzoyl peroxide (4.8 mg, 0.02 mmol), methyl acrylate (0.18 mL, 2.0 mmol), and *N*,*N*-dimethylaniline (2.5 µL, 0.02 mmol) yielded **4-CL** with 5 mol% of mechanophore **3** incorporated.

Preparation of **S1**. Acetylene dicarboxylate (1.0 g, 8.76 mmol), hexanol (2.20 mL, 17.5 mmol) and *p*-toluenesulfonic acid monohydrate (167 mg, 0.88 mmol) were dissolved in benzene (15 mL). The reaction flask was equipped with a reflux condenser fitted with a Dean-Stark trap and heated at 100 °C. After 18 h, the solution was removed from heat, diluted with $Et_2O$ (20 mL), and washed successively with saturated $NaHCO_3$ solution (2 × 10 mL) and brine (1 × 10 mL).

The organic layer was dried with $MgSO_4$, filtered through a thin pad of Celite, and concentrated under reduced pressure. The crude product was passed through a silica gel plug eluting with hexanes to yield **S1** as a clear liquid (868 mg, 35%). $^1$H NMR (300 MHz, $CDCl_3$) δ 4.23 (t, *J* = 6.7 Hz, 4H), 1.75 – 1.60 (m, 4H), 1.45 – 1.21 (m, 12H), 0.89 (t, *J* = 6.7 Hz, 6H). $^{13}$C NMR (126 MHz, $CDCl_3$) δ 152.1, 74.9, 67.3, 31.4, 28.4, 25.5, 22.6, 14.1. LRMS (DART): $[M+NH_4]^+$ calcd for $C_{16}H_{30}NO_4$, 300.22; found 299.9.

Preparation of **5**. Compounds **S1** (600 mg, 2.12 mmol) and **2** (400 mg, 2.12 mmol) were combined in a sealed vial and heated at 70 °C. The reaction progress was monitored via $^1$H NMR spectroscopy. After 15 h, nearly full conversion of **2** was achieved. The crude product was purified by column chromatography (10% EtOAc/hexanes) to yield compound **5** as a pale yellow liquid (873 mg, 87%). $^1$H NMR (300 MHz, $CDCl_3$) δ 7.40 – 7.27 (m, 5H), 6.93 (dd, *J* = 3.6, 1.8 Hz, 1H), 5.66 (t, *J* = 1.7 Hz, 1H), 5.59 (d, *J* = 1.6 Hz, 1H), 4.56 (d, *J* = 11.9 Hz, 1H), 4.47 (d, *J* = 11.9 Hz, 1H) 4.33 (t, *J* = 1.7 Hz, 2H), 4.25 – 4.08 (m, 4H), 1.79 – 1.48 (m, 4H), 1.44 – 1.09 (m, 12H), 0.95 – 0.74 (m, 6H). $^{13}$C NMR (126 MHz, $CDCl_3$) δ 163.04, 163.00, 156.0, 152.8, 152.5, 137.8, 137.0, 128.4, 127.7, 85.9, 85.6, 72.5, 66.1, 65.6, 31.4, 28.5, 25.5, 22.5, 14.0. LRMS (DART): $[M+H]^+$ calcd for $C_{28}H_{39}O_6$, 471.27; found 471.1. HRMS (ESI): $[M+NH_4]^+$ calcd for $C_{28}H_{42}NO_6$, 488.3012; found 488.3013.

Preparation of **4-ads**. In a screw cap vial under $N_2$ atmosphere, compound **5** (47 mg, 0.10 mmol), 1,6-hexanediol dimethacrylate (25 mg, 0.10 mmol) and recrystallized benzoyl peroxide (4.8 mg, 0.02 mmol) were dissolved in freshly distilled methyl acrylate (0.45 mL, 5 mmol). *N*,*N*-Dimethylaniline was added (2.5 µL, 0.02 mmol) and the vial was sealed with a Teflon-lined

screw cap and immediately transferred to a freezer (-10 °C). After 40 h, the vial was opened and MeOH (5 mL) was added. After 1 h, the solution was decanted and replaced with a fresh portion of MeOH, and the soaking process repeated until no reactants were observed by GC. The remaining solids were dried on a Schlenk line to yield **4-ads** as a rubbery orange solid (111 mg). The final loading of **5** and 1,6-hexanediol dimethacrylate within the polymer network were determined via $^1$H NMR analysis of the combined MeOH soaking solutions and determined to be 7 mol% and 11 mol%, respectively.

An analogous procedure using **5** (94 mg, 0.20 mmol), 1,6-hexanediol dimethacrylate (51 mg, 0.20 mmol), benzoyl peroxide (9.6 mg, 0.04 mmol), methyl acrylate (0.36 mL, 4.0 mmol), and *N*,*N*-dimethylaniline (5.2 µL, 0.04 mmol) yielded **4-ads** with 17 mol% of mechanophore **5** and 19 mol% of crosslinker incorporated.

To confirm the presence of **5** within the network, a 10.3 mg sample (17 mol% **5** according to protocol above) was placed in $CD_2Cl_2$ for 26 h. The solution was then transferred away from the swollen network into an NMR tube containing 1,4-dicyanobenzene as an internal standard. The amount of **5** present in the $CD_2Cl_2$ as determined by $^1$H NMR spectroscopy was 3.2 mg, or 71% of the theoretical amount.

Preparation of **S2**. Acetylene dicarboxylate (5.0 g, 43.8 mmol), 1,6-hexanediol (25.9 g, 219 mmol), hexanol (55 mL, 438 mmol) and *p*-toluenesulfonic acid monohydrate (833 mg, 4.38 mmol) were dissolved in benzene (70 mL). The reaction flask was equipped with a reflux condenser fitted with a Dean-Stark trap and heated at 100 °C. After 20 h, ca. 1.5 mL of water had

collected in the trap. The solution was removed from heat, diluted with $Et_2O$ (50 mL), and cooled to -10 °C for 1 h causing a precipitate to form. The solution was decanted and the solids rinsed with additional portions of $Et_2O$. The combined organic layers were washed successively with saturated $NaHCO_3$ solution (2 × 50 mL), water (4 × 50 mL), and brine (1 × 50 mL). The organic layer was dried with $MgSO_4$, filtered through a pad of Celite, and concentrated under reduced pressure. Excess hexanol was removed from the resulting liquid via vacuum distillation (35 °C, 0.5 torr) and the crude product purified via column chromatography (40% EtOAc/hexanes) to yield **S2** as a yellow oil (5.36 g, 41%). $^1$H NMR (300 MHz, $CDCl_3$) δ 4.25 (t, *J* = 6.5 Hz, 2H), 4.21 (t, *J* = 6.5 Hz, 2H), 3.65 (t, *J* = 6.5 Hz, 2H), 1.79 – 1.52 (m, 6H), 1.47 – 1.24 (m, 10H), 0.89 (t, *J* = 6.7 Hz, 3H). $^{13}$C NMR (126 MHz, $CDCl_3$) δ 151.9, 74.8, 74.6, 67.1, 66.9, 62.7, 32.5, 31.3, 28.2, 28.2, 25.5, 25.33, 25.27, 22.4, 13.9. LRMS (DART): $[M+NH_4]^+$ calcd for $C_{16}H_{30}NO_5$, 316.21; found 316.0.

Preparation of **S4**. Compounds **S2** (2.50 g, 8.4 mmol) and **2** (1.73 g, 9.22 mmol) were combined in a sealed vial and heated at 70 °C. The reaction progress was monitored via $^1$H NMR spectroscopy. After 18 h, nearly full conversion of **2** was achieved. The reaction mixture was removed from heat and triturated with hexanes (3 × 15 mL) to remove excess unreacted starting materials. Residual solvent was removed under reduced pressure to yield the intermediate alcohol (**S3**) as an orange oil (3.20 g, 78%).

To a solution of **S3** (387 mg, 0.76 mmol) in dry pyridine (5 mL) under $N_2$ atmosphere was added methacrylic anhydride (450 µL, 3.0 mmol). The solution was stirred at room temperature and monitored via TLC (85% EtOAc/hexanes). After 18 h, the reaction mixture was diluted with

$Et_2O$ (10 mL) and washed successively with water (2 × 10 mL), 10 wt% $CuSO_4$ solution (3 × 10 mL), and saturated $NaHCO_3$ solution (2 × 10 mL). The organic layer was dried with $MgSO_4$, filtered through a thin pad of Celite, and concentrated under reduced pressure. The crude product was purified by column chromatography (20% EtOAc/hexanes) to yield **S4** as a pale yellow oil (98 mg, 23%). $^1$H NMR (300 MHz, $CDCl_3$) δ 7.38 – 7.27 (m, 5H), 6.93 (d, *J* = 1.8 Hz, 1H), 6.09 (s, 1H), 5.66 (s, 1H), 5.59 (d, *J* = 1.5 Hz, 1H), 5.55 (s, 1H), 4.54 (d, *J* = 11.9 Hz, 1H), 4.46 (d, *J* = 11.9 Hz, 1H ), 4.32 (s, 2H), 4.25 – 4.09 (m, 6H), 1.94 (s, 3H), 1.77 – 1.51 (m, 8H), 1.46 – 1.25 (m, 10H), 0.94 – 0.82 (m, 3H). $^{13}$C NMR (126 MHz, $CDCl_3$) δ 167.5, 162.99, 162.97, 162.92, 162.89, 156.0, 153.0, 152.8, 152.7, 137.8, 137.01, 136.96, 136.5, 128.4, 127.8, 127.7, 125.6, 85.9, 85.6, 72.5, 66.1, 65.6, 65.4, 64.6, 31.4, 28.53, 28.49, 28.47, 28.4, 25.7, 25.5, 22.5, 18.4, 14.0. LRMS (ESI): $[M+H]^+$ calcd for $C_{32}H_{43}O_8$, 555.30; found 555.3.

*General procedure for compression studies.* A sample of polymer network (approx. 15 mg) was loaded into a KBr pellet press and pressure applied via a Carver laboratory press with attached manometer. The sample was compressed at the desired pressure (calculated by dividing load by area of the pellet press surface, 6.34 mm radius) for 30 min. The sample was transferred to a vial containing $CH_2Cl_2$ and a known concentration of 1,3,5-trimethoxybenzene as internal standard. After 2 h, a sample of the soak solution was analyzed via GC-MS and the % activation determined by dividing the observed furan (**2**) by the total amount present in the polymer sample (determined as mol% in the original synthesis; see above).

*CoGEF analysis of mechanophores***.** Density functional theory (DFT) calculations were performed at the B3LYP 6-31G* (d) level of theory using the Gaussian 09 program package. To

simulate the effects of bond angle deformation on the oxanorbornadiene, relaxed PES scans were performed. Starting from the equilibrium geometry, the angle highlighted (Fig. 2.11) was increased incrementally by 5° (1° near the $E_a$ of the retro-Diels Alder reaction) and constrained while optimizing the geometry of the rest of the molecule. This angle was chosen so as to utilize a single internal coordinate in the system capable of capturing the envisioned bending motion of each half of the dienophile. At the onset of the cycloreversion reaction, optimization of the resulting geometry of the cycloreversion products failed. Thus, an estimation of the $E_a$ was obtained from the last successfully optimized structure obtained from the PES scan. The unoptimized cycloreversion products were then utilized as starting points for a new PES scan along the same internal coordinate, providing a simulation of the effects of further deformation upon the resulting alkyne.

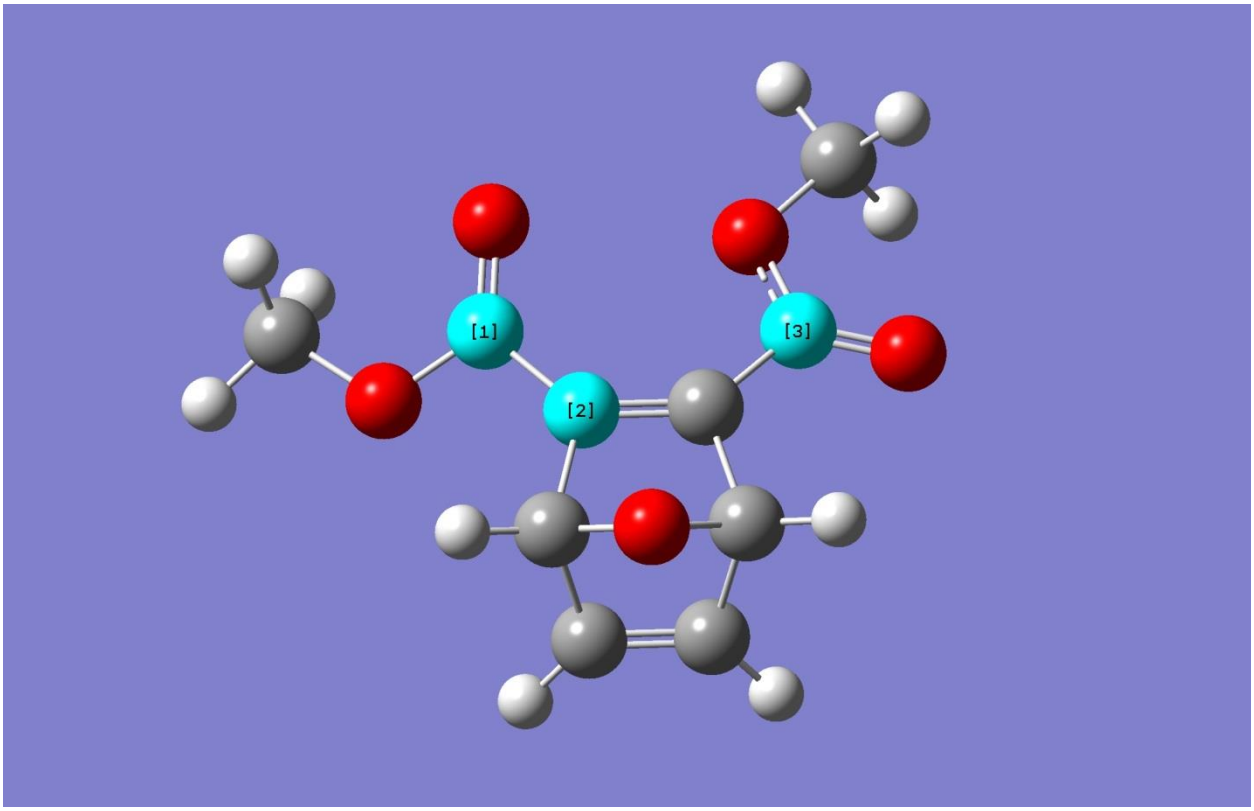


**Figure 2.11**. C1-C2-C3 bond angle utilized for CoGEF calculations.

In addition, the effect of elongation of specific internuclear axes was probed to investigate the calculated effects that bond stretching motions could have on the mechanophore (Table 2.1). In three cases (entries 1-3), bond homolysis was observed, and the calculated activation energies for each are significantly higher than the estimated activation energy for cycloreversion based on bond angle deformation. In the fourth case (entry 4), cycloreversion was observed, albeit at a slightly higher calculated activation energy than that observed from the above bond angle deformation calculations.

**Table 2.1**. Results of CoGEF calculations based on internuclear elongations.

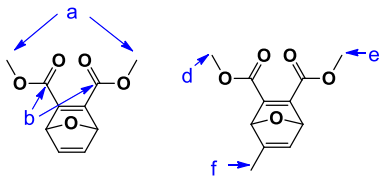


| **entry** | **elongation axis** | **result** | $E_a$ **(kcal/mol)** |
|---|---|---|---|
| 1 | a - a | homolysis of a – O bond | 115 |
| 2 | b - b | homolysis of b – alkene bond | 88 |
| 3 | e - f | homolysis of e – O bond | 80 |
| 4 | d - f | cycloreversion to furan and acetylene diester | 50 |

*General procedure for Raman microscopy*. A thin sample of polymer network was placed on a freshly cleaved piece of highly ordered pyrolytic graphite (HOPG). Due to residual fluorescence of the sample, photobleaching at 785 nm was performed for 45 min prior to collection of the Raman spectrum. Spectra were obtained using an excitation wavelength of 785 nm and are presented in Figure 2.12.

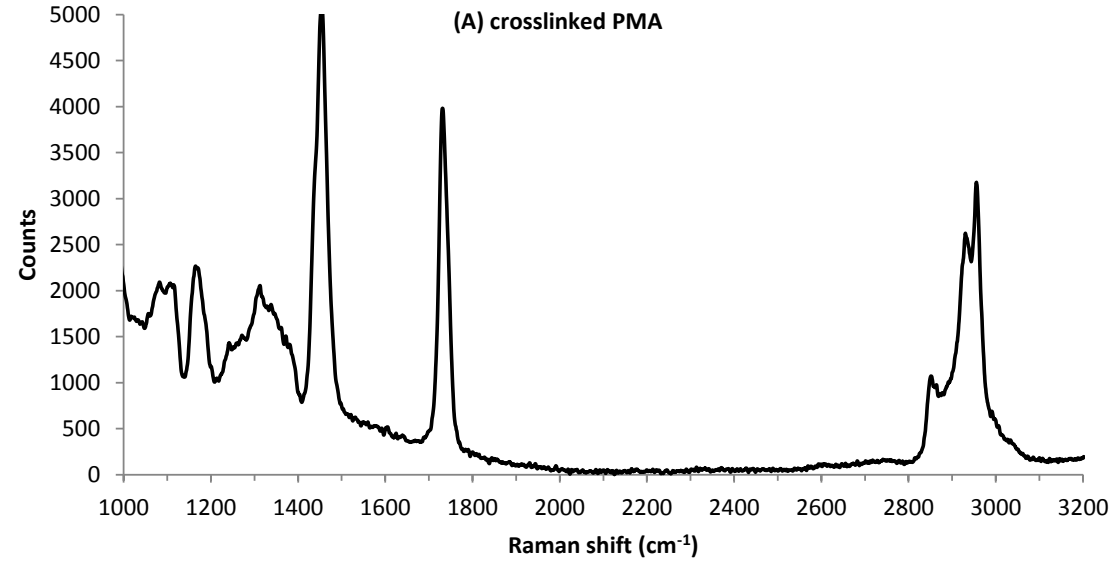
(A) crosslinked PMA
Counts
5000
4500
4000
3500
3000
2500
2000
1500
1000
500
0
1000
1200
1400
1600
1800
2000
2200
2400
2600
2800
3000
3200
Raman shift (cm-1)

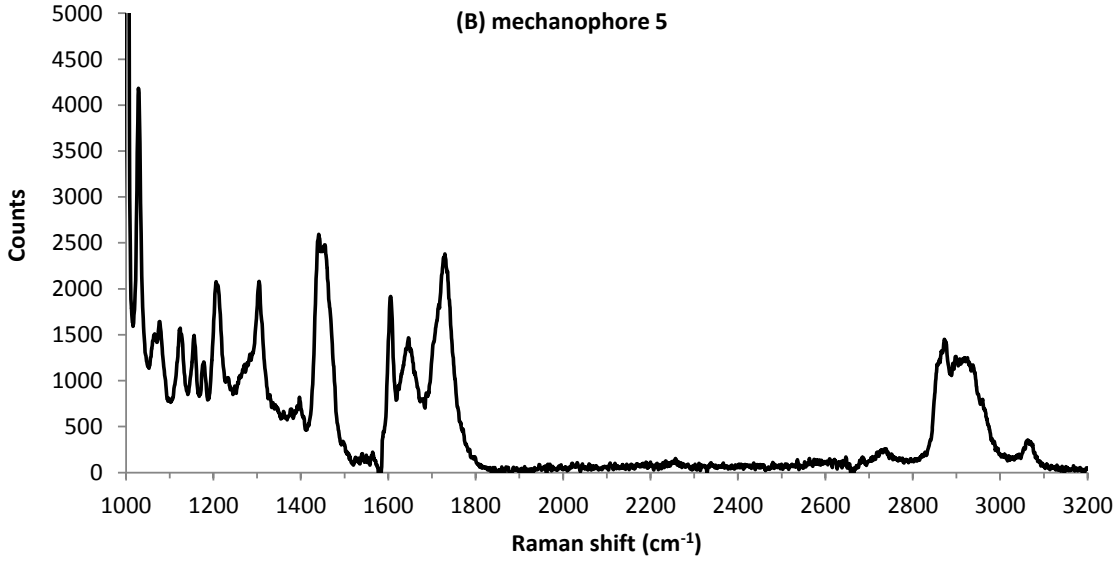
(B) mechanophore 5
Counts
5000
4500
4000
3500
3000
2500
2000
1500
1000
500
0
1000
1200
1400
1600
1800
2000
2200
2400
2600
2800
3000
3200
Raman shift (cm-1)

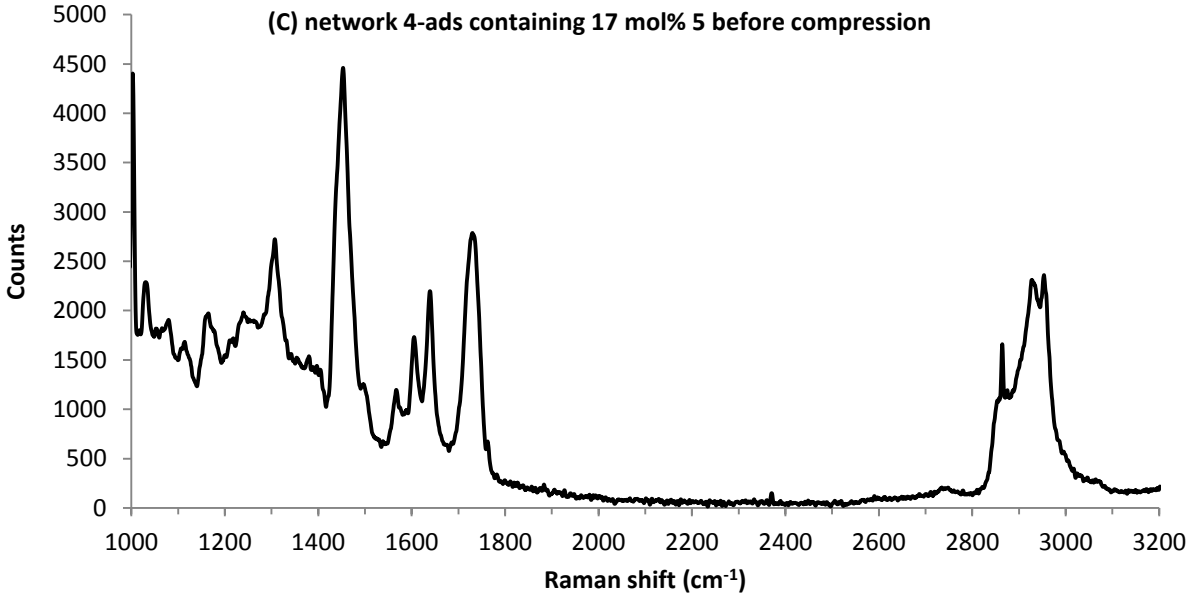
(C) network 4-ads containing 17 mol% 5 before compression
Counts
5000
4500
4000
3500
3000
2500
2000
1500
1000
500
0
1000
1200
1400
1600
1800
2000
2200
2400
2600
2800
3000
3200
Raman shift (cm-1)

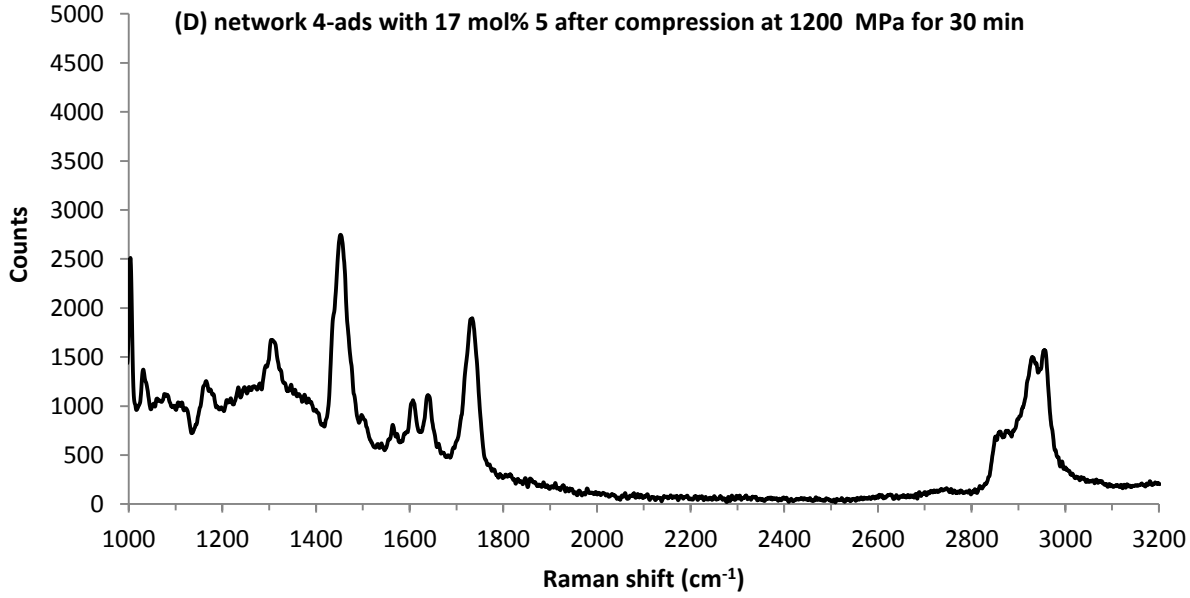
(D) network 4-ads with 17 mol% 5 after compression at 1200 MPa for 30 min
Counts
5000
4500
4000
3500
3000
2500
2000
1500
1000
500
0
1000
1200
1400
1600
1800
2000
2200
2400
2600
2800
3000
3200
Raman shift (cm-1)

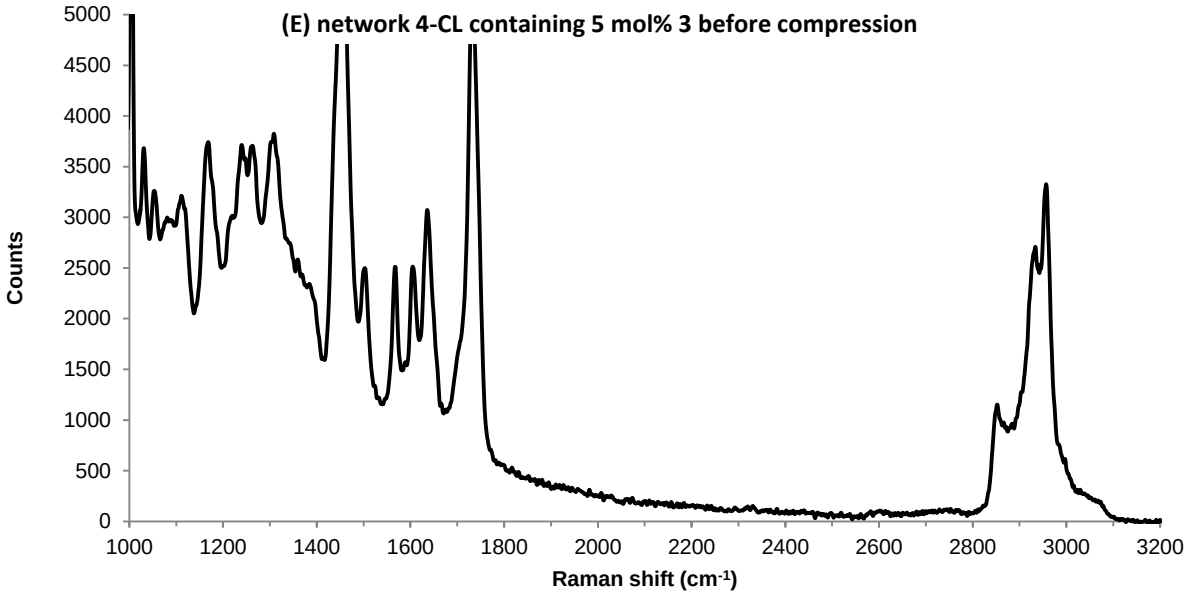
(E) network 4-CL containing 5 mol% 3 before compression
Counts
Raman shift (cm-1)
0
500
1000
1500
2000
2500
3000
3500
4000
4500
5000
1000
1200
1400
1600
1800
2000
2200
2400
2600
2800
3000
3200

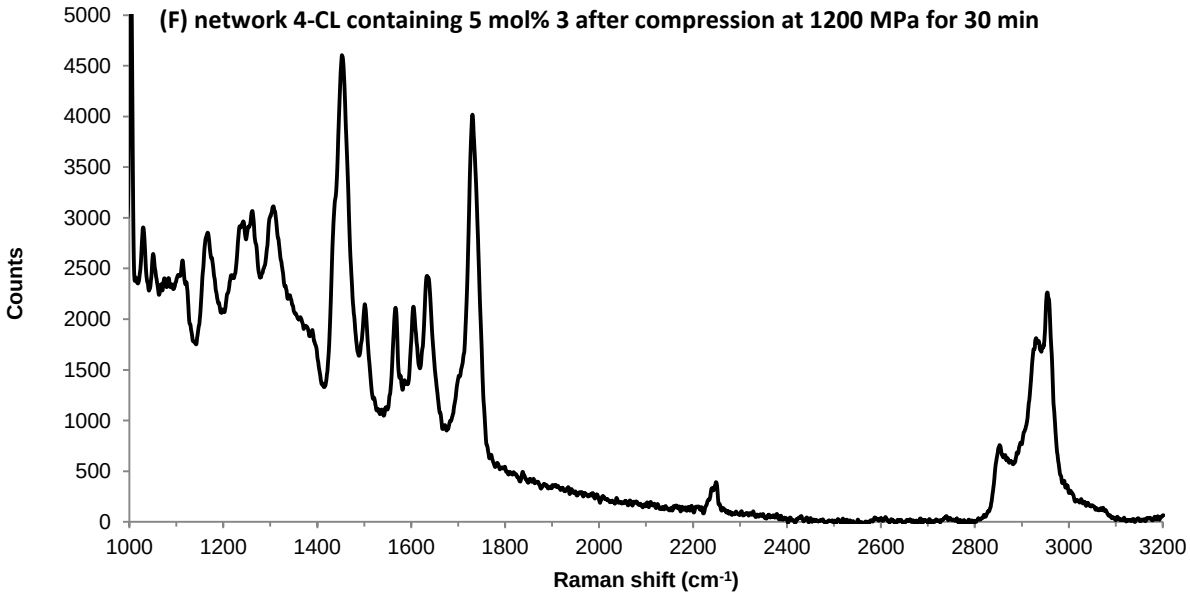
(F) network 4-CL containing 5 mol% 3 after compression at 1200 MPa for 30 min
Counts
Raman shift (cm-1)
0
500
1000
1500
2000
2500
3000
3500
4000
4500
5000
1000
1200
1400
1600
1800
2000
2200
2400
2600
2800
3000
3200

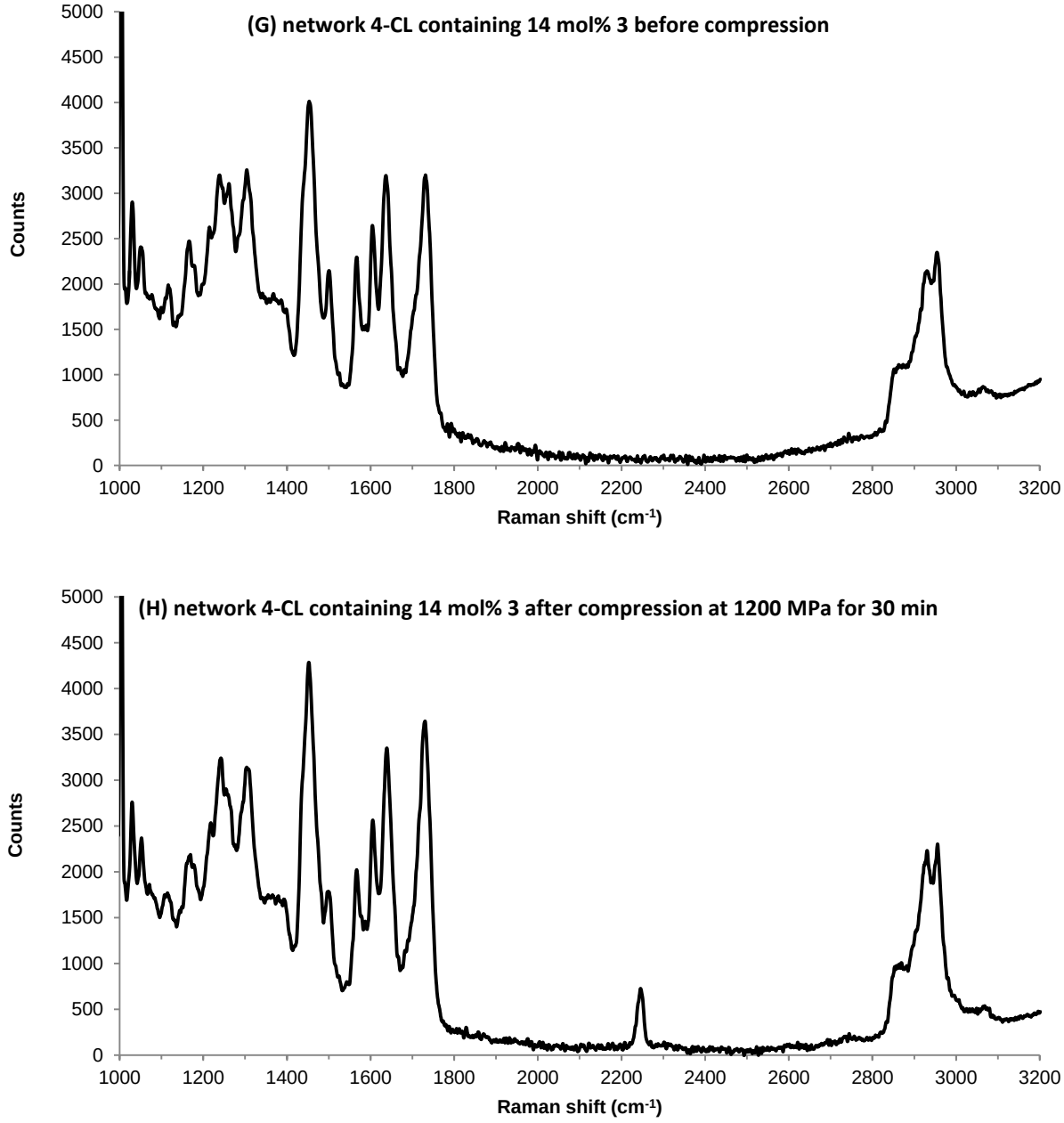


**Figure 2.12**. Raman spectra of (A) PMA crosslinked with **6**, (B) control mechanophore **5** (neat), (C) network **4-ads** containing 17 mol% **5** before compression, (D) network **4-ads** containing 17 mol% **5** after compression at 1200 MPa for 30 min, (E) network **4-CL** containing 5 mol% **3** before compression, (F) network **4-CL** containing 5 mol% **3** after compression at 1200 MPa for 30 min, (G) network **4-CL** containing 14 mol% **3** before compression, (H) network **4-CL** containing 14 mol% **3** after compression at 1200 MPa for 30 min.

*Verification of mechanophore stability under crosslinking conditions***.** Linear poly(methyl acrylate) incorporating **S4** as a repeat unit was synthesized in bulk. In a screw cap vial under $N_2$ atmosphere, compound **S4** (26 mg, 0.047 mmol) and recrystallized benzoyl peroxide (2.3 mg, 9 μmol) were dissolved in freshly distilled methyl acrylate (85 μL, 0.94 mmol). *N*,*N*-Dimethylaniline was added (1.1 μL, 9 μmol) and the vial was sealed with a Teflon-lined screw cap and immediately transferred to a freezer (-10 °C). After 20 h, the vial was opened and the residue dissolved in $CH_2Cl_2$. The polymer was isolated by adding the $CH_2Cl_2$ solution dropwise into an excess of cold MeOH, causing precipitation of the polymer. The solution was decanted from the resulting solids. The solids were rinsed with additional portions of MeOH and dried on a Schlenk line. $^1$H NMR analysis (Figure 2.13) indicated incorporation of **S4** as a repeat unit, as no protons from the terminal acrylate were detected and the bridgehead proton signals remained intact (Figure 2.13, inset).

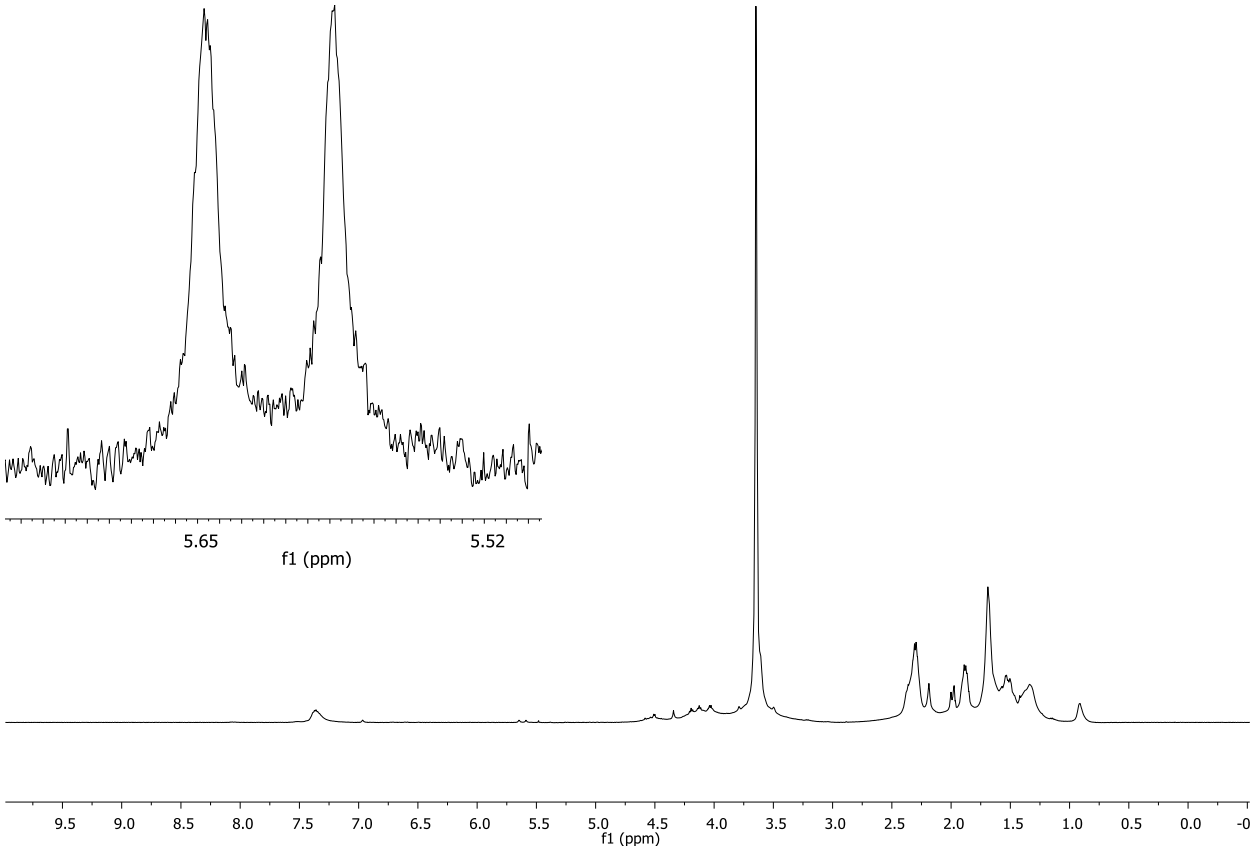


**Figure 2.13**. $^{1}$H NMR spectrum of linear polymer with control mechanophore **S4** incorporated into the main chain (solvent = $CD_3CN$). Inset: resonances corresponding to intact oxanorbornadiene (bridgehead protons)

*2.4.b Experimental for Multiple Activation Cycles in Elastomeric Polyurethane*

**Scheme 2.5**. Synthesis of mechanophore **7**.

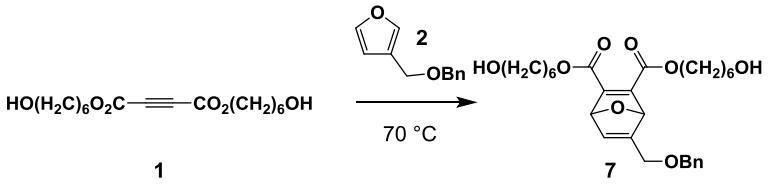


Preparation of **7**. Compounds **1** (1.50 g, 4.77 mmol) and **2** (898 mg, 4.77 mmol) were combined in a screw cap vial, sealed, and heated at 70 °C. The reaction progress was monitored via $^{1}$H NMR spectroscopy. After 18 h, nearly full conversion of **2** was achieved. The reaction mixture was removed from heat and the crude product purified by column chromatography (75% EtOAc/hexanes) to yield **7** as a pale orange oil (1.34 g, 56%). $^{1}$H NMR (300 MHz, $CDCl_3$) δ 7.40 – 7.27 (m, 5H), 6.94 (s, 1H), 5.66 (s, 1H), 5.60 (s, 1H), 4.52 (d, *J* = 12.0 Hz, 1H), 4.45 (d, *J* = 12.0 Hz, 1H), 4.33 (s, 2H), 4.25 – 4.15 (m, 4H), 3.64 (t, *J* = 6.4 Hz, 2H), 3.62 (t, *J* = 6.4 Hz, 2H) 1.75 – 1.62 (m, 4H), 1.57 (m, 4H), 1.45 – 1.33 (m, 8H). $^{13}$C NMR (126 MHz, $CDCl_3$) δ 163.0, 155.9, 152.8, 152.5, 137.71, 137.70, 128.4, 127.7, 85.9, 85.5, 72.4, 66.9, 66.1, 65.41, 65.39, 62.59, 62.56, 32.5, 28.4, 25.57, 25.56, 25.31, 25.30. LRMS (ESI): $[M+H]^+$ calcd for $C_{28}H_{39}O_8$, 503.26; found 503.3.

*Preparation of crosslinked network incorporating* **7**. In a screw cap vial under $N_2$ atmosphere, compound **7** (100.5 mg, 0.2 mmol), methylene diphenyl diisocyanate (307.8 mg, 1.23 mmol), and DABCO (2.2 mg, 0.02 mmol) were dissolved in anhydrous THF (3.0 mL). After 10 min, 1 kDa poly(ethylene glycol) (1.00 g, 1.0 mmol) and tris(hydroxymethyl)ethane (2.4 mg, 0.02 mmol) were added. The vial was sealed with a Teflon-lined screw cap. After 48 h under ambient conditions, full gelation of the reaction mixture was observed. The vial was then unsealed and

cured at 30 °C for 48 h, and the remaining solids were dried on a Schlenk line for 18 h yielding the polymer network as a rubbery solid (1.495 g). The weight% of mechanophore was determined from the initial loading of compound **7** divided by the final mass of polymer obtained.

*Preparation of control network incorporating* **5**. In a screw cap vial under $N_2$ atmosphere, 1,6-hexanediol (23.6 mg, 0.2 mmol), methylene diphenyl diisocyanate (307.8 mg, 1.23 mmol), and DABCO (2.2 mg, 0.02 mmol) were dissolved in anhydrous THF (3.0 mL). After 10 min, 1 kDa poly(ethylene glycol) (1.00 g, 1.0 mmol) and tris(hydroxymethyl)ethane (2.4 mg, 0.02 mmol) were added. The vial was sealed with a Teflon-lined screw cap. After 2 h, a solution of compound **5** (94.1 mg, 0.2 mmol) in anhydrous THF (0.5 mL) was added, the vial resealed, and allowed to react for an additional 47 h, during which full gelation of the reaction mixture was observed. The vial was unsealed and cured at 30 °C for 48 h, and the remaining solids were dried on a Schlenk line for 18 h yielding the polymer network as a rubbery solid (1.436 g). The weight% of mechanophore was determined from the initial loading of compound **9** divided by the final mass of polymer obtained.

*General procedure for compression studies*. A sample of polymer network (approx. 20 – 30 mg) was loaded into a KBr pellet press and pressure applied via a Carver laboratory press with attached manometer. The sample was compressed at the desired pressure (calculated by dividing load by area of the pellet press surface, 6.34 mm radius) for 1 min. For samples subjected to multiple compressions, the compressed polymer sample was extracted from the KBr press,

folded in half with forceps, and recompressed (Figure 2.14). Compression of the folded material initially resulted in a thin disk (< 0.1 mm) consisting of the two halves of the original sample adhered to each other; thus, after extraction and subsequent folding for additional compressions, a new portion of material was incorporated into the folding region each time. After the desired number of compressions was reached, the sample was transferred to a vial containing $CH_2Cl_2$ and a known concentration of anisole as internal standard. After 2 h, a sample of the soak solution was analyzed via GC-MS and the % activation determined by dividing the observed furan (**2**) by the total amount present in the polymer sample (determined as wt% in the original synthesis; see above).

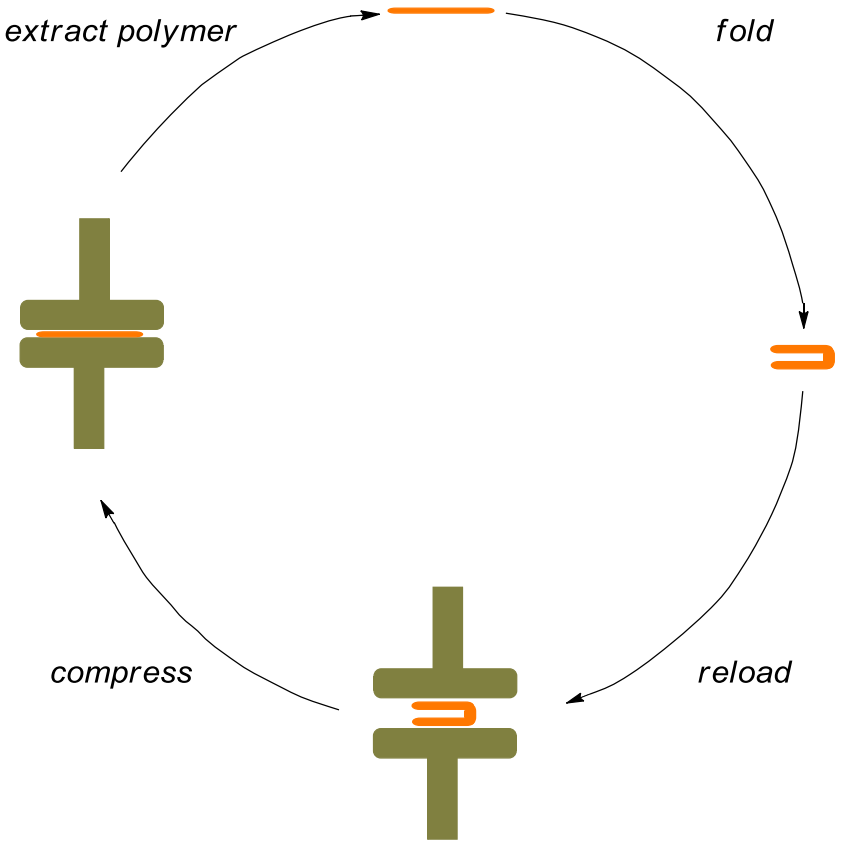


**Figure 2.14**. Idealized depiction of compression and subsequent folding process for multiple compression-activation cycles.

*Effect of folding on % activation*. A sample of polymer containing **7** was compressed at 35 MPa for 1 min, the polymer extracted, and recompressed without folding. The process was repeated until the sample had been compressed three times. The % activation was determined as above, which was found to be 3.6% (average of three unique samples).

*General procedure for mechanical testing*. A rectangular sample was cut out of the original cured material and the length, width, and depth measured. Prior to each DMA measurement, the dimensions were re-measured with electronic calipers. The sample was loaded into the DMA and subjected to a three-point flexural test (5 mm support span width, static force scan, 10.0 mN to 50.0 mN, 10.0 mN/min). The slope of the initial linear portion of the force-deflection curve was used to calculate the flexural modulus from the equation:

$$E_{flex} = L^3 m / 4bd^3$$

where:

$L$ = support span width (mm)

$m$ = slope of force-deflection curve (N/mm)

$b$ = width of sample (mm)

$d$ = depth of sample (mm)

*Confirmation of mechanophore stability under crosslinking and curing conditions*. In a screw cap vial under $N_2$ atmosphere, compound **7** (50.2 mg, 0.1 mmol), methylene diphenyl diisocyanate (150.0 mg, 0.6 mmol), and DABCO (1.2 mg, 0.01 mmol) were dissolved in

anhydrous THF (1.5 mL). After 10 min, 1 kDa poly(ethylene glycol) (499.5 mg, 0.5 mmol) was added. After 2.5 h, 0.5 mL of methanol was added to the viscous solution to terminate the polymerization. The polymer was cured at 30 °C for 48 h, and the remaining solids were dried on a Schlenk line for 18 h. $^{1}$H NMR analysis (Figure 2.15) showed that the ratio of mechanophore to MDI repeat unit in the final polymer matched the initial feed ratio, as calculated by the integrals of furfuryl methylene protons to aromatic MDI protons (Figure 2.15, inset).

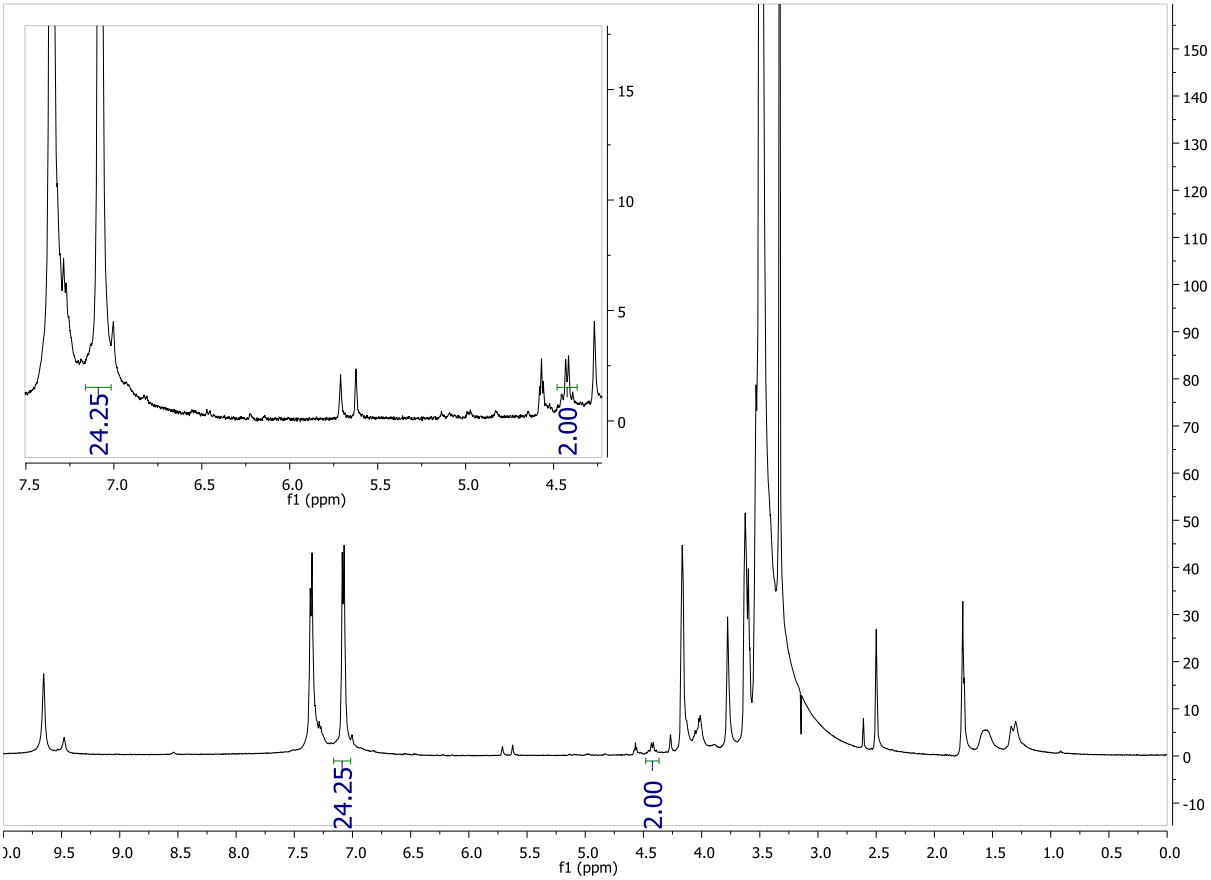


**Figure 2.15**. $^{1}$H NMR spectrum of linear polyurethane incorporating mechanophore **7** (500 MHz, DMSO-$d_6$), with intact oxanorbornadiene signals indicating minimal degradation during polymerization and curing. Inset: magnified 4.25 – 7.5 ppm region, with integrals corresponding to initial feed ratio.

*Effect of compression on previously synthesized poly(methyl acrylate) networks*. Compression of poly(methyl acrylate) networks synthesized in Section 2.2.a resulted in substantial macroscopic failure, even at the lowest pressures examined (Figure 2.16).

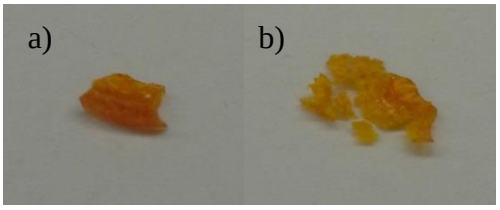


**Figure 2.16**. Images of crosslinked poly(methyl acrylate) networks a) before and b) after compression at 35 MPa for 1 minute.

**Table 2.2**. Raw data for pressure vs. activation plot (Figure 2.5) for active mechanophore network (containing **7**) and control network (containing **5**).

| Pressure (MPa) | Activation (with **7**) | Activation (with **5**) |
|---|---|---|
| 0 | 1.5% | 2.0% |
| | 1.1% | 2.0% |
| | 1.0% | 2.1% |
| 35 | 3.5% | 3.6% |
| | 2.6% | 2.7% |
| | 3.2% | 3.2% |
| 88 | 5.1% | 1.3% |
| | 4.6% | 2.0% |
| | 3.6% | 2.8% |
| 176 | 5.9% | 2.5% |
| | 5.4% | 3.0% |
| | 6.4% | 1.4% |
| 352 | 6.5% | 1.4% |
| | 5.8% | 2.1% |
| | 5.4% | 2.1% |

**Table 2.3**. Raw data for compressions vs. activation plot (Figure 2.6) for active mechanophore network (containing **7**) and control network (containing **5**).

| # compressions | Activation (with **7**) 35 MPa | Activation (with **7**) 88 MPa | Activation (with **5**) 35 MPa |
|---|---|---|---|
| 1 | 3.5% | 5.1% | 3.6% |
| | 2.6% | 4.6% | 2.7% |
| | 3.2% | 3.6% | 3.2% |
| 3 | 4.7% | 5.5% | 2.2% |
| | 4.8% | 5.9% | 2.6% |
| | 4.7% | 5.5% | 2.1% |
| 5 | 4.7% | 5.6% | 1.9% |
| | 4.5% | 6.2% | 1.5% |
| | 4.5% | 5.5% | 2.0% |
| 7 | 5.3% | 5.3% | 2.1% |
| | 4.6% | 5.8% | 1.8% |
| | 6.4% | 6.7% | 2.0% |
| 9 | 5.2% | 6.8% | 2.5% |
| | 4.5% | 7.4% | 1.0% |
| | 7.6% | 7.3% | 1.0% |
| 15 | 5.7% | 5.8% | 2.4% |
| | 6.1% | 6.2% | 0.7% |
| | 7.0% | 7.2% | 1.7% |

**Table 2.4**. Raw data for compressions vs. flexural modulus (Figures 2.7 and 2.8).

| Trial | Compressions / pressure | Dimensions (mm) | Modulus (MPa) | % uncompressed modulus |
|---|---|---|---|---|
| 1 | 0 | 7.57 x 2.71 x 2.38 | .0268 | 100 |
| | 1 / 35 MPa | 7.56 x 2.72 x 2.33 | .0248 | 92.6 |
| | 3 / 35 MPa | 7.43 x 2.77 x 2.32 | .0237 | 88.6 |
| | 5 / 35 MPa | 7.55 x 2.89 x 2.39 | .0211 | 78.7 |
| | 7 / 35 MPa | 7.49 x 2.74 x 2.30 | .0246 | 91.9 |
| | 9 / 35 MPa | 7.49 x 2.86 x 2.16 | .0210 | 78.6 |
| 2 | 0 | 10.21 x 2.34 x 2.02 | .0217 | 100 |
| | 1 / 35 MPa | 10.10 x 2.20 x 1.92 | .0242 | 111 |
| | 3 / 35 MPa | 10.30 x 2.35 x 2.09 | .0204 | 94.1 |
| | 5 / 35 MPa | 10.35 x 2.35 x 1.97 | .0190 | 87.6 |
| | 7 / 35 MPa | 10.30 x 2.30 x 1.93 | .0187 | 86.0 |
| | 9 / 35 MPa | 10.40 x 2.54 x 1.87 | .0133 | 61.3 |
| 3 | 0 | 8.04 x 2.37 x 2.23 | .0292 | 100 |
| | 1 / 35 MPa | 8.04 x 2.45 x 2.30 | .0257 | 88.1 |
| | 3 / 35 MPa | 7.97 x 2.59 x 2.39 | .0256 | 87.8 |
| | 5 / 35 MPa | 7.99 x 2.66 x 2.42 | .0213 | 73.1 |
| | 7 / 35 MPa | 7.93 x 2.56 x 2.39 | .0251 | 86.2 |
| | 9 / 35 MPa | 7.90 x 2.65 x 2.15 | .0191 | 65.6 |
| 4 | 0 | 7.01 x 2.71 x 1.12 | .00596 | 100 |
| | 1 / 88 MPa | 7.15 x 2.71 x 1.05 | .00391 | 65.6 |
| | 3 / 88 MPa | 7.16 x 2.59 x 1.10 | .00339 | 56.9 |
| | 5 / 88 MPa | 7.34 x 2.63 x 1.01 | .00328 | 55.0 |
| | 7 / 88 MPa | 7.01 x 2.65 x 1.07 | .00321 | 53.9 |
| | 9 / 88 MPa | 7.68 x 3.00 x 0.95 | .000760 | 12.8 |
| 5 | 0 | 7.88 x 2.69 x 1.45 | .00636 | 100 |
| | 1 / 88 MPa | 8.05 x 2.83 x 1.31 | .00377 | 59.3 |
| | 3 / 88 MPa | 8.16 x 2.73 x 1.26 | .00350 | 55.1 |
| | 5 / 88 MPa | 8.34 x 2.82 x 1.29 | .00257 | 40.5 |
| | 7 / 88 MPa | 7.77 x 3.20 x 1.21 | .00203 | 31.9 |
| | 9 / 88 MPa | 8.10 x 3.32 x 1.12 | .00154 | 24.2 |
| 6 | 0 | 6.76 x 2.65 x 2.30 | .0298 | 100 |
| | 1 / 88 MPa | 6.93 x 2.72 x 2.61 | .0234 | 78.4 |
| | 3 / 88 MPa | 6.97 x 2.74 x 2.42 | .0209 | 70.1 |
| | 5 / 88 MPa | 7.01 x 2.66 x 2.49 | .0184 | 61.5 |
| | 7 / 88 MPa | 7.16 x 2.75 x 2.50 | .0158 | 52.9 |
| | 9 / 88 MPa | 6.90 x 2.33 x 2.17 | .0189 | 63.4 |

*2.4.c Experimental for Effects of Oxanorbornadiene Substitution*

**Scheme 2.6**. Synthesis of small molecule components.

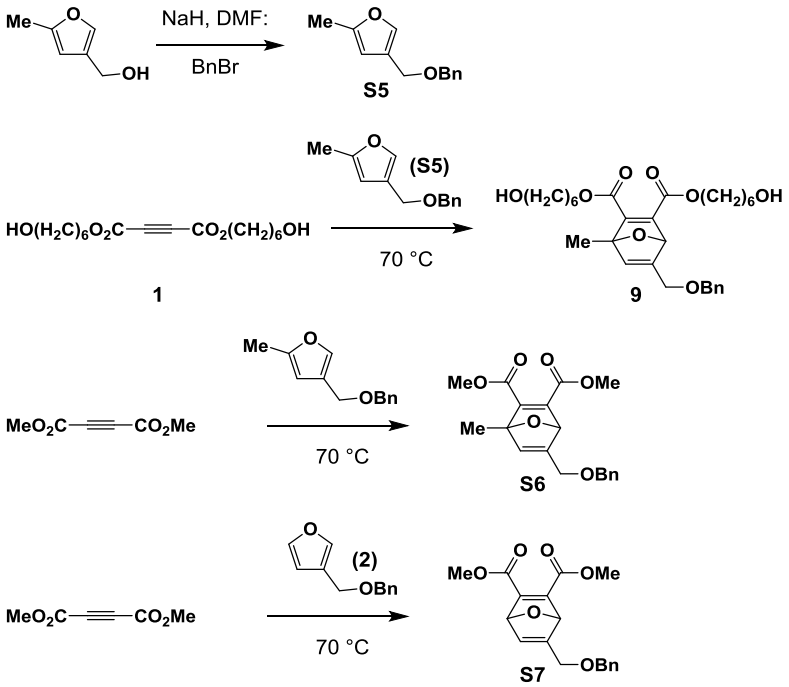


5-methylfuran-3-methanol was synthesized as previously described.[26]

Preparation of **S5**. Compound **S5** was prepared in a manner identical to **2**, substituting 5-methylfuran-3-methanol (274 mg, 2.44 mmol) for 3-furanmethanol. $^{1}$H NMR (300 MHz, $CDCl_3$) δ 7.39 – 7.26 (m, 5H), 7.25 (s, 1H), 6.03 (s, 1H), 4.51 (s, 2H), 4.35 (s, 2H), 2.27 (s, 3H). $^{13}$C NMR (126 MHz, $CDCl_3$) δ 153.1, 139.1, 138.4, 128.5, 127.9, 127.7, 123.1, 106.6, 71.8, 63.6, 13.7. LRMS (EI) $[M]^+$ calcd for $C_{13}H_{14}O_2$ 202.10; found 202.1.

Preparation of **9**. Compound **9** was prepared in a manner identical to **7**, substituting **S5** (150 mg, 0.74 mmol) for **2**. $^{1}$H NMR (500 MHz, $CDCl_3$) δ 7.39 – 7.26 (m, 5H), 6.70 (s, 1H), 5.52 (s,1H), 4.51 (d, J = 11.9 Hz, 1H), 4.46 (d, J = 11.9 Hz, 1H), 4.27 (s,2H), 4.26 – 4.18 (m, 2H), 4.11 (t, J =

6.7 Hz, 2H), 3.68 – 3.57 (m, 4H), 1.78 (s, 3H), 1.75 – 1.65 (m, 4H), 1.66 – 1.48 (m, 8H), 1.48 – 1.38 (m, 4H), 1.39 – 1.31 (m, 4H). $^{13}$C NMR (126 MHz, $CDCl_3$) δ 164.8, 162.7, 157.3, 156.6, 150.7, 140.0, 137.9, 128.5, 127.9, 94.6, 84.3, 72.5, 66.2, 65.6, 65.4, 62.8, 32.6, 28.6, 28.6, 25.7, 25.47, 25.46, 15.5. LRMS (ESI) $[M+NH_4]^+$ calcd for $C_{29}H_{44}NO_8$ 534.31; found 534.4.

Preparation of **S6**. Dimethylacetylene dicarboxylate (0.09 mL, 0.74 mmol) and **S5** (150 mg, 0.74 mmol) were combined in a sealed vial and heated at 70 °C. The reaction progress was monitored via $^1$H NMR spectroscopy. After 15 h, nearly full conversion of **S5** was achieved. The crude product was purified by column chromatography (10% EtOAc/hexanes) to yield compound **S6** as a pale yellow liquid (127 mg, 50%). $^1$H NMR (500 MHz, $CDCl_3$) δ 7.39 – 7.26 (m, 5H), 6.71 (s, 1H), 5.53 (s, 1H), 4.51 (d, J = 11.8 Hz, 1H), 4.45 (d, J = 11.8 Hz, 1H), 4.27 (s, 2H), 3.84 (s, 3H), 3.70 (s, 3H), 1.78 (s, 3H). $^{13}$C NMR (126 MHz, $CDCl_3$) δ 165.0, 162.9, 157.3, 156.7, 151.1, 140.0, 137.9, 128.5, 127.8, 94.6, 84.3, 72.5, 66.2, 53.6, 52.4, 52.3, 15.5. LRMS (ESI): $[M+Na]^+$ calcd for $C_{19}H_{20}NaO_6$, 367.12; found 367.6.

Preparation of **S7**. **S7** was prepared in a manner identical to **S6**, substituting **2** (250 mg, 1.33 mmol) for **S5**. $^1$H NMR (300 MHz, $CDCl_3$) δ 7.42 – 7.27 (m, 5H), 6.94 (d, J = 1.7 Hz, 1H), 5.68 (s, 1H), 5.61 (d, J = 1.4 Hz, 1H), 4.54 (d, J = 11.8 Hz, 1H), 4.47 (d, J = 11.8 Hz, 1H), 4.32 (s, 2H), 3.82 (s, 3H), 3.75 (s, 3H). $^{13}$C NMR (126 MHz, $CDCl_3$) δ 163.3, 156.1, 153.3, 152.9, 137.2, 128.6, 127.9, 86.0, 85.7, 72.6, 66.2, 52.5, 52.4. (ESI): $[M+Na]^+$ calcd for $C_{18}H_{18}NaO_6$, 353.10; found 353.2.

*Preparation of crosslinked network incorporating* **9**. The crosslinked network was prepared in a manner analogous to that described in Section 2.4.b, substituting **9** (34.2 mg, 0.066 mmol) for **7**. Yield = 479 mg, 7.1 wt% mechanophore.

*Preparation of mixed crosslinked network containing **7** and **9**.*

In a screw cap vial under $N_2$ atmosphere, compound **7** (35.0 mg, 0.07 mmol), compound **9** (36.0 mg, 0.07 mmol) methylene diphenyl diisocyanate (214.5 mg, 0.86 mmol), and DABCO (1.6 mg, 0.014 mmol) were dissolved in anhydrous THF (2.5 mL). After 10 min, 1 kDa poly(ethylene glycol) (697 mg, 0.697 mmol) and tris(hydroxymethyl)ethane (1.7 mg, 0.014 mmol) were added. The vial was sealed with a Teflon-lined screw cap. After 48 h under ambient conditions, full gelation of the reaction mixture was observed. The vial was then unsealed and cured at 30 °C for 48 h, and the remaining solids were dried on a Schlenk line for 18 h yielding the polymer network as a rubbery solid (1.078 g, 3.2 wt% **7**, 3.3 wt% **9**). The weight% of each mechanophore was determined from the initial loading of compounds **7** and **9** divided by the final mass of polymer obtained.

*General procedure for compression studies.* Compression studies were performed as described in Section 2.4.b.

*Thermolysis of oxanorbornadienes***.** In separate scintillation vials, compounds **S6** (17.2 mg, 0.05 mmol) and **S7** (16.5 mg, 0.05 mmol) were dissolved in 0.5 mL portions of DMSO-$d_6$. Nitrobenzene (5.0 μL, 0.05 mmol) was added as an internal standard, and the solutions were transferred to separate NMR tubes. The NMR tubes were heated at 140 °C and monitored by

NMR spectroscopy for retrocyclization and/or decomposition of the oxanorbornadiene adducts (Figure 2.17). While retrocyclization was observed, judged by the appearance of the corresponding furan in each case, its concentration reached a maximum of only 25-30% of the initial oxanorbornadiene concentration. While each benzyl furfuryl ether is not completely stable at 140 °C, the rate constant of decomposition is an order of magnitude greater than that of oxanorbornadiene decomposition; therefore, it appears the thermolysis of oxanorbornadiene results in a combination of both retrocyclization and nonspecific degradation. First-order rate constants for the disappearance of oxanorbornadiene were calculated from the slope of ln[oxanorbornadiene] versus time plots (Figure 2.18).

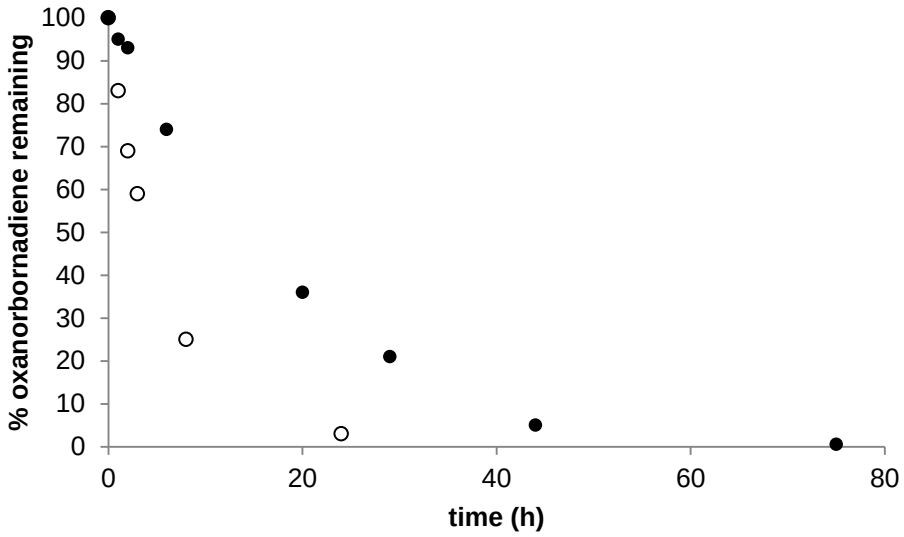


**Figure 2.17**. Disappearance of oxanorbornadienes **S6** (○) and **S7** (●) upon thermolysis at 140 °C.

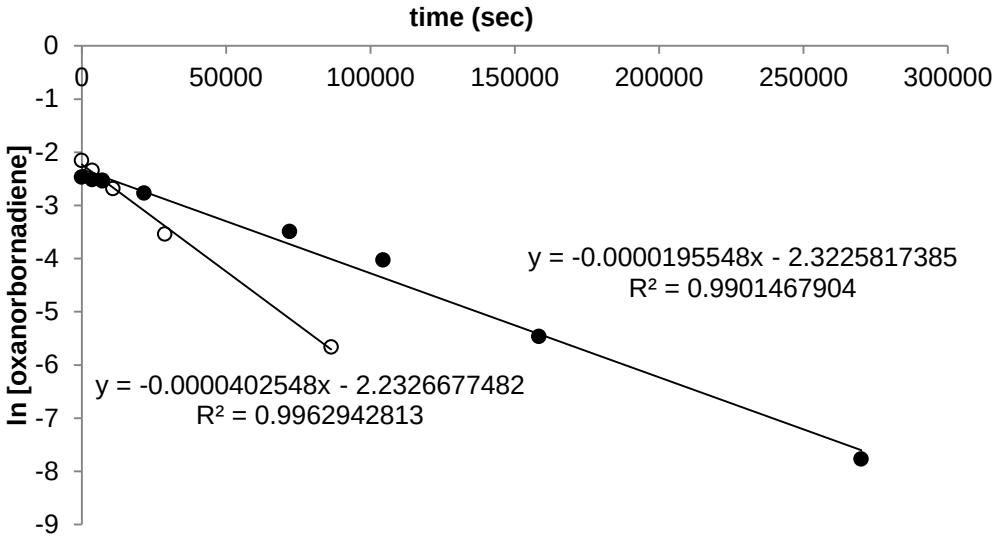


**Figure 2.18**. First-order rate plot for disappearance of oxanorbornadienes **S6** (○) and **S7** (●) upon thermolysis at 140 °C. $k_{\mathbf{S6}} = 4.03 \times 10^{-5}$ s$^{-1}$; $k_{\mathbf{S7}} = 1.96 \times 10^{-5}$ s$^{-1}$.

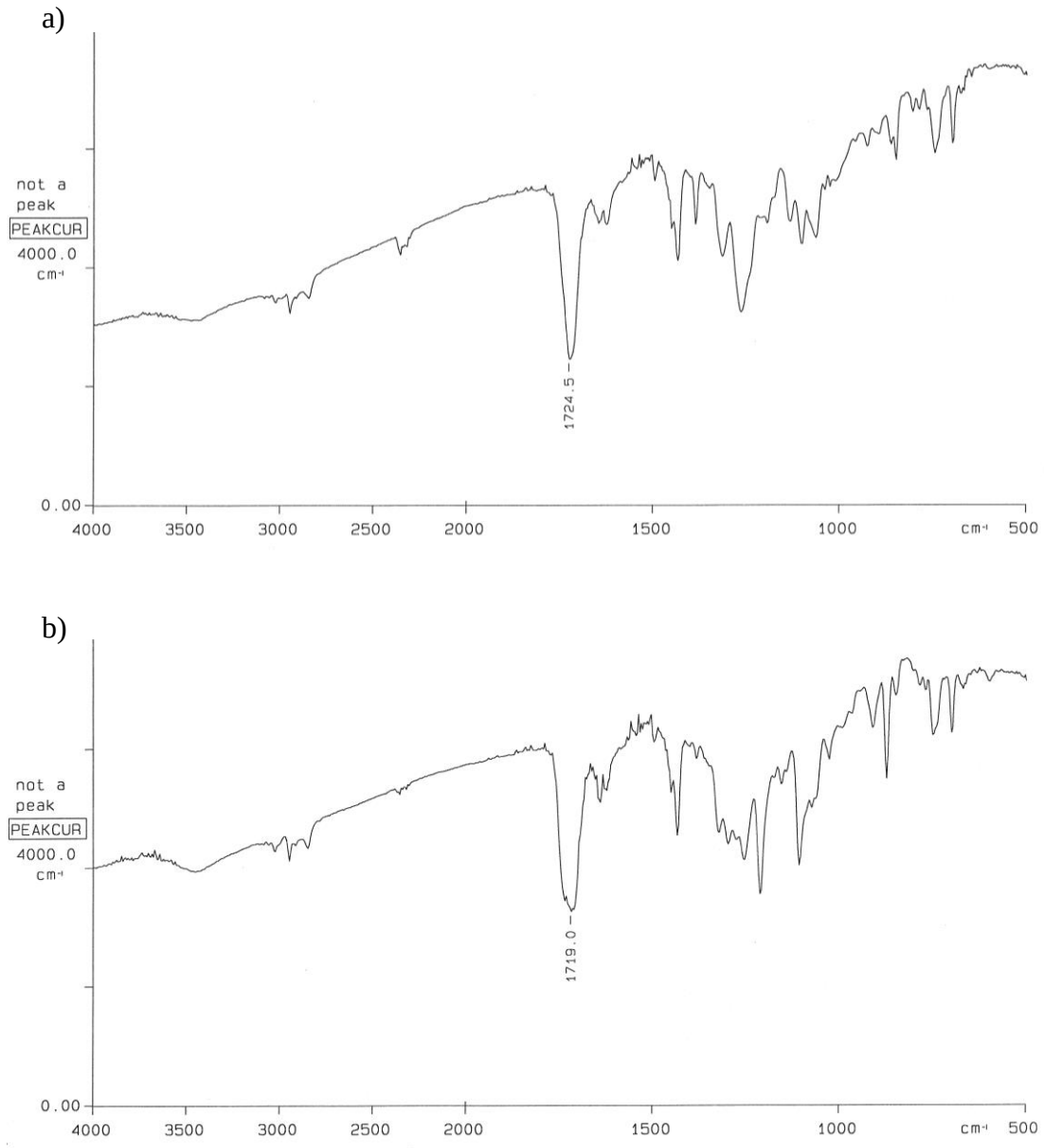


**Figure 2.19**. Infrared spectra of (a) **S6** and (b) **S7**, showing shift in carbonyl stretching frequencies.

**Notes and References to Chapter 2**

[1] Boulatov, R. *Pure Appl. Chem.* **2011**, *83*, 25.
[2] (a) Sletten, E. M.; Bertozzi, C. R. *Acc. Chem. Res.* **2011**, *44*, 666. (b) Hall, H. K., Jr.; Zbinden, R. *J. Am. Chem. Soc.* **1958**, *80*, 6428.
[3] Beyer, M. K.; Clausen-Schaumann, H. *Chem. Rev.* **2005**, *105*, 2921.
[4] (a) Gilman, J. J. *Mat. Res. Soc. Symp. Proc.* **2004**, *800*, AA7.6.1. (b) Gilman, J. J. *Science* **1996**, *274*, 65.
[5] For a discussion on shock-driven changes in electronic structure that manifest mechanochemical reactions, see: Luty, T.; Ordon, P.; Eckhardt, C. J. *J. Chem. Phys.* **2002**, *117*, 1775.
[6] Jezowski, S. R.; Zhu, L.; Wang, Y.; Rice, A. P.; Scott, G. W.; Bardeen, C. J.; Chronister, E. L. *J. Am. Chem. Soc.* **2012**, *134*, 7459. Pressure-induced mechanochromism has been demonstrated in spiropyrans and bianthrones, in which the smaller volume of the colored (product) form lead to pressure-induced changes in thermodynamic equilibria: (a) Wilson, D. G.; Drickamer, H. G. *J. Chem. Phys.* **1975**, *63*, 3649. (b) Fanselow, D. L.; Drickamer, H. G. *J. Chem. Phys*, **1974**, *61*, 4567.
[7] Lenhardt, J. M.; Black, A. L.; Beiermann, B. A.; Steinberg, B. D.; Rahman, F.; Samborski, T.; Elsakr, J.; Moore, J. S.; Sottos, N. R.; Craig, S. L. *J. Mater. Chem.* **2011**, *21*, 8454.
[8] A related approach utilizes mechanical force to disrupt non-covalent interactions, leading to release of active species. For recent representative examples and reviews, see: (a) Izawa, H.; Kawakami, K.; Sumita, M.; Tateyama, Y.; Hill, J. P.; Ariga, K. *J. Mater. Chem. B.* **2013**, *1*, 2155. (b) Hyun, D. C.; Moon, G. D.; Park, C. J.; Kim, B. S.; Xia, Y.; Jeong, U. *Angew. Chem. Int. Ed.* **2011**, *50*, 724. (c) Lee, K. Y.; Peters, M. C.; Mooney, D. J. *Adv. Mater.* **2001**, *13*, 837. (d) Lee, K. Y.; Peters, M. C.; Anderson, K. W.; Mooney, D. J. *Nature* **2000**, *408*, 998. (e) Uhrich, K. E.; Cannizzaro, S. M.; Langer, R. S.; Shakesheff, K. M. *Chem. Rev.* **1999**, *99*, 3181. (f) Langer, R. *Nature* **1998**, *392*, 5.
[9] Klukovich, H. M.; Kouznetsova, T. B.; Kean, Z. S.; Lenhardt, J. M.; Craig, S. L. *Nat. Chem.* **2013**, *5*, 110.
[10] Kryger, M. J.; Munaretto, A. M.; Moore, J. S. *J. Am. Chem. Soc.* **2011**, *133*, 18992.
[11] Beyer, M. K. *J. Chem. Phys.* **2000**, *112*, 7307.
[12] CoGEF experiments in which internuclear distances were elongated (i.e., stretch-activating) are included in the Experimental. Notably, direct elongation of distance between the ester functionalities resulted in bond homolysis.
[13] Gaussian 09, Revision A.1, Frisch, M. J.; Trucks, G. W.; Schlegel, H. B.; Scuseria, G. E.; Robb, M. A.; Cheeseman, J. R.; Scalmani, G.; Barone, V.; Mennucci, B.; Petersson, G. A.; Nakatsuji, H.; Caricato, M.; Li, X.; Hratchian, H. P.; Izmaylov, A. F.; Bloino, J.; Zheng, G.; Sonnenberg, J. L.; Hada, M.; Ehara, M.; Toyota, K.; Fukuda, R.; Hasegawa, J.; Ishida, M.; Nakajima, T.; Honda, Y.; Kitao, O.; Nakai, H.; Vreven, T.; Montgomery, Jr., J. A.; Peralta, J. E.; Ogliaro, F.; Bearpark, M.; Heyd, J. J.; Brothers, E.; Kudin, K. N.; Staroverov, V. N.; Kobayashi, R.; Normand, J.; Raghavachari, K.; Rendell, A.; Burant, J. C.; Iyengar, S. S.; Tomasi, J.; Cossi, M.; Rega, N.; Millam, J. M.; Klene, M.; Knox, J. E.; Cross, J. B.; Bakken, V.; Adamo, C.; Jaramillo, J.; Gomperts, R.; Stratmann, R. E.; Yazyev, O.; Austin, A. J.; Cammi, R.; Pomelli, C.; Ochterski, J. W.; Martin, R. L.; Morokuma, K.; Zakrzewski, V. G.; Voth, G. A.; Salvador, P.;

Dannenberg, J. J.; Dapprich, S.; Daniels, A. D.; Farkas, Ö.; Foresman, J. B.; Ortiz, J. V.; Cioslowski, J.; Fox, D. J. Gaussian, Inc., Wallingford CT, 2009.
[14] Diesendruck, C. E.; Steinberg, B. D.; Sugai, S. N.; Silberstein, M. N.; Sottos, N. R.; White, S. R.; Braun, P. V.; Moore, J. S. *J. Am. Chem. Soc.* **2012**, *134*, 12446.
[15] (a) Petrović, Z. S.; Javni, I.; Divjaković, V. *J. Polym. Sci., Part B: Polym. Phys.* **1998**, *36*, 221. (b) Petrović, Z. S.; Ferguson, J. *Prog. Polym. Sci.* **1991**, *16*, 695.
[16] Limitations on the dimensions of the compressed materials precluded more traditional tensile testing, thus the use of flexural moduli to provide an internal comparison of the samples.
[17] (a) Yi, J.; Boyce, M. C.; Lee, G. F.; Balizer, E. *Polymer* **2006**, *47*, 319. (b) Qi, H. J.; Boyce, M. C. *Mech. Mater.* **2005**, *37*, 817.
[18] Buckley, C. P; Prisacariu, C.; Martin, C. *Polymer* **2010**, *51*, 3213.
[19] Degen, C. M.; May, P. A.; Moore, J. S.; White, S. R.; Sottos, N. R. *Macromolecules* **2013**, *46*, 8917.
[20] Kingsbury, C. M.; May, P. A.; Davis, D. A.; White, S. R.; Moore, J. S.; Sottos, N. R. *J. Mater. Chem.* **2011**, *21*, 8381.
[21] Church, D. C.; Peterson, G. I.; Boydston, A. J. *ACS Macro Lett.* **2014**, *3*, 648.
[22] Brown, C. L.; Craig, S. L. *Chem. Sci.* **2015**, *6*, 2158.
[23] (a) Gossweiler, G. R.; Kouznetsova, T. B.; Craig, S. L. *J. Am. Chem. Soc.* **2015**, *137*, 6148. (b) Wang, J.; Kouznetsova, T. B.; Kean, Z. S.; Fan, L.; Mar, B. D.; Martínez, T. J.; Craig, S. L. *J. Am. Chem. Soc.* **2014**, *136*, 15162.
[24] Chung, Y.; Duerr, B. F.; McKelvey, T. A.; Nanjappan, P.; Czarnik, A. W. *J. Org. Chem.* **1989**, *54*, 1018.
[25] Nyori, R.; Sato, T.; Kobayashi, H. *Bull. Chem. Soc. Jpn.* **1983**, *56*, 2661.
[26] Friedrich, M.; Wachtler, A.; de Meijer, A. *Synlett* **2002**, *4*, 619.

# Chapter 3. Flex Activation of N-heterocyclic Carbene – Carbodiimide Adducts

## Section 1: Introduction

### *3.1.a Small Molecule Release in Polymer Mechanochemistry*

Investigations of targeted bond scission in polymer mechanochemistry over the past decade have yielded a wide variety of mechanophore designs and functionalities.[1] While the homolytic scission of weak bonds[2] and opening of strained rings[3–6] have provided valuable insights, application-driven development of mechanophores has yielded materials capable of further translating mechanochemical bond scission to a specific output. Advances in mechanochromism,[7] mechanoluminescence,[8] and force-activated catalysis[9] are prime examples of this type of functionality, as mechanophore activation results in an easily detectable spectroscopic signal or serves to turn on catalytic activity. This type of input-output response holds promise for addressing challenges in sensory materials, self-healing systems, and drug delivery.

Of particular note in this context are mechanophores capable of releasing small molecules as a result of activation. In effect, this decouples the fate of the polymer from that of the released molecule; that is, further chemistry brought about by the small molecule is not influenced or affected by the polymer from which it was released. To date, three mechanophores capable of small-molecule release have been demonstrated in the literature (Figure 3.1). Moore and coworkers were first to develop this concept by exploring the activation of a *gem*-dichlorocyclopropane based on a 1,3-disubstituted indene.[10] Upon scission and isomerization of the cyclopropane, the driving force for rearomatization is of sufficient strength to spontaneously

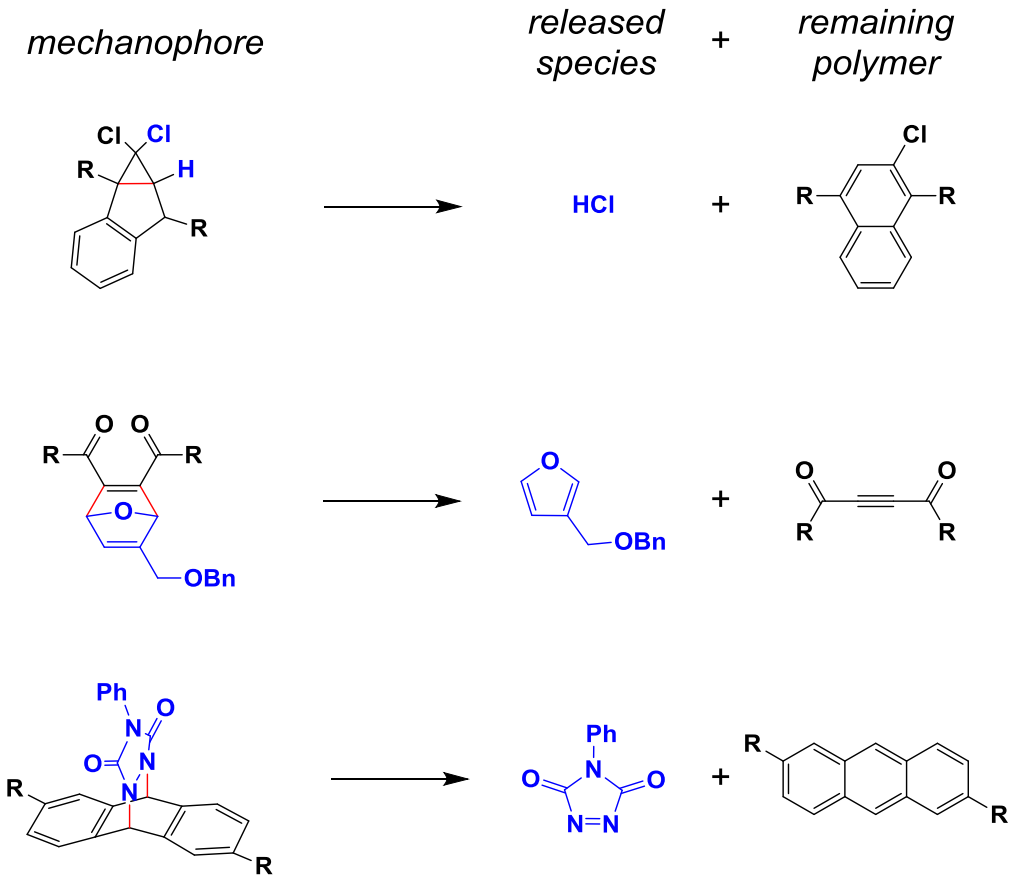


**Figure 3.1**. Mechanophores capable of small molecule release and the product of activation. Red = mechanochemically active bonds, blue = released species; R = site of polymer attachment.

expel HCl. However, no attempts to further utilize the released acid for other chemical transformations were reported. Similarly, no further reactions mediated or activated by the benzyl furfuryl ether released by the oxanorbornadiene mechanophore we have developed (see Chapter 2) have been demonstrated,[11] nor by the released triazolinedione investigated by Craig and coworkers.[12] Therefore, an important unrealized capability of polymer mechanochemistry is the release of a small molecule that activates or participates in further chemical transformations.

In designing a system capable of this type of activation, we considered a particularly attractive goal in this context to be the release of an organocatalyst, since the efficiency of activation in mechanochemical processes is generally low, especially in the solid state.[4c,10,11]

Stoichiometric consumption of a released species would therefore result in only small amounts of conversion, a limitation which would be avoided by releasing a catalytically-active molecule. In considering the mode of mechanochemical activation, flex-activated mechanophores are well-suited to small molecule release. A hallmark of these types of mechanophores is the scission of covalent bonds orthogonal to the main polymer chain, which is easily coupled to small-molecule release; furthermore, they are capable of multiple activation cycles, enabling the tuning of the concentration of released species.[11b] Therefore, we sought to develop a flex-activated mechanophore that enabled the direct release of a catalytically-active species.

*3.1.b N-heterocyclic Carbene – Carbodiimide Adducts*

Consistent with previous studies of flex activation, we sought a transformation in which the geometric changes that occur during the course of the reaction are consistent with linearization of the polymer backbone that occurs during elongation. One such possibility is the conversion of $sp^2$-hybridized carbons to *sp*, the key transformation in the oxanorbornadiene mechanophore. In surveying the literature, we sought a system that combined this characteristic with the release of an organocatalyst. Recently, Johnson and coworkers reported stable covalent adducts between N-heterocyclic carbenes (NHCs) and carbodiimides (CDIs).[13] Formed via the

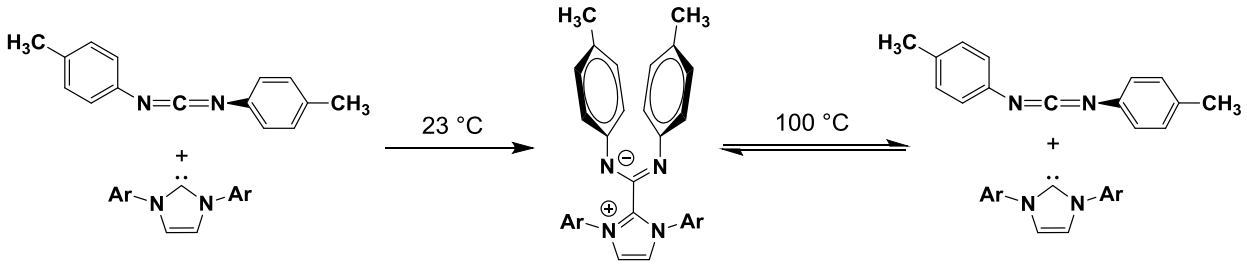


**Figure 3.2**. Synthesis of NHC-CDI adducts and dynamic equilibrium established at high temperatures, studied by Johnson and coworkers.

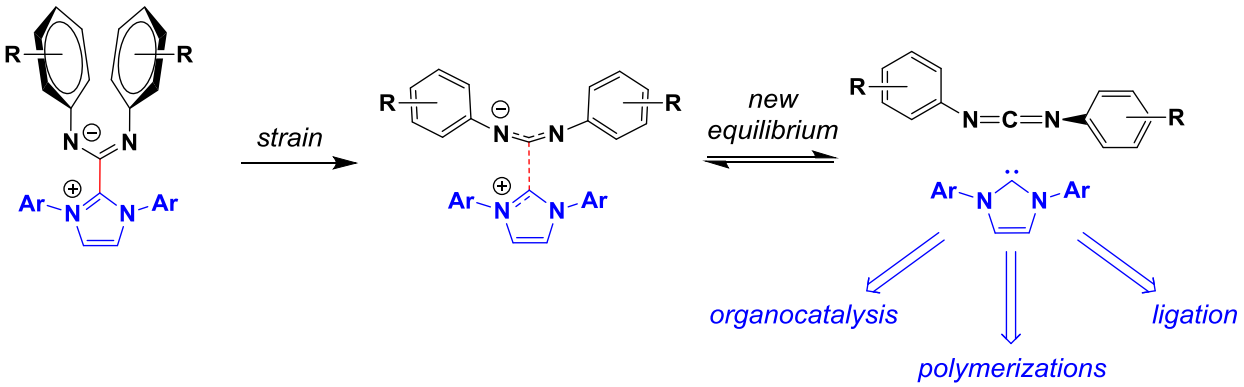


**Figure 3.3**. Generalized depiction of force-induced redistribution of NHC-CDI adduct equilibrium, leading to NHC release. Red = mechanochemically active bonds, blue = released species; R = site of polymer attachment.

reaction of 1,3-diarylimidazol(in)-2-ylidenes and diarylcarbodiimides (Figure 3.2), these bench-stable zwitterions exist fully in the bound form at room temperature, but at ca. 100 °C dynamic equilibrium is established between the adduct and free NHC and CDI. We hypothesized that, by incorporating the CDI portion of the adduct within a polymer chain, linearization of the amidinate upon elongation would perturb the ground state equilibrium to the extent that free NHC could be released (Figure 3.3). This type of mechanically-biased equilibrium has previously been documented and quantified for the spiropyran–merocyanine transition,[7b] and a similar effect would enable the release of a small molecule in this case. NHCs are an extraordinarily versatile class of compounds, capable of functioning as organocatalysts,[14] polymerization initiators and mediators,[15] and transition metal ligands.[16] The diverse range of transformations that would be enabled by this mechanochemical NHC release would greatly expand the utility of polymer mechanochemistry.

## Section 2: Results and Discussion

We first conducted a CoGEF (Constrained Geometries Simulate External Force) study to determine if the geometric distortions that would occur as a result of polymer elongation were

consistent with the desired mechanochemical reaction. This method, utilized by us and others in the modeling of polymer mechanochemistry,[4a,6c,11a,17] incrementally distorts the ground state of the putative mechanophore along a specified axis, angle, or bond. By re-optimizing the geometry of the rest of the molecule at each step, the effect of precise geometric distortions can be determined. As a model for the envisioned polymeric NHC-CDI, the adduct between 1,3-

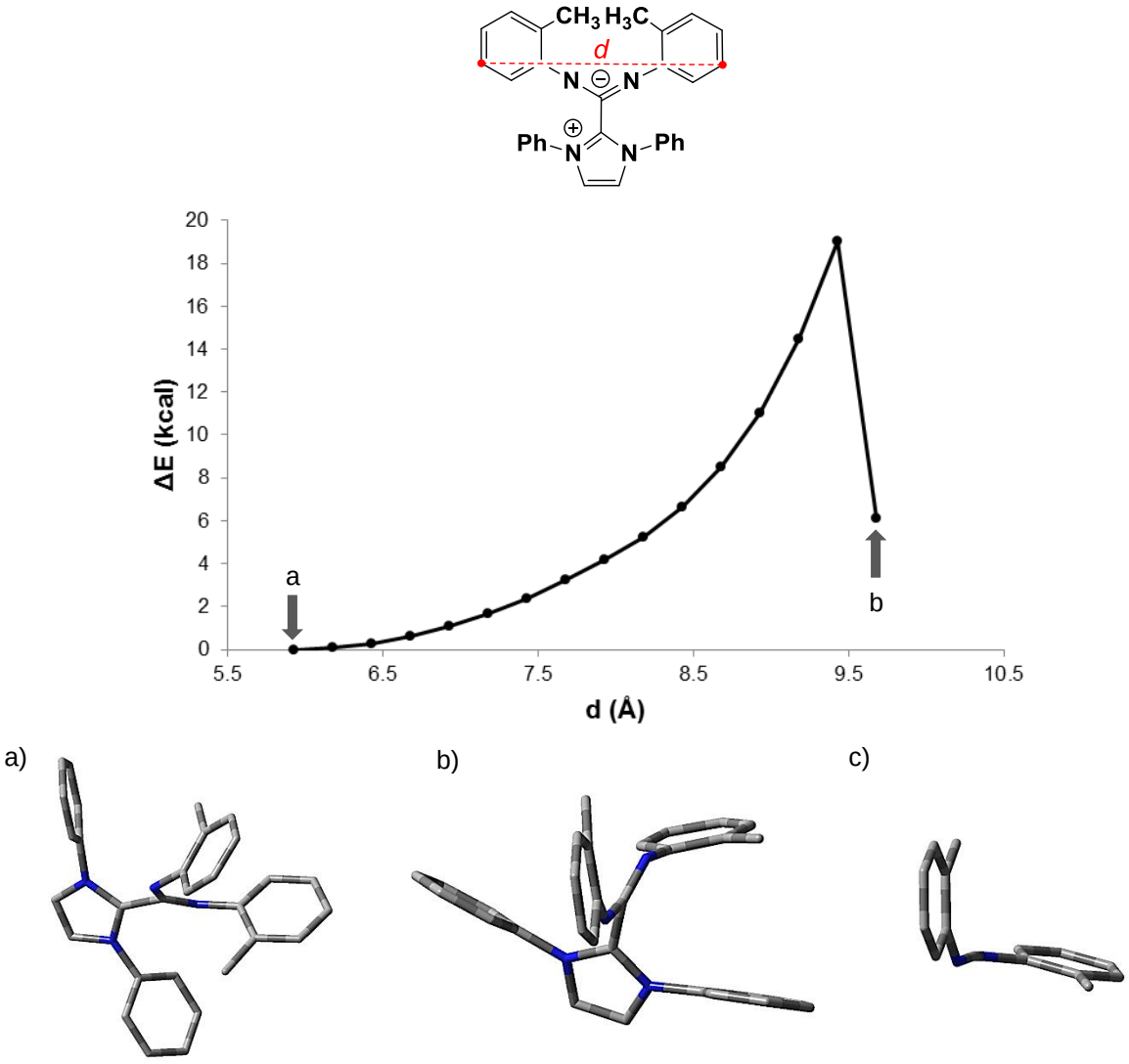


**Figure 3.4**. Calculated potential energies (kcal/mol) resulting from incremental increase in distance *d*. (a) Minimized ground state of NHC-CDI adduct; (b) extended conformation, exhibiting orthogonal carbodiimide aryl rings; (c) minimized structure of di-*o*-tolylcarbodiimide. Hydrogens omitted for clarity. Density functional theory (DFT) calculations were performed at the B3LYP 6-31G* (d) level of theory using the Gaussian program package.

diphenylimidazolylidene and di-*o*-tolylcarbodiimide was subjected to elongation along the axis indicated in Figure 3.4,[18] with the axis chosen to correspond to attachment points for a monomer unit derived from 2,4-tolylene diisocyanate (see below). In the ground state (Figure 3.4a), the aryl rings of the carbodiimide are in a face-on conformation. As *d* is increased, the potential energy rises to the point at which a conformational change occurs, with an onset of ca. 19 kcal (Figure 3.4b). Interestingly, this more extended conformation exhibits a rotation of the carbodiimide aryl rings, which become nearly orthogonal to each other. The aryl groups in di-*o*-tolylcarbodiimide are similarly rotated (Figure 3.4c), as would be expected for two disparate pi systems converging at a *sp* carbon. Thus, it appears that the amidinate begins to exhibit diimide character upon elongation, consistent with the desired mechanochemical reactivity.

Along with these computational studies, we considered different synthetic routes toward incorporating the diarylcarbodiimide unit in a polymer backbone. A particularly attractive option was the work of Campbell, which demonstrated in the early 1960s the conversion of isocyanates to carbodiimides in the presence of a phospholene oxide catalyst.[19] Subsequent extension of this work led to the synthesis of poly(carbodiimides) using diisocyanates as precursors,[20] and the use of aromatic diisocyanates led to polymers of high molecular weights comprised of diarylcarbodiimide repeat units. Our planned synthetic route was thus to polymerize 2,4-tolylene diisocyanate (TDI), followed by post-polymerization functionalization with discretely made 1,3-bis(2,6-diisopropylphenyl)imidazolylidene (DiPP) to form the desired polymeric NHC-CDI adducts.

To this end, TDI was first reacted with a substoichiometric amount of poly(tetramethylene glycol) to obtain flexible macrodiisocyanates so as to impart a degree of elasticity in the final polymer. Similar to the strategy employed for the synthesis of elastomeric

**Scheme 3.1**. Synthesis of polymeric NHC-CDI adducts.[a]

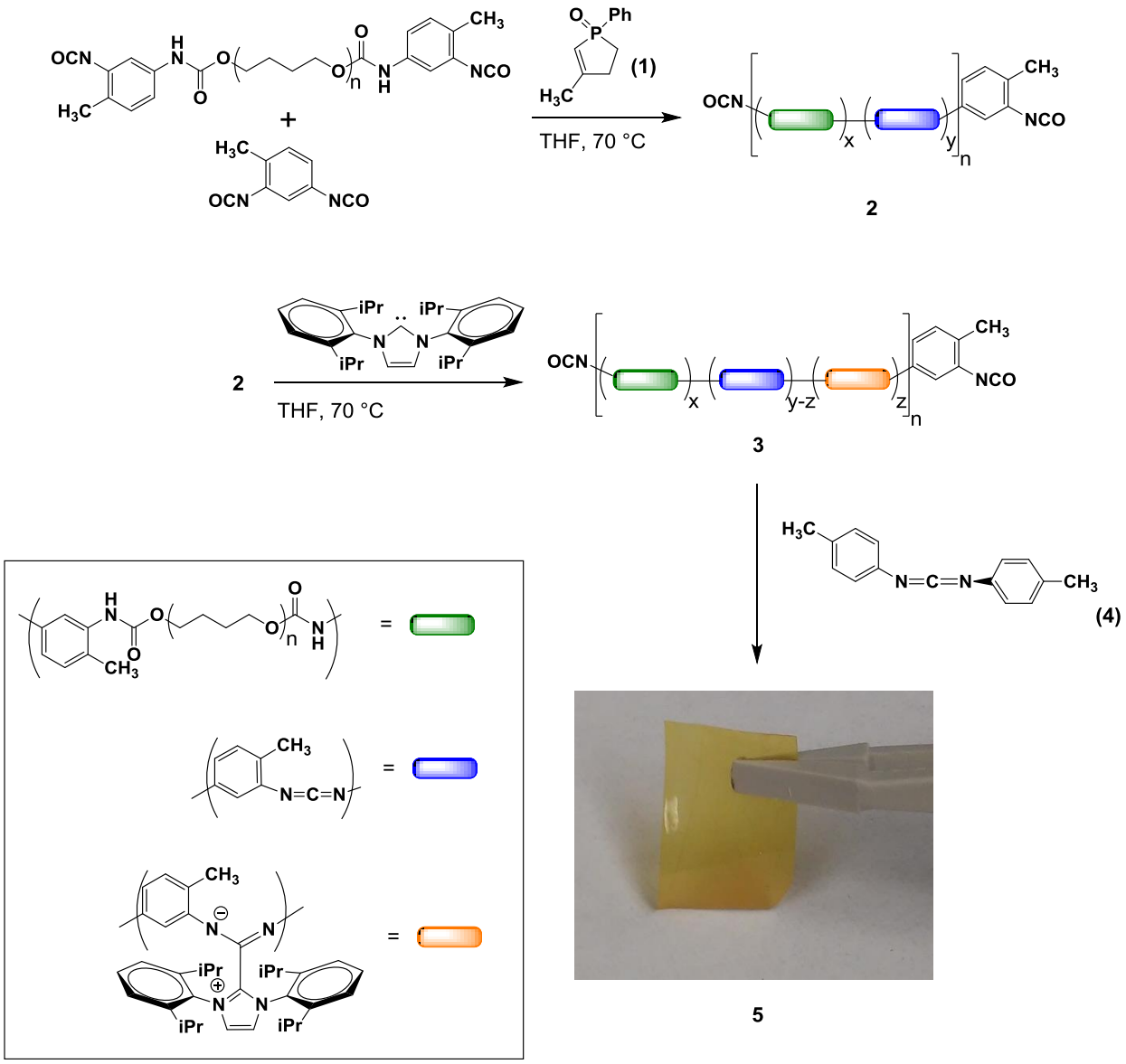


[a] For simplicity, only one regioisomer of each repeat unit arising from TDI is shown.

polyurethane networks in Chapter 2, the flexible polyether segments lowered the modulus of the final material and increased the % strain to break.[21] Polymerization was effected via the addition of a solution of phospholene oxide catalyst **1** to the macrodiisocyanate/TDI mixture, and heating at 70 °C for 2 h resulted in prepolymer **2** (Scheme 3.1). After cooling, a separately prepared solution of DiPP was added to the polymerization solution, which immediately turned a bright

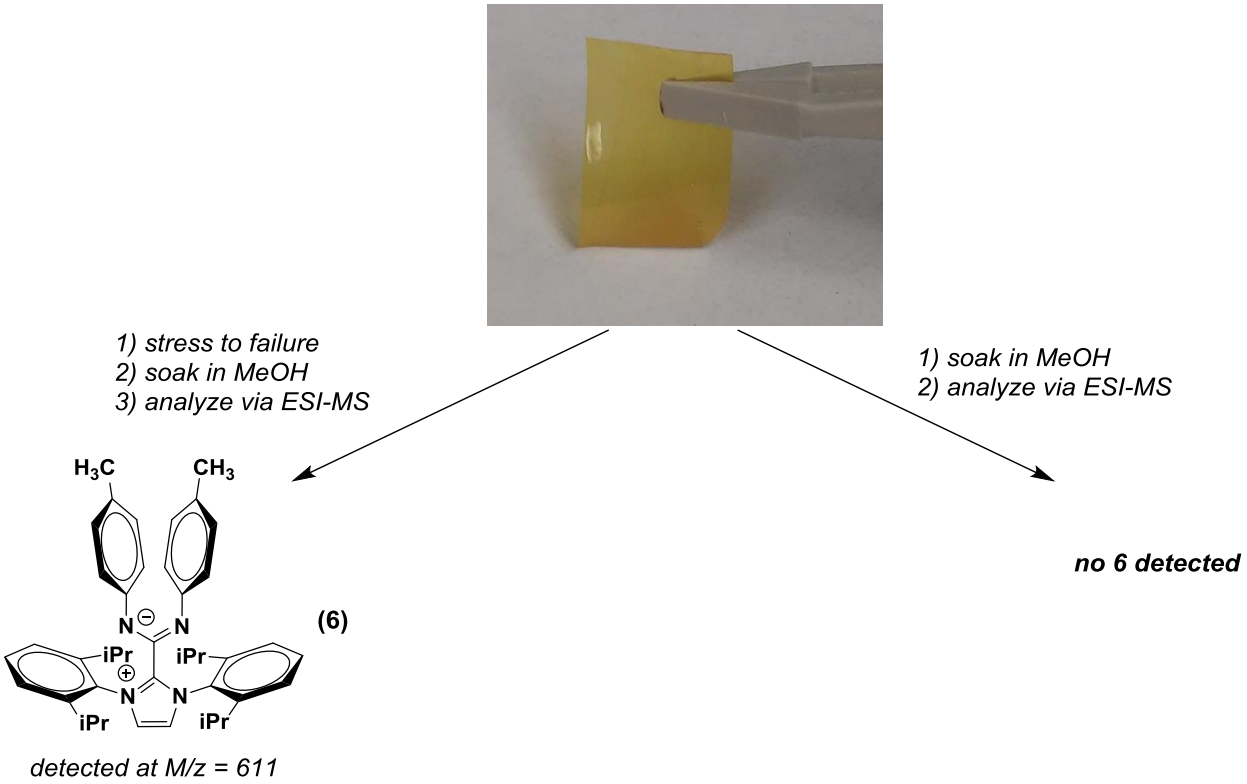


**Figure 3.5**. Results of testing of film **5**, resulting in detection of small molecule adduct **6** arising from crossover of NHC.

orange and yielded polymer **3**. The UV-vis spectrum of **3** exhibited a similar $\lambda_{onset}$ and a peak centered at $\lambda$ = 370 nm compared to an analogous small molecule NHC-CDI **6**, indicating the presence of the desired polymeric adduct (see Experimental). To trap any mechanochemically generated DiPP, ditolylcarbodiimide **4** was added; the presence of small molecule adduct **6** upon the application of force would indicate a crossover of DiPP from **3** to **4**, and thus support the mechanochemical generation of free NHC. Finally, the solution was cast into a Delrin mold and cured under ambient conditions for 60 h to form thin film **5**, consisting of polymer **3** impregnated with **4**.

To assess the mechanochemical reactivity of the NHC-CDI adduct, samples of **5** were cut into rectangular strips of ca. 40 mg and manually elongated to break (generally 50-100% strain). After soaking the strained samples in MeOH for 2 h, the solution was analyzed by electrospray

ionization-mass spectrometry (ESI-MS). As a control, samples of **5** were soaked in MeOH for 2 h without being subject to force and analyzed in an identical manner. In strained samples, a peak corresponding to the mass of the desired small molecule adduct **6** was detected (Figure 3.5), indicating mechanochemical NHC release and trapping by **4**. Importantly, this mass was not detected in unstrained samples, nor in films in which the polymeric NHC-CDI adduct was not present (see Experimental). Thermolysis conducted without the application of force to a sample of **5** also led to detection of the same mass, confirming the dynamic nature of the NHC-CDI equilibrium at elevated temperatures and supporting the ability of the NHC to migrate from polymer to small molecule in the solid state.

Encouraged by these results, we sought to utilize the mechanochemically-generated NHC to effect a secondary transformation. NHCs have been demonstrated to be extremely efficient polymerization initators for a variety of monomers,[15] and the initation of a secondary polymerization reaction upon the application of stress could enable advances in self-healing or reinforcing materials. In particular, the polymerization of lactide seemed an attractive option as it proceeds extremely rapidly when initiated by diaryl imidazolylidenes.[22] Thus, film **7**, analogous to **5** but using lactide in place of **4** as the substrate for reaction with NHC, was prepared and manually elongated to failure. However, no lactide conversion to poly(lactic acid) was detected by NMR or ESI-MS after soaking in $CDCl_3$ or MeOH, respectively. Testing of NHC release in THF, $CH_2Cl_2$, DMF, and MeOH solution was also conducted using thin films consisting solely of **3** and dissolved lactide to test for initiation under solution. Unfortunately, significant dissolution and/or plasticization of films was observed, leading to little or no strain to break and no conversion of lactide. Thus, the use of flex-activated NHC-CDI adducts to perform

organocatalytic transformations has so far been unsuccessful, and is an ongoing subject of investigation in our group.

**Section 3: Conclusions**

In summary, we have investigated the mechanochemical flex activation of NHC-CDI adducts in the solid state. By incorporating a small molecule carbodiimide to serve as a trapping agent and straining films consisting of polymeric NHC-CDI adducts, crossover of the NHC from the polymer to the small molecule was observed by ESI-MS in strained samples. Controls indicated this effect to be likely of mechanochemical origin, as crossover was not observed in the absence of force nor was the putative crossover adduct peak observed in the absence of NHC-CDI adduct in the polymer. Further attempts to utilize the released NHC as a polymerization initiator have thus far been unsuccessful, likely due to the lack of efficient mass transport in the solid state versus in solution; however, difficulties arising from plasticization of solid samples have so far precluded activation and NHC release under solution. Additionally, in cases in which NHC release was observed, the qualitative nature of ESI-MS prevents calculation of % activation of the mechanophore. Solving these complications is a subject of ongoing investigation.

**Section 4: Experimental**

*General Considerations***.** Tetrahydrofuran was obtained from a solvent purification system. $^{1}$H and $^{13}$C NMR spectra were recorded on Bruker AVance 300 MHz or 500 MHz spectrometers. Chemical shifts are reported in delta (δ) units, expressed in parts per million (ppm) downfield from tetramethylsilane using the residual protio-solvent as an internal standard ($CDCl_3$, $^{1}$H: 7.26 ppm and $^{13}$C: 77.0 ppm; DMSO-$d_6$, $^{1}$H: 2.49 ppm and $^{13}$C: 39.5 ppm). LRMS was performed on

a Bruker Esquire equipped with an electrospray ionization (ESI) source. UV-Vis spectroscopy was performed on a Varian Cary 5000 spectrophotometer. IR spectroscopy was performed with a Perkin Elmer Spectrum RX I FTIR spectrometer. All reagents and solvents were obtained from commercial sources and used as received unless otherwise specified. 1,3-bis(2,6-diisopropylphenyl)imidazolium chloride,[23] 3-methyl-1-phenylphospholene oxide **1**,[24] and compound **6**[13] were synthesized as previously described.

Preparation of **2**. In a 20 mL scintillation vial under $N_2$ atmosphere, 2,4-tolylene diisocyanate (0.42 mL, 3 mmol) and poly(tetramethylene glycol) (MW = 650; dried *in vacuo* at 60 °C for 2 d prior to use) (98 mg, 0.15 mmol) were dissolved in THF (5 mL). The vial was sealed with a septum and the contents heated at 70 °C for 30 min. At this time, a stock solution of catalyst **1** (0.2 mL, 0.10 mmol; stock solution 100 mg/mL in THF) was added, and the solution began bubbling rapidly as $CO_2$ evolved. The polymerization proceeded for 2 h after which it was cooled to room temperature, yielding random copolymer **2** which was used immediately without any further purification.

Preparation of **3**. In a 20 mL scintillation vial under $N_2$ atmosphere, 1,3-bis(2,6-diisopropylphenyl)imidazolium chloride (127 mg, 0.30 mmol) and potassium *tert*-butoxide (37 mg, 0.30 mmol) were dissolved in THF (2 mL). The solution was stirred under $N_2$ for 2 h, during which time the solution changed color from a light pink to pale yellow. The resulting solution was taken up and filtered through a 0.45 micron PTFE syringe filter, then added to the solution of freshly prepared **2**. Upon addition, a bright yellow color was observed, which deepened to a vivid orange as addition of the NHC solution was completed. The reaction was stirred under $N_2$

atmosphere at ambient temperature for 30 min. Random copolymer **3** was used immediately without any further purification. The intractable nature of the polymer upon precipitation or curing precluded more extensive purification and characterization; nevertheless, NMR (Figure 3.6), IR (Figure 3.7), and UV-Vis analysis (Figure 3.8) of **3** support the proposed structure.

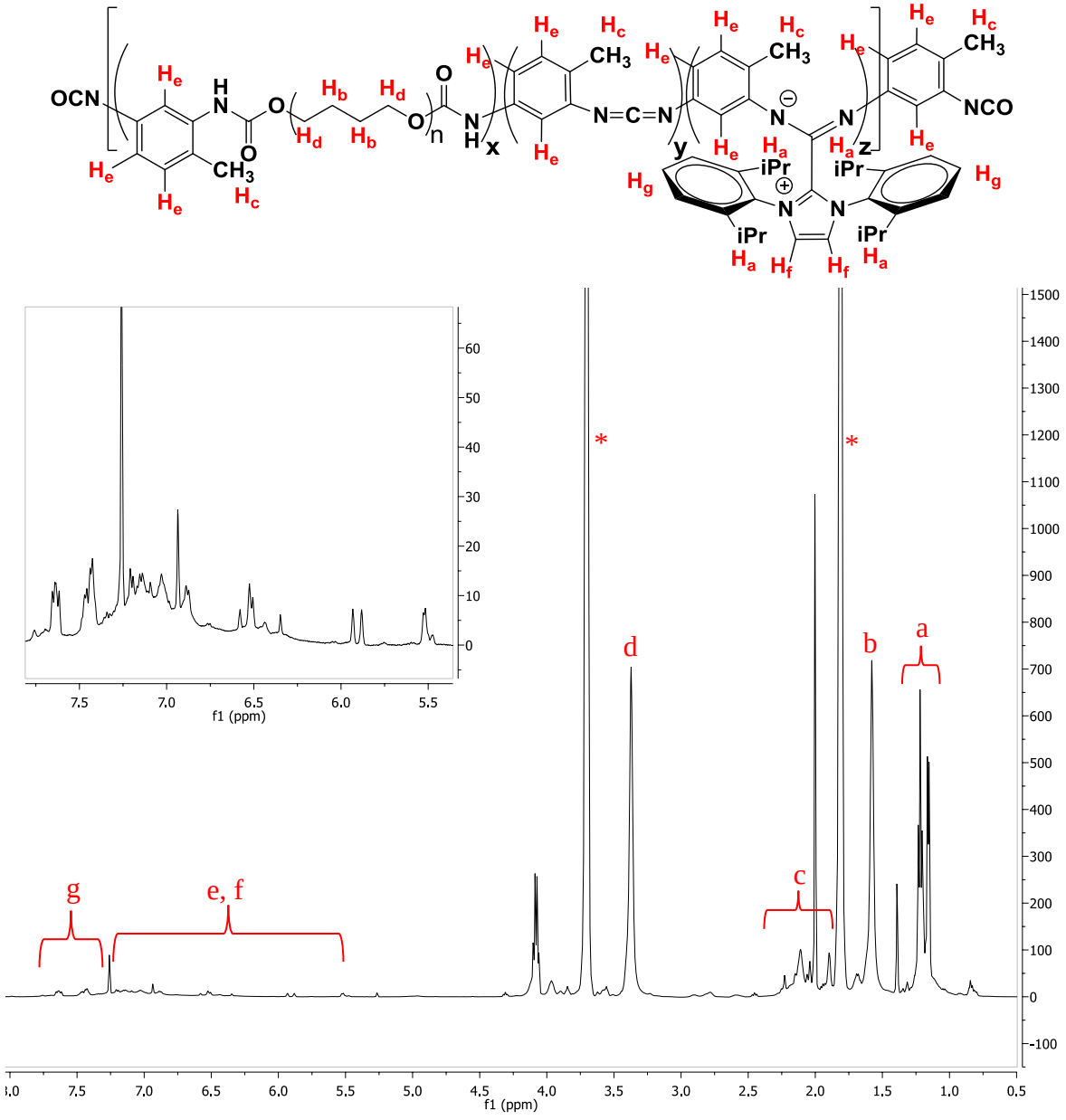


**Figure 3.6**. NMR analysis of concentrated THF solution of polymer **5**. Note broadening associated with backbone aryl groups ($H_c$, $H_e$) due to presence of varied regioisomers. Inset = aromatic region, showing broadening in detail. * = THF.

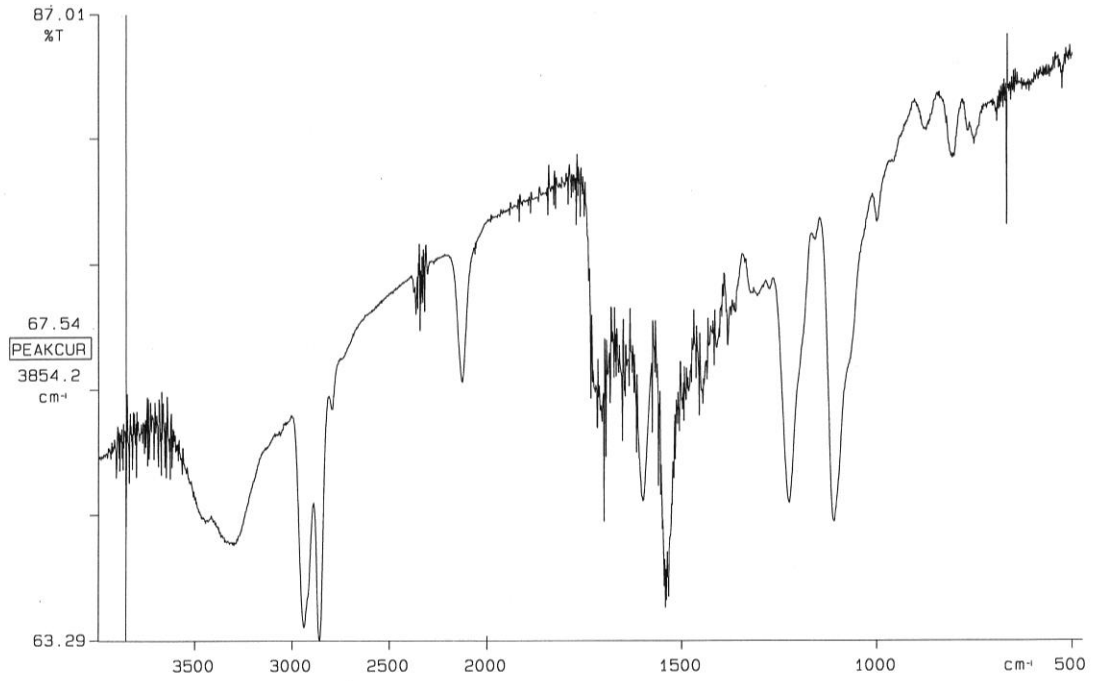


**Figure 3.7**. IR spectrum of polymer **3**. Note carbodiimide stretching frequency (ca. 2100 $cm^{-1}$).

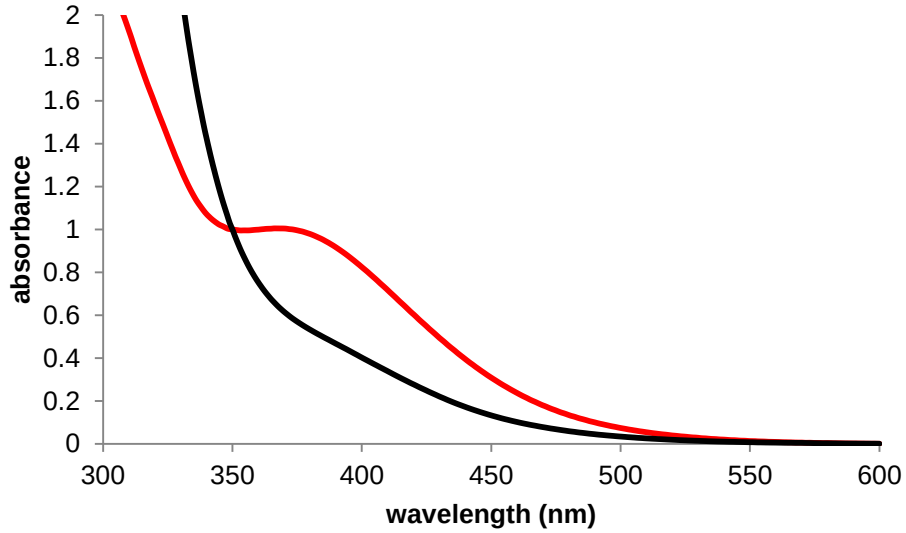


**Figure 3.8**. UV-Vis traces of small molecule **6** (red) and polymer **3** (black). Note similar $\lambda_{onset}$ at ca. 550 nm, and peak centered at ca. 370 nm, observed as a shoulder in **3** due to overlap with other absorbances from other polymer components. Peaks normalized to absorbance at 350 nm.

Preparation of **4**. In a flame-dried flask under N2 atmosphere, catalyst **1** (200 mg, 1.04 mmol).was added to neat *p*-tolyl isocyanate (4.0 mL, 31.7 mmol). The reaction was heated at 50 °C and monitored by NMR spectroscopy. After 2.5 h, full conversion of isocyanate was achieved. Vacuum distillation (135 mtorr, 120 °C) yielded **4** as a colorless liquid that crystallized upon standing (3.32 g, 94%). Spectral values were consistent with those reported elsewhere.[25]

Preparation of **5**. A freshly prepared solution of **3** was opened to air and **4** (349 mg, 1.52 mmol) was added. Upon full dissolution of **4**, the solution was cast into a Delrin mold, covered with aluminum foil, and cured under ambient conditions for 60 h, yielding **5** as a thin, flexible film (958 mg).

Preparation of **7**. Film **7** was prepared in a manner identical to **5**, using lactide (219 mg, 1.52 mmol) in place of **4**.

Preparation of films without NHC-CDI adduct. Control films were prepared in a manner identical to **5**, using polymer **2** in place of **3**.

*General procedure for elongation studies.* A rectangular sample of polymer film (approx. 40 mg) was cut and the dimensions measured. The film was clasped at both ends with forceps and elongated manually over the course of approximately 10 seconds until macroscopic failure occurred; the observed strains were estimated to be generally 50–100%. The pieces of film were soaked in 5 mL MeOH or 2 mL $CDCl_3$ for 2 h, and the soak solution was analyzed directly.

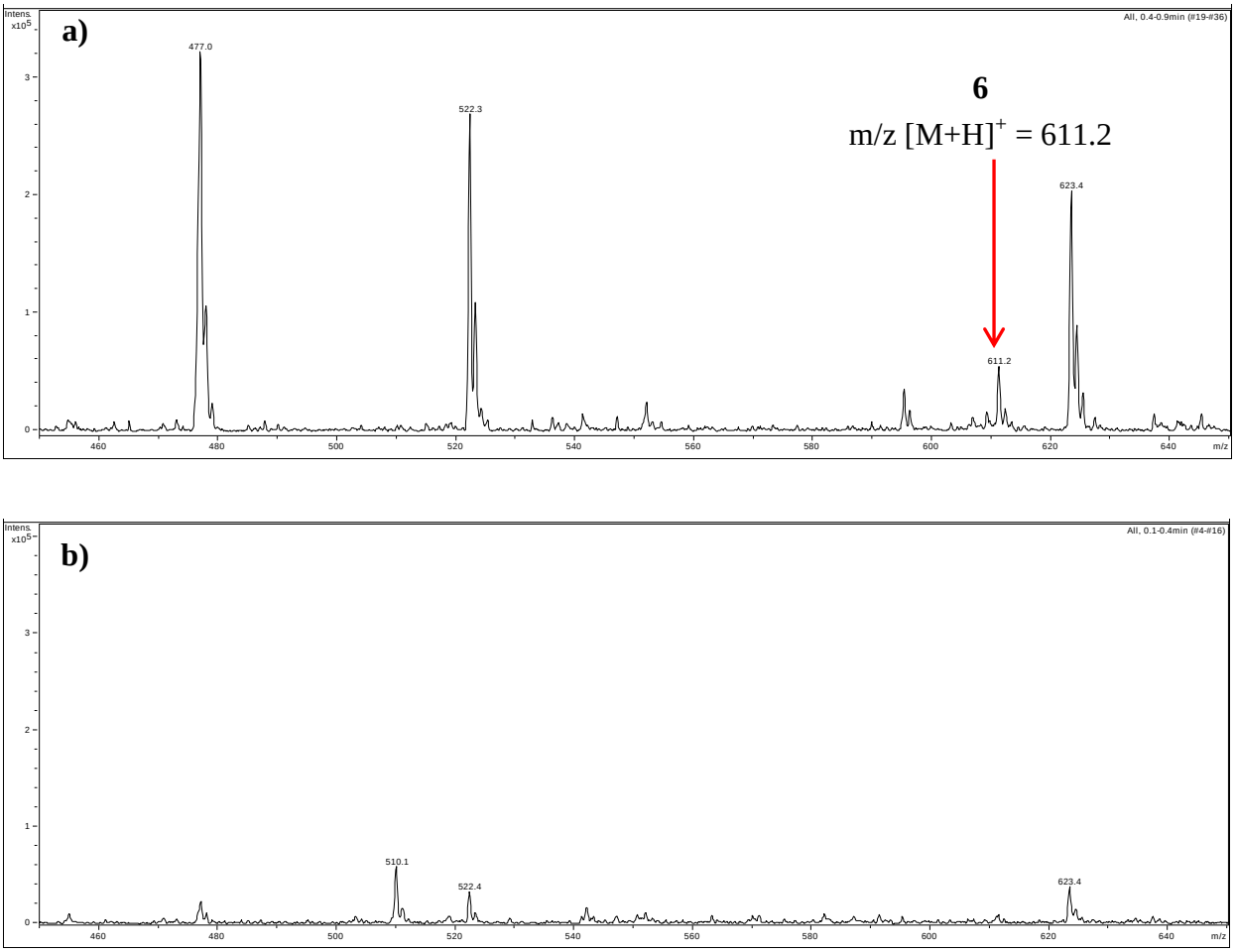


**Figure 3.9**. ESI-MS spectra of (a) sample of **5** elongated to failure, with **6** detected at M/z = 611.2; (b) unstrained sample of **5**. Spectra enlarged from M/z = 450 to 650. Scales on y-axis are identical.

In experiments under solution, the procedure was identical except for taking place under 10 mL of the desired solvent. After straining, solvent was removed under reduced pressure and the residue taken up in MeOH or $CDCl_3$ for analysis.

*General procedure for thermolysis*. Samples of polymer film (approx. 40 mg) were sealed in a 20 mL scintillation vial with a Teflon-lined cap and heated to 100 °C for 2 h. Upon cooling, the MeOH was added, the polymer soaked for 2 h, and the solution analyzed directly by ESI-MS.

*CoGEF analysis of NHC-CDI mechanophore.* Density functional theory (DFT) calculations were

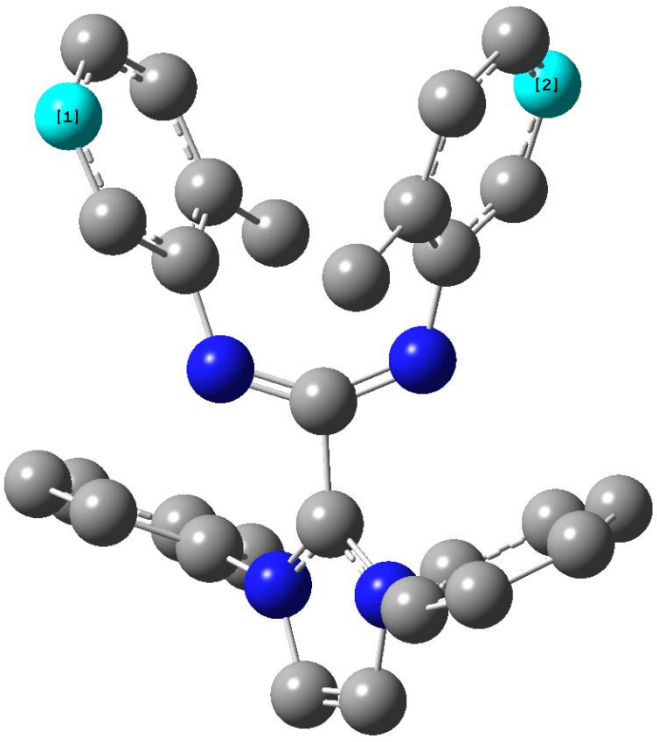


**Figure 3.10**. C1-C2 distance utilized for CoGEF calculations. Hydrogens omitted for clarity.

performed at the B3LYP 6-31G* (d) level of theory using the Gaussian 09 program package. To simulate the effects of elongational force on the NHC-CDI adduct, relaxed PES scans were performed. Starting from the optimized equilibrium geometry, the distance between the two atoms highlighted (Figure 3.10) was increased incrementally by 0.25 Å and constrained while optimizing the geometry of the rest of the molecule. This distance was chosen so as to simulate the point of attachment in a poly(carbodiimide) synthesized from 2,4-tolylene diisocyanate.

**Notes and References for Chapter 3**

[1] For recent reviews, see: (a) Brantley, J. N.; Bailey, C. B.; Wiggins, K. M.; Ketinge-Clay, A. T.; Bielawski, C. W. *Polym Chem.* **2013**, *4*, 3916. (b) May, P. A.; Moore, J. S. *Chem. Soc. Rev.* **2013**, *42*, 7497. (c) Wiggins, K. M.; Brantley, J. N.; Bielawski, C. W. *Chem. Soc. Rev.* **2013**, *42*, 7130. (d) Brantley, J. N.; Wiggins, K. M.; Bielawski, C. W. *Polym. Int.* **2012**, *62*, 2. (e) Ariga, K.; Mori, T.; Hill, J. P. *Adv. Mater.* **2012**, *24*, 158. (f) Caruso, M. M.; Davis, D. A.; Shen, Q.; Odom, S. A.; Sottos, N. R.; White, S. R.; Moore, J. S. *Chem. Rev.* **2009**, *109*, 5755. (g) Beyer, M. K.; Clausen-Schaumann, H. *Chem. Rev.* **2005**, *105*, 2921.

[2] (a) Imato, K.; Irie, A.; Kosuge, T.; Ohishi, T.; Nishihara, M.; Takahara, A.; Otsuka, H. *Angew. Chem. Int. Ed.* **2015**, *127*, 6266. (b) Fitch, K. R.; Goodwin, A. P. *Chem. Mater.* **2014**, *26*, 6771. (c) Park, I.; Sheiko, S. S.; Nese, A.; Matyjaszewski, K. *Macromolecules* **2009**, *42*, 1805 (d) Berkowski, K. L; Potisek, S. L.; Hickenboth, C. R.; Moore, J. S. *Macromolecules* **2005**, *38*, 8975.

[3] For an example of epoxide ring opening, see: Klukovich, H. M.; Kean, Z. S.; Ramirez, A. L. B.; Lenhardt, J. M.; Lin, J.; Hu, X.; Craig, S. L. *J. Am. Chem. Soc.* **2012**, *134*, 9577.

[4] For examples of cyclopropane ring opening, see: (a) Klukovich, H. M.; Kouznetsova, T. B.; Kean, Z. S.; Lenhardt, J. M.; Craig, S. L. *Nat. Chem.* **2013**, *5*, 110. (b) Kean, Z. S.; Craig, S. L. *Polymer* **2012**, *53*, 1035. (c) Lenhardt, J. M.; Black, A. L.; Beiermann, B. A.; Steinberg, B. D.; Rahman, F.; Samborski, T.; Elsakr, J.; Moore, J. S.; Sottos, N. R.; Craig, S. L. *J. Mater. Chem.* **2011**, *21*, 8454. (d) Lenhardt, J. M.; Black, A. L.; Craig, S. L. *J. Am. Chem. Soc.* **2009**, *131*, 10818.

[5] For examples of electrocyclic ring opening of benzocyclobutene, see: (a) Hickenboth, C. R.; Moore, J. S.; White, S. R.; Sottos, N. R.; Baudry, J.; Wilson, S. R. *Nature* **2007**, *446*, 423. (b) Potisek, S. L.; Davis, D. A.; Sottos, N. R.; White, S. R.; Moore, J. S. *J. Am. Chem. Soc.* **2007**, *129*, 13808.

[6] For examples of retro [2+2] cycloaddition, see: (a) Kean, Z. S.; Gossweiler, G. R.; Kouznetsova, T. B.; Hewage, G. B.; Craig, S. L. *Chem. Commun.* **2015**, *51*, 9157. (b) Klukovich, H. M.; Kean, Z. S.; Iacono, S. T.; Craig, S. L. *J. Am. Chem. Soc.* **2011**, *133*, 17882. (c) Kryger, M. J.; Munaretto, A. M.; Moore, J. S. *J. Am. Chem. Soc.* **2011**, *133*, 18992. (d) Kryger, M. J.; Ong, M. T.; Odom, S. A.; Sottos, N. R.; White, S. R.; Martínez, T. J.; Moore, J. S. *J. Am. Chem. Soc.* **2010**, *132*, 4558.

[7] For representative examples, see: (a) Kim, J.-W.; Jung, Y.; Coates, G. W.; Silberstein, M. N. *Macromolecules*, **2015**, *48*, 1335. (b) Lee, C. K.; Davis, D. A.; White, S. R.; Moore, J. S.; Sottos, N. R.; Braun, P. V. *J. Am. Chem. Soc.* **2010**, *132*, 16107. (c) Davis, D. A.; Hamilton, A.; Yang, J.; Cremar, L. D.; Van Gough, D.; Potisek, S. L.; Ong, M. T.; Braun, P. V.; Martínez, T. J.; White, S. R.; Moore, J. S.; Sottos, N. R. *Nature* **2009**, *459*, 68.

[8] (a) Ducrot, E.; Chen, Y.; Bulters, M.; Sijbesma, R. P.; Creton, C. *Science* **2014**, *344*, 186. (b) Chen, Y.; Sijbesma, R. P. *Macromolecules* **2014**, *47*, 3797. (c) Chen, Y.; Spiering, A. J. H.; Karthikeyan, S.; Peters, G. W. M.; Meijer, E. W.; Sijbesma, R. P. *Nature Chem.* **2012**, *4*, 559.

[9] (a) Jakobs, R. T. M.; Ma, S.; Sijbesma, R. P. *ACS Macro Lett.* **2013**, *2*, 613. (b) Piermattei, A.; Karthikeyan, S.; Sijbesma, R. P. *Nat. Chem.* **2009**, *1*, 133. (c) Paulusse, J. M.; Sijbesma, R. P. *Chem. Commun.* **2008**, 4416.

[10] Diesendruck, C. E.; Steinberg, B. D.; Sugai, S. N.; Silberstein, M. N.; Sottos, N. R.; White, S. R.; Braun, P. V.; Moore, J. S. *J. Am. Chem. Soc.* **2012**, *134*, 12446.

[11] (a) Larsen, M. B.; Boydston, A. J. *J. Am. Chem. Soc.* **2014**, *136*, 1276. (b) Larsen, M. B.; Boydston, A. J. *J. Am. Chem. Soc.* **2013**, *135*, 8189.
[12] Gossweiler, G. R.; Hewage, G. B.; Soriano, G.; Wang, Q.; Welshofer, G. W.; Zhao, X.; Craig, S. L. *ACS Macro Lett.* **2014**, *3*, 216.
[13] Zhukhovitskiy, A. V.; Geng, J.; Johnson, J. A. *Chem. Eur. J.* **2015**, *15*, 5685.
[14] For recent reviews of NHC organocatalysis, see: (a) Flanigan, D. M.; Romanov-Michailidis, F.; White, N. A.; Rovis, T. *Chem. Rev.* **2015**, DOI: 10.1021/acs.chemrev.5b00060. (b) Bugaut, X.; Glorius, F. *Chem. Soc. Rev.* **2012**, *41*, 3511. (c) Enders, D.; Niemeier, O.; Henseler, A. *Chem. Rev.* **2007**, *107*, 5606.
[15] For recent reviews of NHCs in the context of polymer chemistry, see: (a) Naumann, S.; Dove, A. P. *Polym. Chem.* **2015**, *6*, 3185. (b) Fèvre, M.; Pinaud, J.; Gnanou, Y.; Vignolle, J.; Taton, D. *Chem. Soc. Rev.* **2013**, *42*, 2142.
[16] For recent reviews of NHCs as ligands, see: (a) Hopkinson, M. N.; Richter, C.; Schedler, M.; Glorius, F. *Nature* **2014**, *510*, 485. (b) Bézier, D.; Sortais, J.-B.; Darcel, C. *Adv. Synth. Catal.* **2013**, *355*, 19. (c) Fortman, G. C.; Nolan, S. P. *Chem. Soc. Rev.* **2011**, *40*, 5151. (d) Hahn, F. E.; Jahnke, M. C. *Angew. Chem. Int. Ed.* **2008**, *47*, 3122.
[17] Beyer, M. K. *J. Chem. Phys.* **2000**, *112*, 7307.
[18] Gaussian 09, Revision A.1, Frisch, M. J.; Trucks, G. W.; Schlegel, H. B.; Scuseria, G. E.; Robb, M. A.; Cheeseman, J. R.; Scalmani, G.; Barone, V.; Mennucci, B.; Petersson, G. A.; Nakatsuji, H.; Caricato, M.; Li, X.; Hratchian, H. P.; Izmaylov, A. F.; Bloino, J.; Zheng, G.; Sonnenberg, J. L.; Hada, M.; Ehara, M.; Toyota, K.; Fukuda, R.; Hasegawa, J.; Ishida, M.; Nakajima, T.; Honda, Y.; Kitao, O.; Nakai, H.; Vreven, T.; Montgomery, Jr., J. A.; Peralta, J. E.; Ogliaro, F.; Bearpark, M.; Heyd, J. J.; Brothers, E.; Kudin, K. N.; Staroverov, V. N.; Kobayashi, R.; Normand, J.; Raghavachari, K.; Rendell, A.; Burant, J. C.; Iyengar, S. S.; Tomasi, J.; Cossi, M.; Rega, N.; Millam, J. M.; Klene, M.; Knox, J. E.; Cross, J. B.; Bakken, V.; Adamo, C.; Jaramillo, J.; Gomperts, R.; Stratmann, R. E.; Yazyev, O.; Austin, A. J.; Cammi, R.; Pomelli, C.; Ochterski, J. W.; Martin, R. L.; Morokuma, K.; Zakrzewski, V. G.; Voth, G. A.; Salvador, P.; Dannenberg, J. J.; Dapprich, S.; Daniels, A. D.; Farkas, Ö.; Foresman, J. B.; Ortiz, J. V.; Cioslowski, J.; Fox, D. J. Gaussian, Inc., Wallingford CT, 2009.
[19] Campbell, T. W.; Monagle, J. J.; Foldi, V. S. *J. Am. Chem. Soc.* **1962**, *84*, 3673.
[20] Campbell, T. W.; Smeltz, K. C. *J. Org. Chem.* **1963**, *28*, 2069.
[21] Analogous films synthesized without the addition of polyether were extremely brittle and showed little to no elongation prior to macroscopic failure.
[22] Connor, E. F.; Nyce, G. W.; Myers, M.; Möck, A.; Hedrick, J. L. *J. Am. Chem. Soc.* **2002**, *124*, 914.
[23] Hintermann, L. *Beilstein J. Org. Chem.* **2007**, *3*, No. 22.
[24] McCormack, W. B. *Org. Synth.* **1963**, *43*, 73.
[25] Zhu, C.; Xu, D.; Wei, Y. *Synthesis* **2011**, *5*, 711.

# Chapter 4. 3D Printed Mechanochromic Materials[1]

## Section 1: Introduction

Three-dimensional printing (3DP) is a method of additive manufacturing that enables the construction of 3D objects based upon a digital model. Although the basic methods for 3DP have been known for decades, the area has seen a recent surge of interest as researchers continue to develop new materials that enhance the capabilities of 3DP and as broader communities find new applications that benefit from software-reconfigurable rapid prototyping.[1–3] When a digital model is supplied to the printer, the printing system uses slicing software that converts the 3D model to 2D slice descriptions, and a G-code generator converts the slice descriptions into numerically controlled machine instructions. With this approach to manufacturing, the time and resources required for production of a single prototype of an envisioned object are streamlined. In contrast to traditional manufacturing techniques, such as injection or compression molding, the advantages of 3DP include increased customizability, ease of use, orthogonality to existing manufacturing techniques, and accessibility to the technique by a wide user base of a variety of backgrounds and skill levels. Fused filament fabrication (FFF), for instance, has become accessible in private homes for printing the likes of toys, housewares, art pieces, and accessories for portable electronics.

An exciting and potentially transformative area of growth is the integration of functional polymeric materials with 3DP technologies.[1,2] As these areas merge, the capabilities afforded by designer polymer synthesis can be incorporated into rapidly customizable objects and devices.[4,5]

[1] Reproduced with permission from Peterson, G. I.; Larsen, M. B.; Ganter, M. A.; Storti, D. W.; Boydston, A. J. "3D-Printed Mechanochromic Materials" *ACS Appl. Mater. Interfaces* **2015**, *7*, 577.

Examples of 3D-printed functional materials and devices include drug delivery platforms,[6] tissue scaffolds,[7,8] energy storage devices,[9] electrically conductive materials,[10] and force-sensors.[11]

We envisioned the ability to incorporate mechanochemically-responsive units into materials amenable to 3DP techniques to produce printed objects with well-defined shapes and regions capable of chemo-mechanical coupling. Recent advances in polymer mechanochemistry have given rise to systems that translate macroscopic mechanical force into specific chemical reactivity.[12] In the solid state, mechanoresponsive polymers and materials have shown promise for applications including mechanochromic and mechanoluminescent force sensors,[13,14] mechano-catalysis,[15] self-reinforcing materials,[15,16] and scaffolds for small molecule release.[13a,17,18] Among the various mechanophores reported in the literature, we were particularly interested in the mechanochromic spiropyran systems that have been extensively studied in the field, as the ease of determining qualitative activation in this system is unmatched.[13] Upon application of force across the $C_{spiro}$-O bond (Figure 4.1), isomerization of the spiropyran to its highly colored purple merocyanine isomer can be accomplished, effectively enabling the self-reporting of stress accumulation within a macroscopic material via readily identifiable color change.

In this section, we characterize the mechanical properties of the printed materials and explore the extent to which polymer degradation occurs during filament formation and extrusion

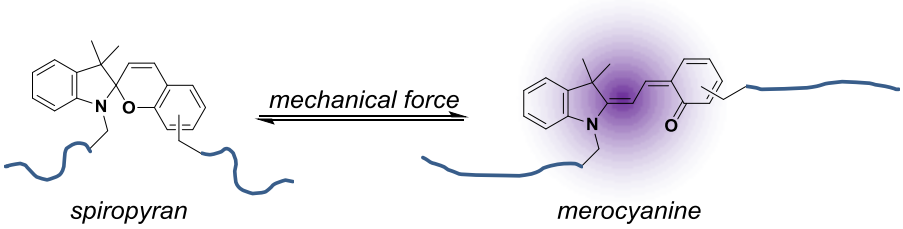


**Figure 4.1**. Generalized depiction of the mechanochemical isomerization of a spiropyran moiety to its merocyanine form.

printing. We also examine the incorporation of different spiropyran moieties into 3D printed PCL. Specifically, we prepare multicomponent specimens that display selective activation of specific regions in the materials, depending on the stimulus being applied. These results include the first demonstration of a spiropyran that is uniquely responsive to mechanical force without displaying the same photoresponsiveness observed from all previously reported spiropyran mechanophores. We also showcase the unique abilities of 3DP in contrast with other traditional manufacturing techniques by demonstrating rapid customization of the dynamic sensing range of a force sensor. The utility of this paradigm and its suitability for broad adoption is supported by presenting illustrative results obtained using only inexpensive entry-level 3DP technology and freely available software.

## Section 2: Results and Discussion

### *4.2.a Spatial Localization of Mechanochromic Responses*

Three spiropyran containing polymers were prepared via ring opening polymerization of

**Scheme 4.1**. Synthesis of polymers **3**, **4**, and **8**.

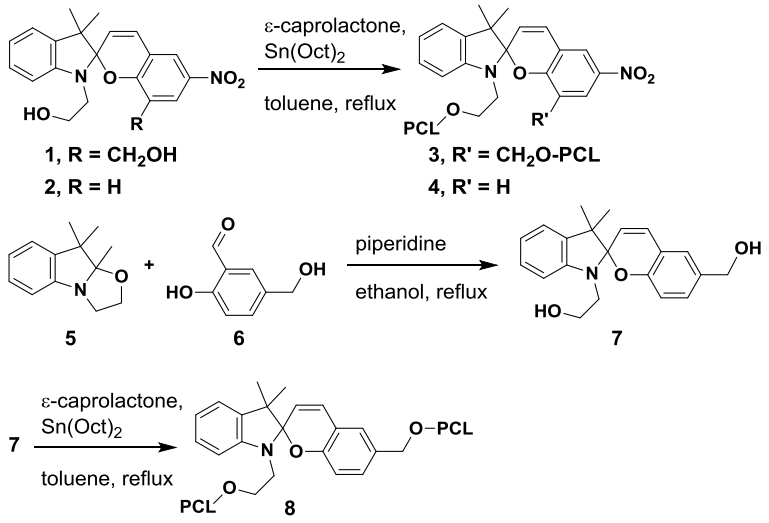

ε-caprolactone from spiropyran alcohol initiators (Scheme 4.1). Polymers **3** ($M_w$ = 90.0 kDa, Đ = 1.16) and **8** ($M_w$ = 82.5 kDa, Đ = 1.18) bear chain-centered spiropyrans such that elongation of the polymer results in stress accumulation across the desired $C_{spiro}$-O bond, and isomerization is activated. In contrast, polymer **4** ($M_w$ = 64.9 kDa, Đ = 1.43) has a chain-end spiropyran moiety such that stress will not be accumulated across the necessary bond, and thus it should not be activated by mechanical stimulus. Notably, each of these polymers is of sufficient molecular weight to accumulate tensile forces within the main chain that are great enough to induce mechanochemical activation.

Each polymer was blended with commercial PCL (**C**) at various concentrations (Table 4.1). The wt % of each spiropyran-containing polymer is denoted by the subscript (e.g., $\mathbf{3_{10}}$ is comprised of 10 wt % **3** and 90 wt % **C**). Filament was prepared using a single screw melt extruder. Average batch-to-batch filament diameters ranged from ca. 1.55 to 1.85 mm, with variation along the filament typically being less than ± 0.05 mm. The custom filaments were

**Table 4.1**. Structure, molecular weight, and dispersity data for the synthesized and commercial polymer, and compositions of various filament types.

| Filament | Polymer | $M_w$ (kDa), Đ | Blend | Spiropyran % w/w |
|---|---|---|---|---|
| $\mathbf{3_{10}}$ | **3** | 90.0, 1.16 | 10% w/w with **C** | 0.05 |
| $\mathbf{3_{50}}$ | | | 50% w/w with **C** | 0.25 |
| $\mathbf{3_{100}}$ | | | none | 0.50 |
| $\mathbf{4_{50}}$ | **4** | 64.9, 1.43 | 50% w/w with **C** | 0.39 |
| $\mathbf{8_{50}}$ | **8** | 82.5, 1.18 | 50% w/w with **C** | 0.43 |
| $\mathbf{C_{100}}$ | **C** | 62.7, 1.29 | none | none |

used to print tensile testing specimens using a commercial dual-extrusion head FFF printer. Printing was initially performed using only one of the extrusion heads set at a temperature of 110 °C, a non-heated build plate, and a relatively slow print speed of 20 mm/s (in comparison with 120 – 150 mm/s typically used for printing acrylonitrile-butadiene-styrene or poly(lactic acid) filament). Due to the relatively flexible nature of the filament, retraction was disabled to avoid jamming of the filament during printing.

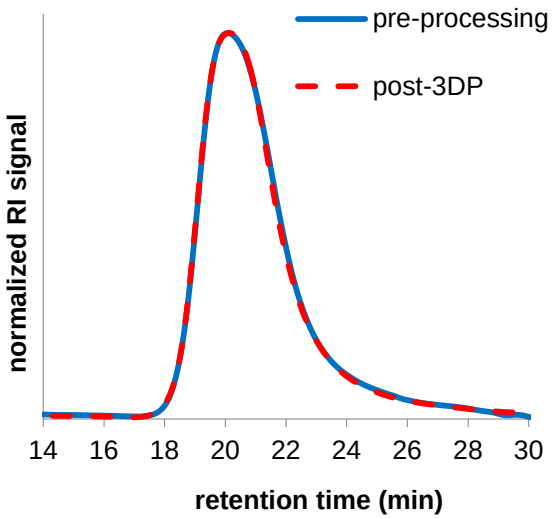


**Figure 4.2**. GPC chromatograms of polymer **3** prior to any filament or print processing and after 3DP.

During the mixing and melt extrusion steps of the filament formation process, no color changes were observed from any of the spiropyran-containing materials. Additionally, no color changes were observed during printing, indicating no thermal activation of the spiropyran was taking place. To determine if any polymer degradation was occurring during the pre-print processing or printing, a printed specimen was subjected to GPC analysis. No detectable changes in polymer molecular weight or dispersity were observed as compared to the virgin polymer (Figure 4.2).

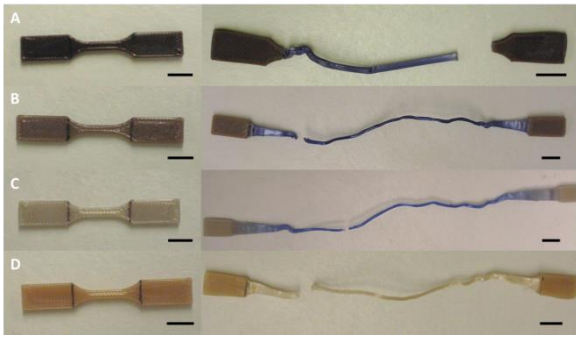


**Figure 4.3**. Tensile test specimens made from (a) $\mathbf{3}_{100}$, (b) $\mathbf{3}_{50}$, (c) $\mathbf{3}_{10}$, and (d) $\mathbf{4}_{50}$ pre- and post-elongation. The vertical marks on the specimen indicate the position of the load frame clamps. Scale bars = 10 mm.

To examine the basic mechanochemical reactivity and mechanical properties of the materials and to ensure a controlled environment for elongation, tensile testing of "dog bone" shaped specimens was performed on an Instron load frame. In all cases in which **3** was present, color change from brown to purple was observed upon elongation and necking of the sample, signifying mechanochemical activation of the spiropyran in accordance with previous studies.[13] While the intensity of the resulting color was directly related to the amount of **3** used in the blend (Figure 4.3), the most apparent contrast between virgin and elongated (activated) materials was observed for blends having lower loading of spiropyran, due to the lighter color of the unactivated material. No spiropyran activation was observed in the test specimens made from $\mathbf{4}_{50}$ in which the mechanophore is located at a chain end, thus confirming the mechanical origin of the color change. Although the Young's modulus and yield strength of each blended material were found to be lower than that of the non-blends (Table 4.2), all are in good agreement with reported values for PCL.[19] Re-filamentizing the commercial material **C** also led to a decrease in Young's modulus and yield strength. As GPC analysis showed no polymer degradation occurring during the processing/printing process (*vide supra*), a possible explanation in the differences of materials properties between $\mathbf{C}_{100}$ and re-extruded $\mathbf{C}_{100}$ could be the variation in

diameter of the filament made in-house, leading to heterogeneity in the structure of the printed objects.

**Table 4.2**. Summary of the materials properties of the test specimens prepared from the various filament types. Values are an average of three experiments ± one standard deviation.

| Filament Type | Modulus (GPa) | Yield Strength (MPa) | Tensile Strength (MPa) | % elongation to break |
|---|---|---|---|---|
| $\mathbf{C_{100}}$ | 0.336 ± 0.042 | 16.57 ± 0.20 | 33.24 ± 1.15 | 709 ± 25 |
| $\mathbf{C_{100}}$ (re-extruded) | 0.225 ± 0.011 | 13.3 ± 0.10 | n. d.[a] | n. d.[a] |
| $\mathbf{3_{10}}$ | 0.268 ± 0.029 | 13.32 ± 0.42 | 29.50 ± 1.12 | 750 ± 81 |
| $\mathbf{3_{50}}$ | 0.300 ± 0.003 | 14.56 ± 0.48 | 27.17 ± 1.94 | 664 ± 37 |
| $\mathbf{3_{100}}$ | 0.351 ± 0.030 | 17.49 ± 0.24 | 14.86 ± 1.71 | 302 ± 12 |
| $\mathbf{4_{50}}$ | 0.300 ± 0.067 | 15.00 ± 0.21 | 26.82 ± 0.31 | 651 ± 12 |
| $\mathbf{3_{50}}$ encased in $\mathbf{C_{100}}$ | 0.308 ± 0.045 | 15.96 ±0.83 | 33.15 ±1.61 | 716 ±56 |

[a]Not determined. Samples necked into the grip region and slipped from the grips in all samples measured.

We next prepared multi-component specimens that highlight the capabilities of 3DP in contrast with other types of traditional manufacturing methods, such as injection or compression molding. A tensile test specimen comprised of discrete regions of photo- and mechano-responsive $\mathbf{3_{50}}$ and photo-responsive$\mathbf{4_{50}}$ was printed in a single session by using two extrusion heads, each loaded with one of the filament types. In this particular dual extrusion technique, the active print head alternates such that only one head is printing at a time. The test specimen body was comprised mainly of $\mathbf{4_{50}}$ which was used as a housing around two surface channels of $\mathbf{3_{50}}$ that spanned the length of the printed specimen (Figure 4.4). Upon elongation of the sample, only the regions containing $\mathbf{3_{50}}$ were activated, signifying the spatio-control over the material's response to external force. Notably, the spiropyran moieties in both materials were still

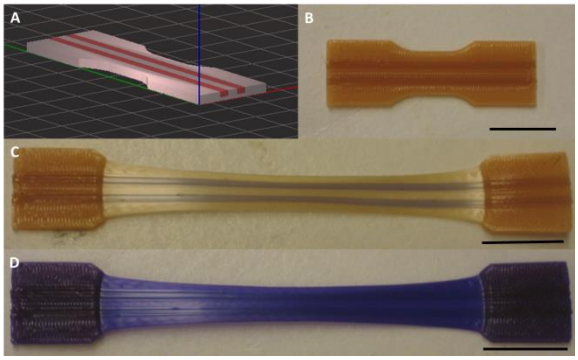


**Figure 4.4**. (a) CAD representation of a multi-component tensile test specimen, with red stripes indicating the location of the mechano-responsive filament $\mathbf{3_{50}}$ (specimen body comprised of $\mathbf{4_{50}}$), (b) test specimen pre-elongation, (c) test specimen post-elongation showing the mechanochromic response of the $\mathbf{3_{50}}$ regions, and (d) test specimen post-elongation after 365 nm UV irradiation showing activation of both the $\mathbf{3_{50}}$ and $\mathbf{4_{50}}$ regions. Scale bars = 20 mm.

susceptible to UV-triggered isomerization and confirmation of spiropyran content throughout the materials was confirmed upon illumination with 365 nm light from a handheld UV lamp.

Absent the electron-withdrawing nitro functionality, the photostationary state of UV-irradiated spiropyrans contains a negligible amount of the corresponding merocyanine isomer, and thus no photochromism is observed.[20,21] However, we found that application of stress across the $C_{spiro}$–O bond still resulted in mechanochromism in this spiropyran. To demonstrate this in a 3D printed specimen, we prepared a multi-component specimen similar to the one depicted in Figure 4.4, but with a body composed of $\mathbf{8_{50}}$ (mechano-responsive, but not photo-responsive), and the surface channels composed of $\mathbf{4_{50}}$, (photo-responsive, but not mechano-responsive) (Figure 4.5a). Irradiation of the specimen with 365 nm UV radiation only led to activation of the regions containing $\mathbf{4_{50}}$ (Figure 4.5b). On the other hand, elongation of the specimen led to activation of the $\mathbf{8_{50}}$ regions but not of the $\mathbf{4_{50}}$ regions (Figure 4.5c), consistent with the results in Figure 4.4. Visually detectable activation of polymer **8** was only readily observed when the polymer was under load; upon relieving the tension on the specimen, the purple color rapidly disappeared. For example, within the ca. 30 s required to remove the sample from the grips in the

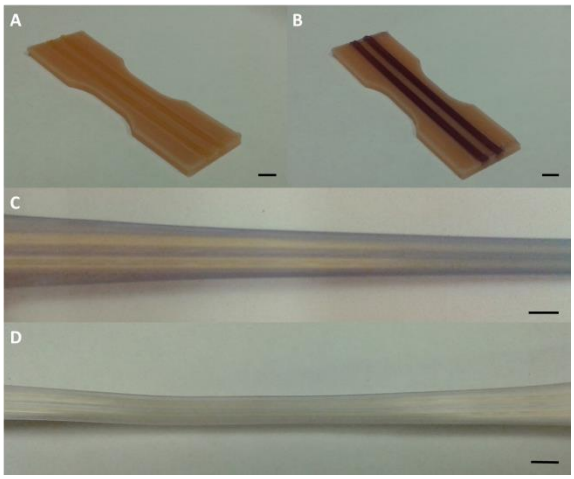


**Figure 4.5**. (a) Test specimen composed of $\mathbf{8}_{50}$ with stripes of $\mathbf{4}_{50}$, (b) test specimen after 365 nm UV irradiation showing the photochromic response of the $\mathbf{4}_{50}$ regions, (c) test specimen under load in the load frame showing the mechanochromic response of the $\mathbf{8}_{50}$ regions, and (d) test specimen ca. 30 s after removal of load showing almost complete loss of the purple color in the $\mathbf{8}_{50}$ regions. Scale bars = 5 mm.

load frame, nearly all of the purple color had disappeared (Figure 4.5d). The reactivity of polymer **8** is significant as it enables the use of these mechanochromic materials in outdoor applications, whereas polymers **3** and **4**, which are both photo-responsive, are rapidly converted to the merocyanine form in direct sunlight.

We then examined the use of 3DP to prepare objects in which a center region of mechanoresponsive $\mathbf{3}_{50}$ was completely encased by $\mathbf{C}_{100}$ (Figure 4.6), a type of structure that would be difficult (if not impossible) to prepare in a single operation via most other manufacturing techniques. Using the dual extrusion method, the target configuration was printed in a single session and then subjected to elongation as before. The $\mathbf{3}_{50}$ region was again activated and the color change was visible from the exterior of the material. The mechanical properties of this specimen design were similar to the specimens comprised solely of **C** (Table 4.2), indicating that the stimuli-responsive properties of $\mathbf{3}_{50}$ can be imparted to larger prints without affecting the bulk properties of the material. Using the same print code and replacing **C** with control filament $\mathbf{4}_{50}$ as the exterior material resulted in a sample in which the $\mathbf{3}_{50}$ region was not visible prior to

elongation (Figure 4.7). Upon tensile testing, the mechanoresponsive core became clearly distinguishable from the encasing filament.

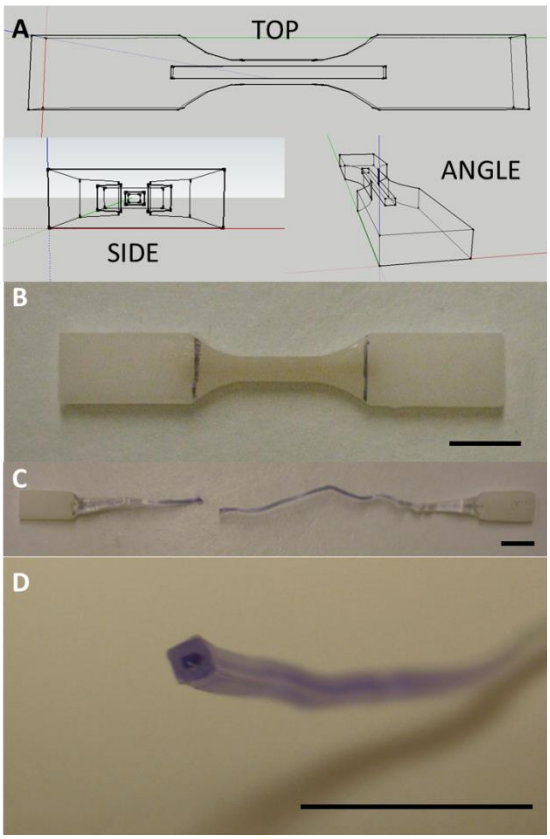


**Figure 4.6**. (a) CAD representations of the tensile test specimen in which the mechano-responsive region is encased by non-mechanoresponsive filament, (b) test specimen in which $3_{50}$ is encased by $C_{100}$ (the vertical lines on the specimen indicate the position of the load frame clamps), (c) test specimen post-elongation showing the mechanochromism of the $3_{50}$ region, and (d) elongated and cut specimen showing the encased filament. Scale bars = 10 mm.

*4.2.b Development of Protoype Force Sensors*

Prototype force sensors were developed to demonstrate the potential engineering applications that can be accessed by integrating mechano-responsive polymers and 3DP technology. An asymmetric tensile test specimen was prepared with multiple embedded regions of $\mathbf{3_{50}}$ spaced evenly within the gauge section (Figure 4.8). Initial testing of dog bones with constant cross-section produced force-extension curves that were flat between initial necking and eventual strain hardening (see Experimental). This led us to pursue an asymmetric dog bone with

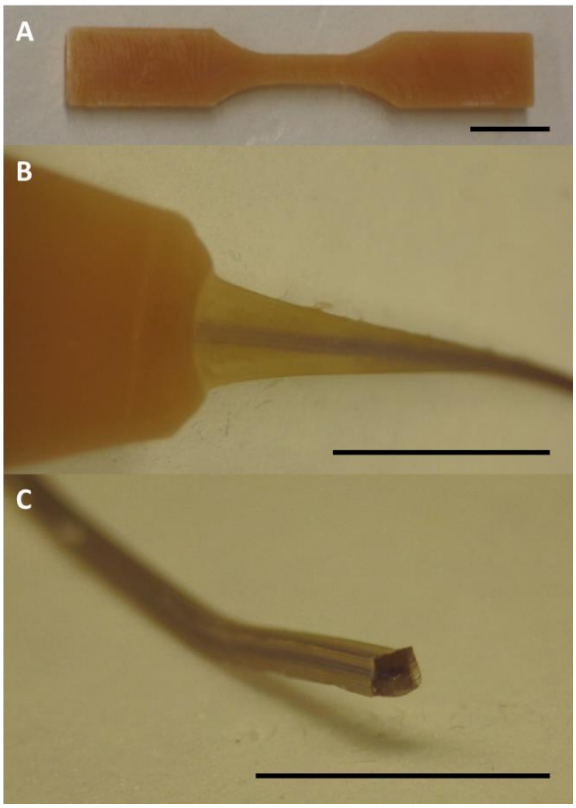


**Figure 4.7**. (a) Tensile test specimen in which $\mathbf{3}_{50}$ is encased by $\mathbf{4}_{50}$, (b) test specimen post-elongation showing the mechanochromism of the $\mathbf{3}_{50}$ region, and (c) elongated and cut specimen showing the encased filament. Scale bars = 10 mm**.**

a variable cross-section. Introducing a section width that varies linearly with displacement along the axis of symmetry resulted in a relationship between the extension and the force required to draw the material that is linear over a broad domain of extension. By controlling the initial location and direction in which the material necks, the design ensures sequential and predictable activation of each mechano-responsive region (see Experimental). The onset of activation of each region is directly related to a specific force that was applied to the specimen (Figure 4.9). By simply counting the number of activated regions, the amount of peak force applied to the material could be quickly estimated with no additional characterization or analysis. Good reproducibility of the force required to activate each region in the sensor is highlighted by the small standard deviations obtained after three test runs (see Table 4.3 in the Experimental).

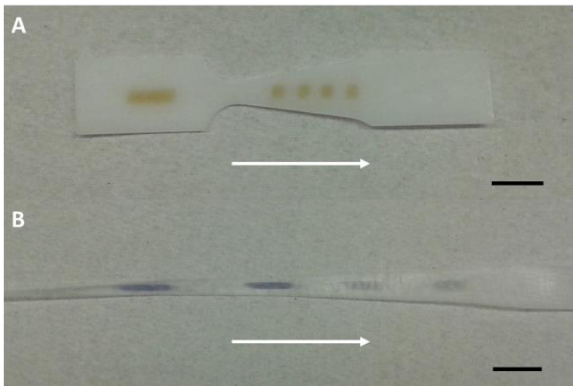


**Figure 4.8**. (a) 1 mm thick force sensor before elongation, and (b) post-elongation. The white arrows indicate the direction of necking. Scale bars = 10 mm.

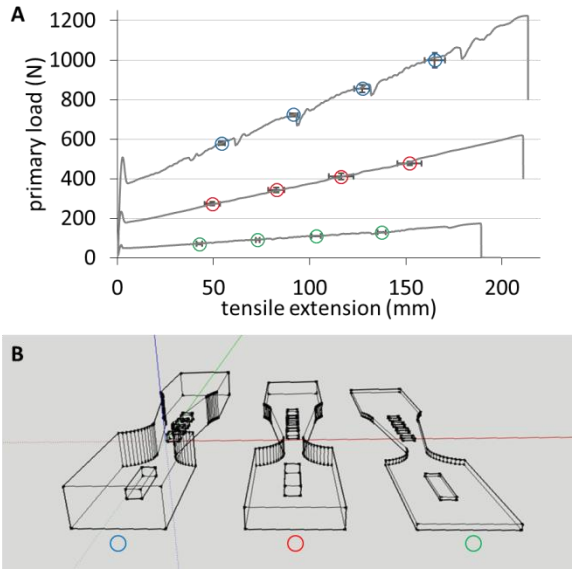


**Figure 4.9**. (a) Representative plots of tensile extension vs load for force sensors of ca. 1 (○), 4 (○), and 7 (○) mm thickness. The markers indicate the onset of the activation of each mechanoresponsive region (average of three runs). Error bars represent ± one standard deviation. (b) CAD representation of each of the force sensors.

One of the advantages of using 3DP to prepare prototypes and end-user products is the ability to quickly modify and optimize designs for a given application. To demonstrate the ease with which this can be accomplished, we modified the thickness of our force sensor to expand the range of detectable loads. By simply changing the thickness dimension in our CAD design we could quickly print different variations of the sensor without any additional tooling. In contrast, a similar process via injection molding would require preparation of a new mold for

each design. By changing the thickness of the specimens, different dynamic ranges were able to be accessed. Specifically, increasing the specimen thickness from 1 mm to 7 mm led to nearly an order of magnitude increase in the forces detectable by the sensor. Furthermore, the number, shape, spacing, and composition of mechano-responsive regions could also be customized based on the needs of the application. Obtaining this level of customizability would be extremely difficult without using 3DP technologies.

**Section 3: Conclusions**

In summary, we have demonstrated the successful 3D printing of a variety of stimuli-responsive polymers and the development of a new spiropyran mechanophore that exhibits selectivity toward mechanical activation by not exhibiting a photochromic response to either natural sunlight or 365 nm UV irradiation. The basic mechanical properties of the different structures prepared with various filament formulations showed some variation, but were within the range of reported values for PCL. The use of 3DP enabled rapid production of multi-component materials such as encased mechano-responsive materials within commercial or control polymers. These materials would generally be difficult or impossible to prepare with other manufacturing techniques. Additionally, rapid modification of a prototype force sensor was demonstrated to show its tunability and the advantages of using 3DP. These demonstrations were borne out through integration of mechanoresponsive polymer technology and the unique features of 3DP. The ability to produce these materials using consumer level equipment is expected to facilitate adoption, use, and exploration by a wide audience.

**Section 4: Experimental**

*General Considerations.* Dry toluene was obtained from a Glass Contour solvent purification system. The monomer, ε-caprolactone, was dried over 4 Å molecular sieves for 48 h prior to use. House $N_2$ was passed through a drying tube before use. All other reagents and solvents were used as obtained from commercial sources. $^{1}H$ and $^{13}C$ spectra were recorded on Bruker AVance 300 and 500 MHz spectrometers. Chemical shifts are reported in delta (δ) units, expressed in parts per million (ppm) downfield from tetramethylsilane using the residual protio-solvent as an internal standard ($CDCl_3$, $^{1}H$: 7.26 ppm, $^{13}C$: 77.0 ppm). MS was performed on a Bruker Esquire equipped with an electrospray ionization (ESI) source. GPC setup consisted of: a Shimadzu pump, three in-line MZ Analysentechnik columns, DAWN Heleos II multi-angle laser light scattering and T-rEX refractive index detectors (Wyatt Technology Corporation), and DMF (0.01 M LiBr) as the mobile phase. UV-Vis spectroscopy was completed using an Agilent 8453 Diode Array UV-Vis spectrometer. Initiator **1** and polymer **3** were prepared following a reported procedure.[13e]

Synthesis of polymer **4**. A flame-dried and $N_2$-purged three-neck round bottom flask fitted with a reflux condenser was charged with initiator **2** (prepared as previously reported,[22] (268 mg, 0.76 mmol) and a stir bar. To the reaction flask was then added ε-caprolactone (29.4 mL, 265 mmol) and dry toluene (30.0 mL). Finally, $Sn(Oct)_2$ (80 μL, 0.251 mmol) was added and the reaction solution was brought to refluxing temperature. After 24 h, the reaction solution was brought to 40 °C, diluted with toluene (~150 mL), and stirred until the polymer was fully dissolved. The polymer solution was then precipitated into an excess of cold MeOH, after which the precipitate

was collected via vacuum filtration and then dried under reduced pressure. The PCL product was obtained as a brown solid in 96% yield (29.0 g).

Synthesis of Initiator **7.** Indole **5** (prepared as previously reported,[13e] 266 mg, 1.31 mmol) and salicylaldehyde **6** (prepared as previously reported,[23] 200 mg, 1.31 mmol) were dissolved in 5 mL of absolute ethanol. Piperidine (0.26 mL, 2.63 mmol) was added and the solution brought to reflux. After 6 h the reaction was judged to be complete by TLC. The reaction was cooled to room temperature and diluted with 20 mL of ethyl acetate and washed successively with water (3 × 20 mL) and brine (1 × 10 mL). The organic layer was dried over $MgSO_4$ and concentrated under reduced pressure to yield **7** as a black crystalline solid in 91% yield (401 mg). $^1$H NMR (300 MHz, $CDCl_3$) δ 7.17 (td, $J$ = 7.7, 1.3 Hz, 1H), 7.11 – 7.05 (m, 3H), 6.86 (td, $J$ = 7.4, 0.8 Hz, 1H), 6.83 (d, $J$ = 10.2 Hz, 1H), 6.68 (d, $J$ = 7.9 Hz, 1H), 6.63 (d, $J$ = 7.8 Hz, 1H), 5.69 (d, $J$ = 10.2 Hz, 1H), 4.57 (s, 2H), 3.79 – 3.70 (m, 2H), 3.56 – 3.45 (m, 1H), 3.40 – 3.26 (m, 1H), 1.30 (s, 3H), 1.17 (s, 3H). $^{13}$C NMR (126 MHz, $CDCl_3$) δ 153.5, 147.3, 136.3, 132.9, 129.3, 129.0, 127.6, 125.9, 121.8, 119.9, 119.3, 118.6, 115.1, 106.6, 104.7, 64.9, 60.8, 52.3, 46.0, 25.8, 20.3. MS (ESI): $[M+H]^+$ calculated for $C_{21}H_{24}NO_3$, 338.18; found 338.4.

Synthesis of Polymer **8.** Polymer **8** was prepared in the same manner as **4**, except using **7** as an initiator (**7** = 164 mg, 0.49 mmol; ε-caprolactone = 18.84 mL, 170.1 mmol; toluene = 20 mL; $Sn(Oct)_2$ = 0.05 mL, 0.16 mmol). The polymer was obtained in 96% yield (18.7 g).

*Filament Production***.** Polymers **3** and **4** were mixed with Makerbot Flexible Filament (**C**), cut into small pieces, melted with a heat gun, and manually mixed with a spatula. After cooling, the

resulting solid mixture was cut into small pieces with scissors and put into an electronically controlled burr mill with dry ice. The polymer was ground into particles no larger than 5 mm in diameter, and then made into filament via melt extrusion (at 63 °C) with a Filabot Wee filament extruder. The filament $\mathbf{3}_{\mathbf{100}}$ was produced without blending in any commercial filament **C**.

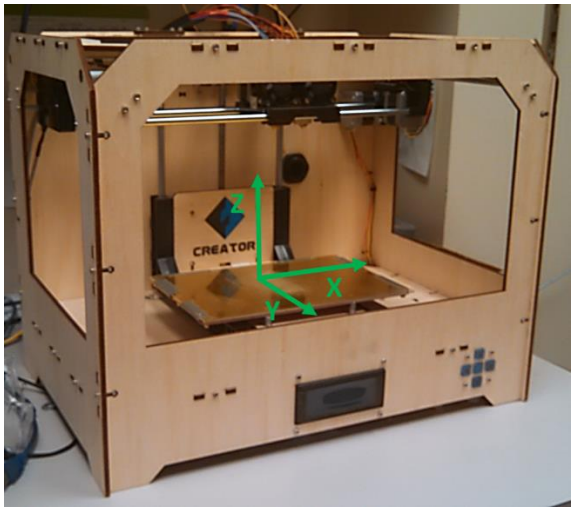


**Figure 4.10**. Flashforge Creator 3D printer used in this study. Axes of the build space are indicated by green arrows.

*3D Printing***.** 3D structures were designed and converted to .STL files using Sketchup 2013 computer aided design (CAD) software. The .STL files were imported into Replicator G (version 0040) and G-code (for Makerbot class machines) was generated using either Slic3r 0.X (for single material prints) or Skeinforge 50 (for multi-material prints) slicing programs. Multi-material prints required generation of G-code for each component individually, followed by their merger using Replicator G. A Flashforge Creator dual-head FFF 3D printer (firmware 7.2) was used to read the G-code and print the 3D object. Objects were printed centered on a non-heated Plexiglas build plate with the long axis of the specimen aligned with the y-axis of the build plate (build space axes shown in Figure 4.10). Objects were built up in the vertical z-axis. The outline

of the specimen was printed first with its thickness depending on the number of shells. For the first layer, the extruded polymer was laid in alignment with the y-axis. For the second, the polymer was laid in alignment with the x-axis. The fill alignment continually alternates such that the layers above or below any one layer are perpendicular to each other. Extrusion nozzles were heated to 110 °C (filament was more prone to jamming at lower temperatures). Additional print parameters included: print speeds set to 20 mm/s, travel speed set to 50 mm/s, retraction disabled when applicable (i.e. when using Slic3r), 2 shells, fill density of 1 (i.e. 100% fill), and layer height of 0.25 mm. To ensure the most accurate filament diameter, each sample of filament was measured with calipers in multiple places along the section to be used for printing and the average diameter was used in the print parameters. Dimensions of each printed specimen are provided below.

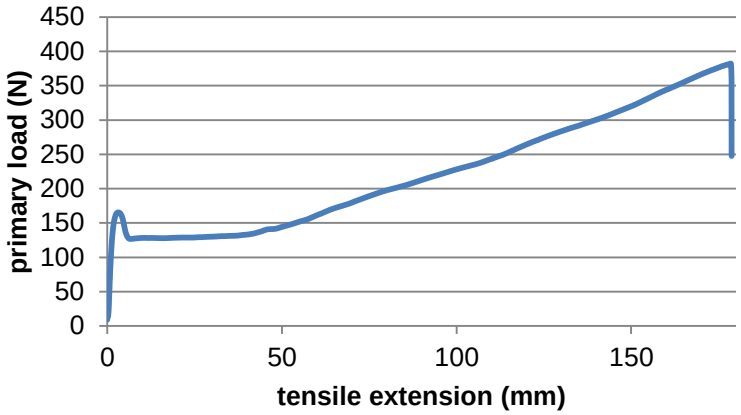


**Figure 4.11**. Plot of load versus extension for a representative symmetric tensile test specimen (as shown in Figure 4.3).

*Mechanical Testing***.** Tensile testing of printed specimens was performed on an Instron 5500R load frame with a 5 kN load cell controlled using Bluehill 3.0 software. All tests were conducted using a crosshead rate of 100 mm/min. Dimensions of each specimen were measured with calipers prior to testing to ensure accurate calculation of stress and strain for each sample. Three

specimens were tested for a given filament type. A typical stress-strain curve for symmetrical dogbone samples is shown in Figure 4.11.

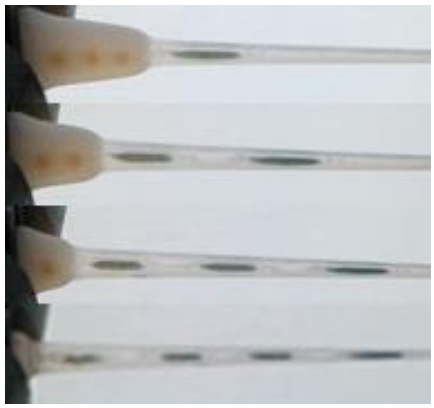

**Figure 4.12**. Images of the 4 mm force sensor undergoing elongation and sequential activation of the mechanoresponsive regions upon continued elongation (top to bottom). The image at the top shows activation of the first region and the bottom image shows activation of the last region.

**Table 4.3**. Extension and load values for the onset of activation of each mechanoresponsive region. Values are an average of three runs ± one standard deviation.

| Specimen Thickness (mm) | Mechanoresponsive Region Number | Average Extension (mm) | Average Primary Load (N) |
|---|---|---|---|
| 1 | 1 | 42.7 ± 1.5 | 70.3 ± 2.5 |
| | 2 | 73.0 ± 1.0 | 89.3 ± 1.5 |
| | 3 | 103.3 ± 2.5 | 109.3 ± 1.5 |
| | 4 | 137.3 ± 2.1 | 127.7 ± 1.5 |
| 4 | 1 | 49.3 ± 4.0 | 272.7 ± 9.3 |
| | 2 | 82.7 ± 4.2 | 342.7 ± 11.4 |
| | 3 | 116.3 ± 6.4 | 411.0 ± 14.7 |
| | 4 | 152.0 ± 6.2 | 477.0 ± 9.0 |
| 7 | 1 | 54.3 ± 1.5 | 579.0 ± 10.0 |
| | 2 | 91.7 ± 2.1 | 722.3 ± 7.5 |
| | 3 | 127.3 ± 4.2 | 855.0 ± 18 |
| | 4 | 165.0 ± 5.3 | 998.7 ± 38.2 |

*Specimen Dimensions*

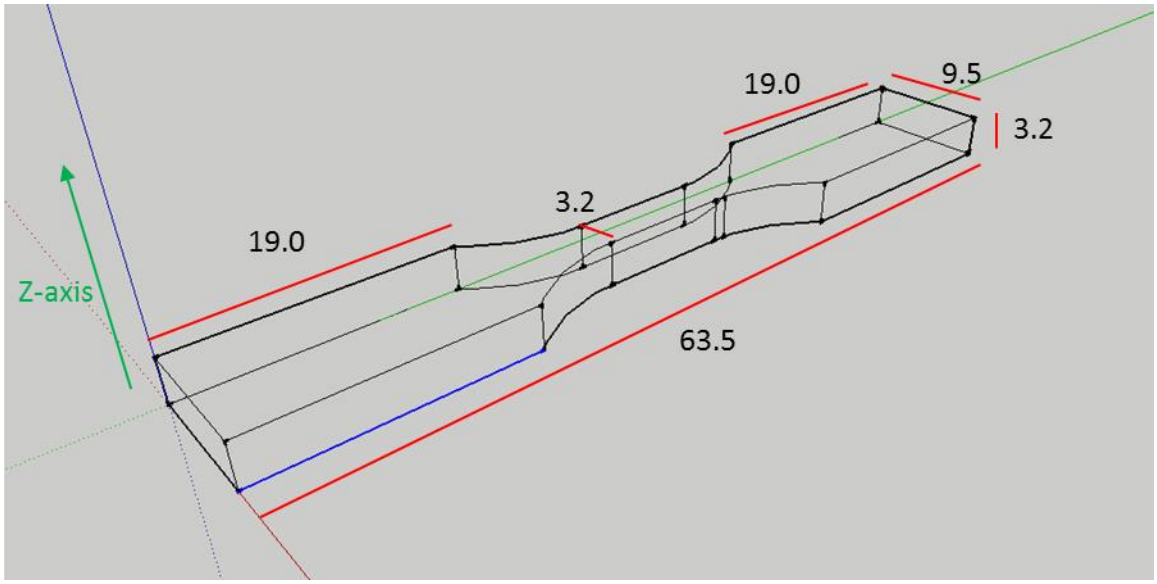


**Figure 4.13**. Tensile test specimen used in Figure 4.3. Radius of filet = 12.7 mm for all curved sections. Listed dimensions are in units of mm.

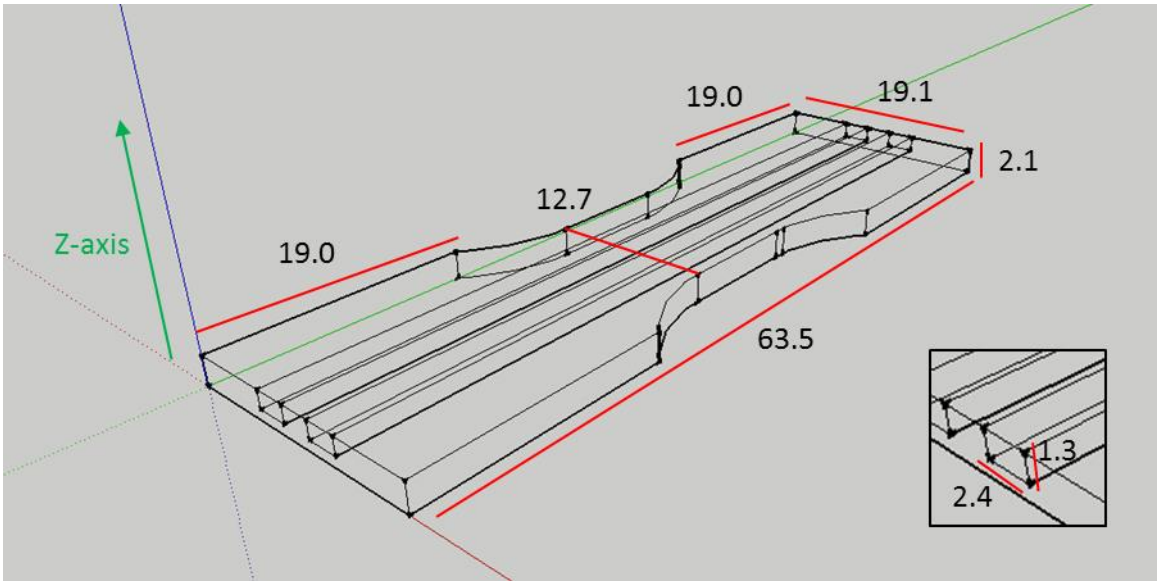


**Figure 4.14**. Tensile test specimen used in Figures 4.4 and 4.5. Radius of filet = 12.7 mm for all curved sections. Listed dimensions are in units of mm.

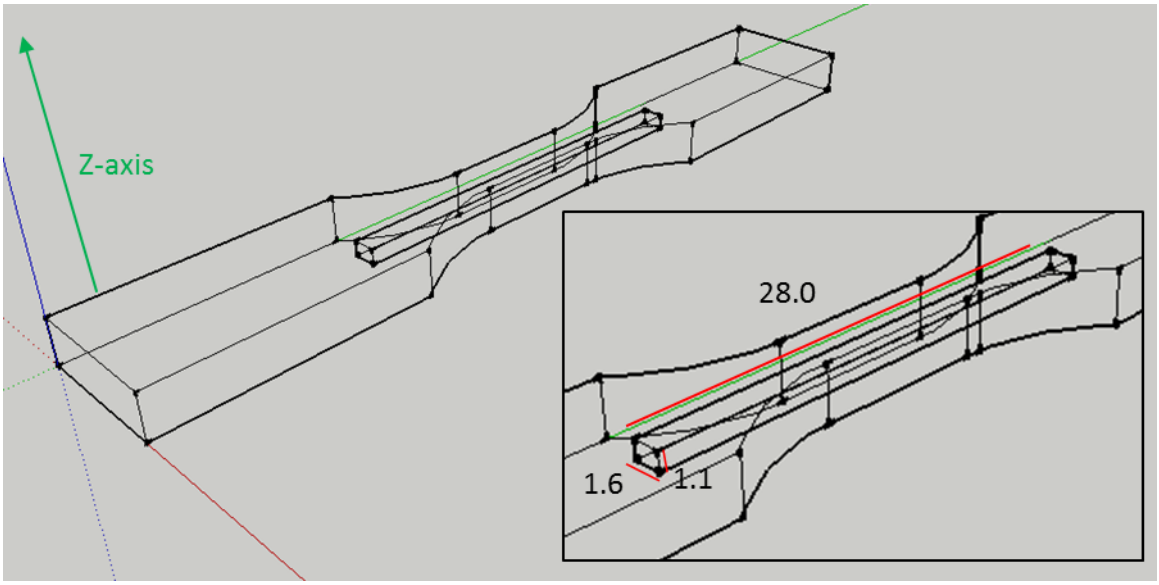


**Figure 4.15**. Tensile test specimen used in Figures 4.6 and 4.7. Dimensions of the specimen "body" are the same as those in Figure 4.12. The embedded rectangle is centered between the top and bottom faces of the specimen (in relation to the z-axis) and between the side walls of the specimen (in both the x- and y-directions). Listed dimensions are in units of mm.

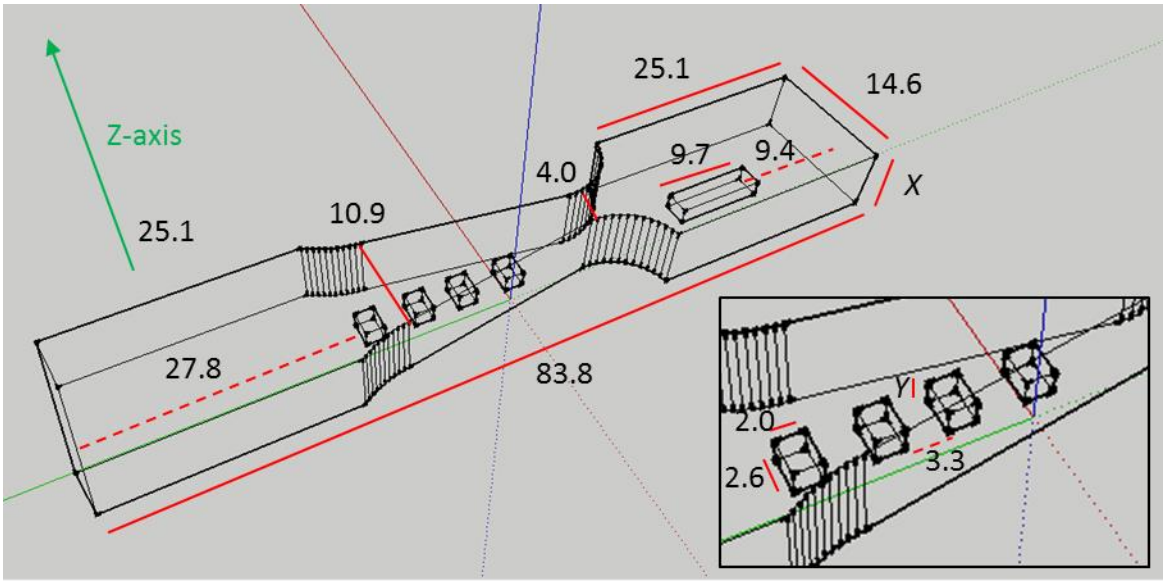


**Figure 4.16**. Tensile test specimen used in Figures 4.8 and 4.9. The embedded rectangles are raised 0.5 mm above the bottom face in the $X$ = 4 and 7 mm specimens and 0.25 mm for the $X$ = 1 mm specimen. The height of the rectangles ($Y$) is 1.8 mm in the $X$ = 4 and 7 mm specimens and 0.5 mm in the $X$ = 1 mm specimen. The rectangles are centered between the 25.1 mm walls of the specimen. The radius of filet for the shallow curves (on the left hand side of the specimen, as drawn) is 10 mm. The radius of filet for the steeper curves (on the right hand side of the specimen, as drawn) is 6 mm. Listed dimensions are in units of mm.

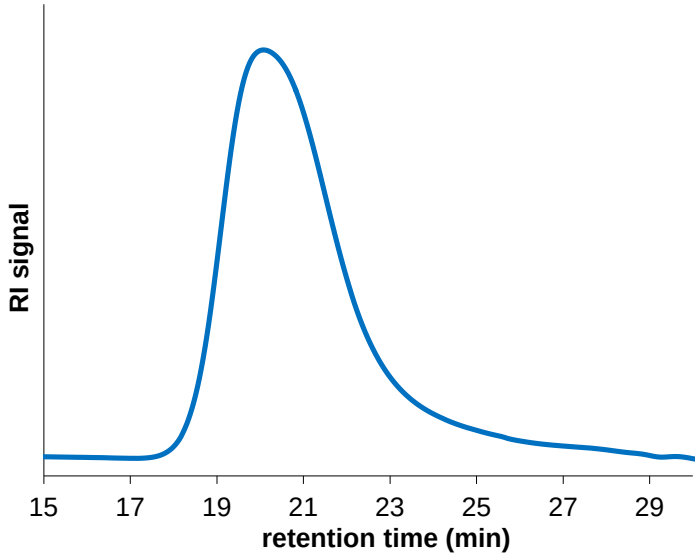


**Figure 4.17**. Gel permeation chromatography (GPC) trace of polymer **3** ($M_w$ = 90.0 kDa, Đ = 1.16).

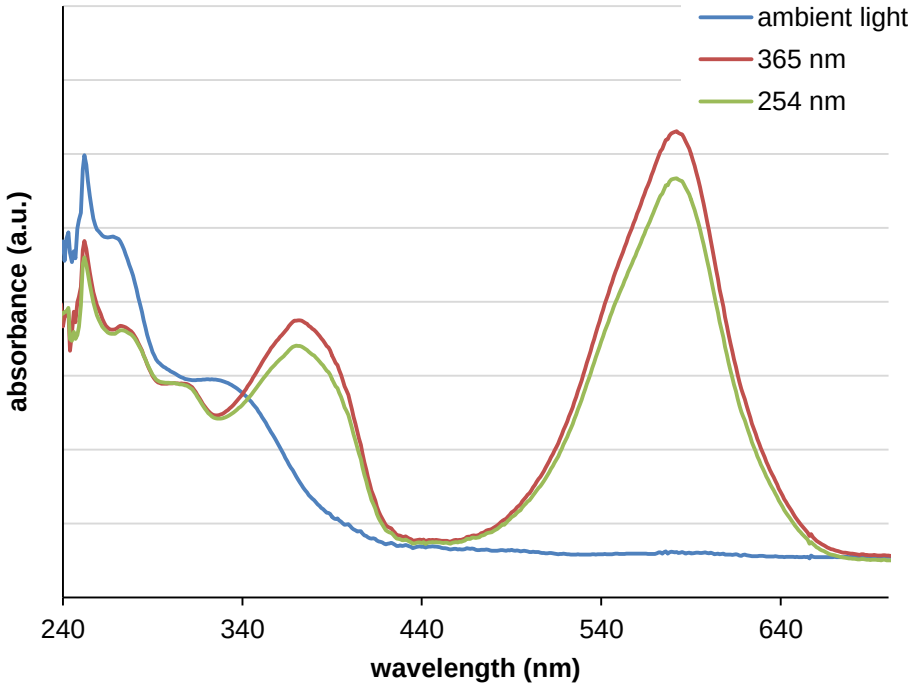


**Figure 4.18**. UV-Vis spectrum of polymer **3** dissolved in ethyl acetate after exposure to ambient light, 1 min of 365 nm UV, or 1 min of 254 nm UV.

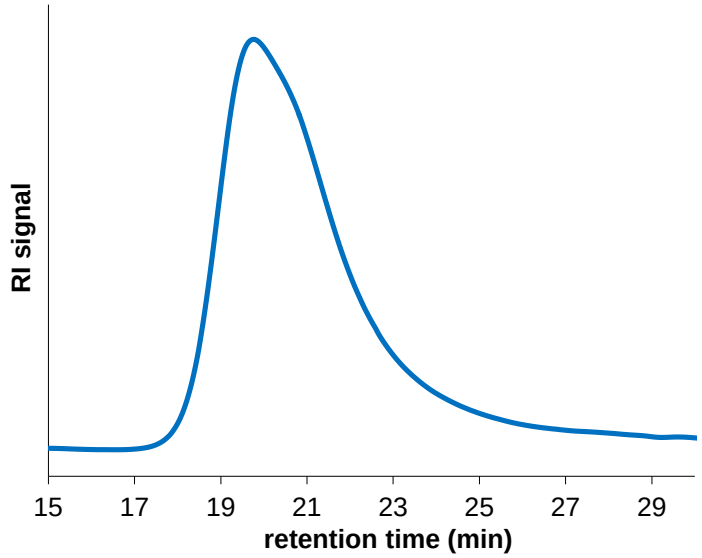


**Figure 4.19**. GPC trace of polymer **4** ($M_w$ = 64.9 kDa, Đ = 1.43).

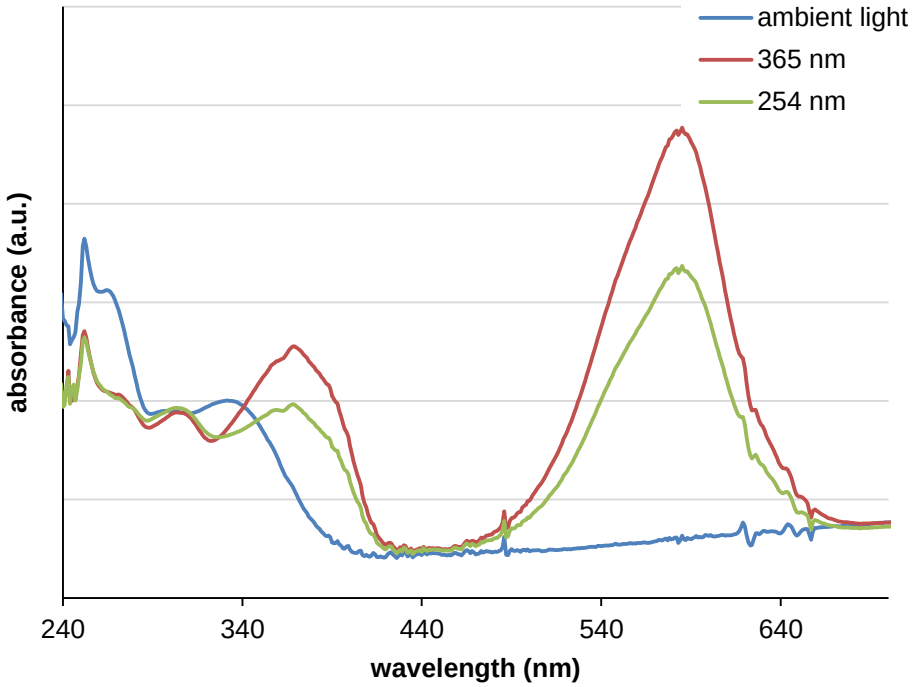


**Figure 4.20**. UV-Vis spectrum of polymer **4** dissolved in ethyl acetate after exposure to ambient light, 1 min of 365 nm UV, or 1 min of 254 nm UV.

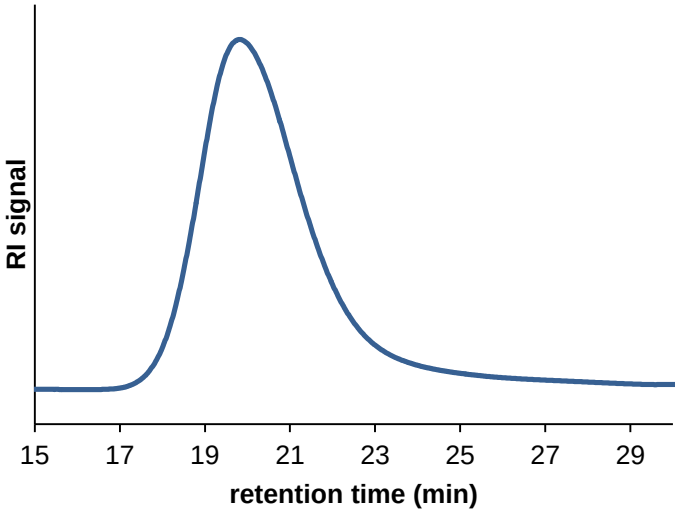


**Figure 4.21**. GPC trace of polymer **8** ($M_w$ = 82.5 kDa, Đ = 1.18).

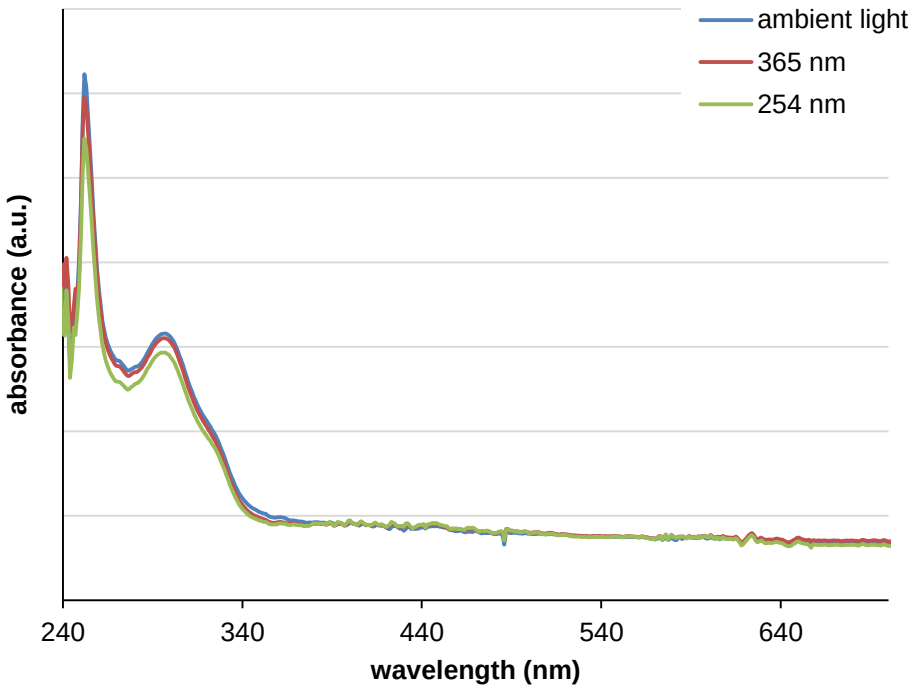


**Figure 4.22**. UV-Vis spectrum of polymer **8** dissolved in ethyl acetate after exposure to ambient light, 1 min of 365 nm UV, or 1 min of 254 nm UV.

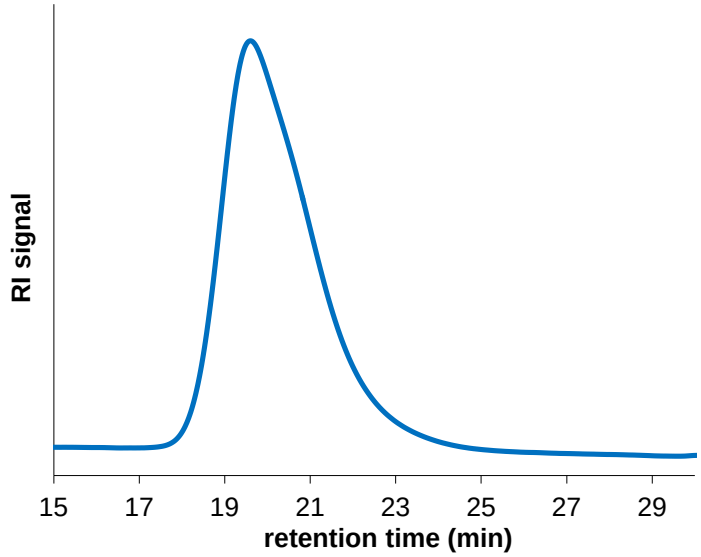


**Figure 4.23**. GPC trace of the Makerbot Flexible Filament ($M_w$ = 62.7 kDa, Đ = 1.29).

**Notes and References for Chapter 4**

[1] Hofmann, M. *ACS Macro Lett.* **2014**, *3*, 382.
[2] Gross, B. C.; Erkal, J. L.; Lockwood, S. Y.; Chen, C.; Spence, D. M. *Anal. Chem.* **2014**, *86*, 3240.
[3] Jones, N. *Nature* **2012**, *487*, 22.
[4] Wang, X.; Guo, Q.; Cai, X.; Zhou, S.; Kobe, B.; Yang, J. *ACS Appl. Mater. Interfaces* **2014**, *6*, 2583.
[5] Bakarich, S. E.; Gorkin III, R.; in het Panhuis, M.; Spinks, G. M. *ACS Appl. Mater. Interfaces* **2014**, *6*, 15998.
[6] (a) Khaled, S. A.; Burley, J. C.; Alexander, M. R.; Roberts, C. J. *Int. J. Pharm.* **2014**, *461*, 105. (b) Yu, D.-G.; Shen, X.-X.; Branford-White, C.; Zhu, L.-M.; White, K.; Yang, X. L. *J. Pharm. Pharmacol.* **2009**, *61*, 323.
[7] For recent reviews, see: (a) Derby, B. *Science* **2012**, *338*, 921. (b) Melchels, F. P. W.; Domingos, M. A. N.; Klein, T. J.; Malda, J.; Bartolo, P. J.; Hutmacher, D. W. *Prog. Polym. Sci.* **2012**, *37*, 1079. (c) Billiet, T.; Vandenhaute, M.; Schelfhout, J.; Van Vlierberghe, S.; Dubruel, P. *Biomaterials* **2012**, *33*, 6020.
[8] Xu, N.; Ye, X.; Wei, D.; Zhong, J.; Chen, Y.; Xu, G.; He, D. *ACS Appl. Mater. Interfaces* **2014**, *6*, 14952.
[9] (a) Zhao, C.; Wang, C.; Gorkin III, R.; Beirne, S.; Shu, K.; Wallace, G. G. *Electrochem. Commun.* **2014**, *41*, 20. (b) Sun, K.; Wei, T.-S.; Ahn, B. Y.; Seo, J. Y.; Dillon, S. J.; Lewis, J. A. *Adv. Mater.* **2013**, *25*, 4539.
[10] (a) Mannoor, M. S.; Jiang, Z.; James, T.; Kong, Y. L.; Malatesta, K. A.; Soboyejo, W. O.; Verma, N.; Gracias, D. H.; McAlpine, M. C. *Nano Lett.* **2013**, *13*, 2634. (b) Leigh, S. J.; Bradley, R. J.; Purssell, C. P.; Billson, D. R.; Hutchins, D. A *PLoS ONE* **2012**, *7*, e49365. (c) Czyzewski, J.; Burzynski, P.; Gawel, K.; Meisner, J. *J. Mater. Process. Tech.* **2009**, *209*, 5281. (d) Espalin, D.; Muse, D.; MacDonald, E.; Wicker, R. *Int. J. Adv. Manuf. Technol.* **2014**, *72*, 963.
[11] (a) Muth, J. T.; Vogt, D. M.; Truby, R. L.; Menguc, Y.; Kolesky, D. B.; Wood, R. J.; Lewis, J. A. *Adv. Mater.* **2014**, *26*, 6307. (b) Kim, K.; Zhu, W.; Qu, X.; Aaranson, C.; McCall, W. R.; Chen, S.; Sirbuly, D. J. *ACS Nano* **2014**, *8*, 9799.
[12] For recent reviews, see: (a) May, P. A.; Moore, J. S. *Chem. Soc. Rev.* **2013**, *42*, 7497. (b) Wiggins, K. M.; Brantley, J. N.; Bielawski, C. W. *Chem. Soc. Rev.* **2013**, *42*, 7130. (c) Brantley, J. N.; Wiggins, K. M.; Bielawski, C. W. *Polym. Int.* **2012**, *62*, 2. (d) Caruso, M. M.; Davis, D. A.; Shen, Q.; Odom, S. A.; Sottos, N. R.; White, S. R.; Moore, J. S. *Chem. Rev.* **2009**, *109*, 5755. (e) Beyer, M. K.; Clausen-Schaumann, H. *Chem. Rev.* **2005**, *105*, 2921.
[13] (a) Gossweiler, G. R.; Hewage, G. B.; Soriano, G.; Wang, Q.; Welshofer, G. W.; Zhao, X.; Craig, S. L. *ACS Macro Lett.* **2014**, *3*, 216. (b) Grady, M. E.; Beiermann, B. A.; Moore, J. S.; Sottos, N. R. *ACS Appl. Mater. Interfaces* **2014**, *6*, 5350. (c) Lee, C. K.; Beiermann, B. A.; Silberstein, M. N.; Wang, J.; Moore, J. S.; Sottos, N. R.; Braun, P. V. *Macromolecules* **2013**, *46*, 3746. (d) Beiermann, B. A.; Kramer, S. L. B.; Moore, J. S.; White, S. R.; Sottos, N. R. *ACS Macro Lett.* **2012**, *1*, 163. (e) O'Bryan, G.; Wong, B. M.; McElhanon, J. R. *ACS Appl. Mater. Interfaces* **2010**, *2*, 1594. (f) Davis, D. A.; Hamilton, A.; Yang, J.; Cremar, L. D.; Van Gough, D.; Potisek, S. L.; Ong, M. T.; Braun, P. V.; Martinez, T. J.; White, S. R.; Moore, J. S.; Sottos, N. R. *Nature* **2009**, *459*, 68.

[14] (a) Ducrot, E.; Chen, Y.; Bulters, M. J. H.; Sijbesma, R. P.; Creton, C. *Science* **2014**, *344*, 186. (b) Chen, Y.; Spiering, A. J. H.; Karthikeyan, S.; Peters, G. W. M.; Meijer, E. W.; Sijbesma, R. P. *Nat. Chem.* **2012**, *4*, 559.
[15] Jakobs, R. T. M.; Ma, S.; Sijbesma, R. P. *ACS Macro Lett.* **2013**, *2*, 613.
[16] Black Ramirez, A. L.; Kean, Z. S.; Orlicki, J. A.; Champhekar, M.; Elsakr, S. M.; Krause, W. E.; Craig, S. L. *Nat. Chem.* **2013**, *5*, 757.
[17] (a) Larsen, M. B.; Boydston, A. J *J. Am. Chem. Soc.* **2014**, *136*, 1276. (b) Larsen, M. B.; Boydston, A. J. *J. Am. Chem. Soc.* **2013**, *135*, 8189.
[18] Diesendruck, C. E.; Steinberg, B. D.; Sugai, N.; Silberstein, M. N.; Sottos, N. R.; White, S. R.; Braun, P. V.; Moore, J. S. *J. Am. Chem. Soc.* **2012**, *134*, 12446.
[19] Eshraghi, S.; Das, S. *Acta Biomater.* **2010**, *6*, 2467.
[20] (a) Keum, S.-R.; Lee, K.-B.; Kazmaier, P. K.; Buncel, E. *Tetrahedron Lett.* **1994**, *35*, 1015. (b) Keum, S.-R.; Lee, M.-J. *Bull. Korean Chem. Soc.* **1999**, *20*, 1464.
[21] Aramaki, S.; Atkinson, G. H. *J. Am. Chem. Soc.* **1992**, *114*, 438.
[22] Raymo, F. M.; Giordani, S. *J. Am. Chem. Soc.* **2001**, *123*, 4651.
[23] Frédérick, R.; Robert, S.; Charlier, C.; de Ruyck, J.; Wouters, J.; Pirotte, B.; Masereel, B.; Pochet, L. *J. Med. Chem.* **2005**, *48*, 7592.